NTNU
Norwegian University of
Science and Technology

Dynamic Modelling, Vibration and Fatigue Analysis of Slow Rotating Propulsion Systems

Helene Rimstad

Marine Technology
Submission date: July 2018
Supervisor: Amir Nejad, IMT
Co-supervisor: Geir Dahler, DNV GL

Norwegian University of Science and Technology
Department of Marine Technology

NTNU – Trondheim
Norwegian University of
Science and Technology
Department of Marine Technology

MSC THESIS IN MARINE TECHNOLOGY
SPRING 2018

Dynamic Modelling, Vibration and Fatigue Analysis of Slow Rotating Propulsion Systems

Helene Rimstad

Background:

Regulating the greenhouse gas (GHG) emissions from ships was addressed by IMO in the resolution no. MEPC.203(62) issued in 2011 where the Energy Efficiency Design Index (EEDI) was implemented. This was a major step forward in implementing the regulations on energy efficiency of ships. However, EEDI introduction brought serious concerns regarding the sufficiency of propulsion power and of steering devices to maintain the manoeuvrability of ships in the adverse conditions. Ship designers might choose to lower the installed power to achieve EEDI requirements or to operate at slow steaming, super slow steaming and virtual arrival approach. Adverse consequences of slow steaming operation include increased vibration of the power transmission system. In other words the ship drive train is exposed to the Barred Speed Range (BSR) in a longer time which causes whirling and severe vibration of bearings, rotor and driving components.

The aim of the project is to employ state-of-the art tools and methods to build a dynamic model of a representative ship's drive train and to use the model for studying different vibration reduction methods and evaluate the fatigue damage due to high vibration at BSR.

Assignment:

The following tasks should be addressed in the thesis work:
1. Study and utilize the literature on dynamic analysis, modelling of propulsion systems, vibration analysis and vibration reduction
2. Develop and build a dynamic model of a given ship propulsion system in DNV GL Nauticus Machinery Software/ Marine Propulsion.
3. Validate the model by empirical data provided by DNV GL.
4. Study and propose methods reducing the vibration at critical speeds.
5. Develop a model in a multi-body dynamic software (like SIMPACK).
6. Verify the model. Use the simulation results in time domain analysis for fatigue analysis.
7. Discuss the results, conclude the work and give recommendations for future work.
8. Write the MSc thesis report.

NTNU – Trondheim
Norwegian University of
Science and Technology
Department of Marine Technology

In the thesis the candidate shall present his/her personal contribution to the resolution of problem within the scope of the thesis work.

Theories and conclusions should be based on mathematical derivations and/or logic reasoning identifying the various steps in the deduction.

The candidate should utilize the existing possibilities for obtaining relevant literature.

The thesis should be organized in a rational manner to give a clear exposition of results, assessments, and conclusions. The text should be brief and to the point, with a clear language. Telegraphic language should be avoided.

The thesis shall contain the following elements: A text defining the scope, preface, list of contents, summary, main body of thesis, conclusions with recommendations for further work, list of symbols and acronyms, reference and (optional) appendices. All figures, tables and equations shall be numerated.

The supervisor may require that the candidate, in an early stage of the work, present a written plan for the completion of the work. The plan should include a budget for the use of computer and laboratory resources that will be charged to the department. Overruns shall be reported to the supervisor.

The original contribution of the candidate and material taken from other sources shall be clearly defined. Work from other sources shall be properly referenced using an acknowledged referencing system.

The thesis shall be submitted electronically (pdf) in DAIM:

- Signed by the candidate
- The text defining the scope (this text) (signed by the supervisor) included
- Computer code, input files, videos and other electronic appendages can be uploaded in a zip-file in DAIM. Any electronic appendages shall be listed in the main thesis.

The candidate will receive a printed copy of the thesis.

Supervisor (s):
Amir Nejad
Marine Technology Department, NTNU

Geir Dahler
DNV GL - Maritime Advisory

Deadline for thesis report: July 2018 (check the exact date at DAIM)
Description of grades for master thesis at NTNU is found here.

Preface

This master thesis represents the final thirty ECTS of a Master of Science in Marine Technology at the Norwegian University of Science and Technology (NTNU) in Trondheim, Norway. My field of specialization is within marine engineering. The research project is a continuation of a preliminary study that took place during the autumn of 2017, while the rest of the work have been performed between February and July of 2018. The thesis is written in collaboration with DNV GL, department Maritime Advisory - Machinery & Systems, where my contact person has been Geir Dahler.

The mentioned preliminary study, referred to as 'the project thesis', is incorporated into this manuscript. It is therefore not necessary to read both papers, this master thesis covers all of the executed research and studies on the topic.

During an internship in DNV GL the summer of 2017, I got in contact with Geir Dahler, Head of Department Maritime Advisory - Machinery & Systems. A collaboration on a master thesis was agreed upon, where studying torsional vibrations in vessel drive trains became the selected topic. DNV GL had received concerns from their customers regarding propulsion shaft damages, whereas I was eager to work with a timely issue related to the field of marine engineering. After having the research topic in place, followed the search for a suitable supervisor at the Department of Marine Technology (IMT). I was pleased to be informed that Amir Rasekhi Nejad would guide me through the master thesis, he was in fact the professor who had success-

fully taught and introduced me to the field of mechanical vibrations.

The booklet you have in hand is a result of many hours of hard and frustrating, but also enjoyable work. Drive train modelling in two different softwares turned out to be a bigger challenge than expected, which affected the available time for post-processing analyzes and testing of vibration reduction measures. Anyhow, I hope you will enjoy your reading and learn something new within the field of torsional vibration analysis in slow rotating propulsion systems.

Helene Rimstad — 12/07/18, Østevas

Signature of the Author — *Date and Place*

Helene Rimstad

Acknowledgements

I would like to express my gratitude to my supervisor Amir Rasekhi Nejad, Associate Professor at the Department of Marine Technology NTNU, for his contributions throughout the work with the master thesis. Your door is always open, and I am grateful for your excellent support during the past year. I also want to thank DNV GL and Head of Department Maritime Advisory - Machinery & Systems, Geir Dahler, for the provided material and the time spent related to the thesis. Additional appreciations go to Head Engineer Bjørn Tore Bach for the necessary IT and software support, and lastly to my fellow student Sigrid Siksjø Johansen for valuable discussions about modelling in Simpack. This master thesis would not be concluded without the help from each and every one of you.

Summary

In recent years, shipping has experienced a technical transformation motivated by its impact on the environment and the desire to reduce operational costs. Engines with lower power ranges and slow steaming are two examples. These modifications have fulfilled their purpose, but there are also downsides such as increased torsional vibrations. This master thesis presents an approach to the issue. A case study, the drive train of a modern eco-ship, is used for this purpose. It is driven directly by a two-stroke diesel engine, with a torsional vibration damper (TVD) mounted on its free end, and the propeller is fixed pitch. System characteristics are provided by DNV GL. The presented method is general, and can be applied on other propulsion systems as well. The final goal is to identify vibration reduction measures and to evaluate the consequences of severe torsional vibrations.

All vibration analyzes need a steady foundation in terms of an accurate software model. The applied mathematical approach is the one degree of freedom lumped mass method. Masses are modelled as rigid and shafts are massless. Damping is further introduced through the dynamic magnifier model, defining damping as independent of varying rotational speed. Nauticus Torsional Vibration, a software from DNV GL, is used to simulate in frequency domain. Simpack Multi-Body Simulation Software is utilized to introduce the aspect of time. Two software models are thereby constructed, both from the lumped mass model of the drive train. The model in Nauticus Machinery is verified by empirical data from DNV GL. Time limitations resulted in absent propeller damping in Simpack, in addition to a simplified

engine torque. Only the system's free and undamped behavior is therefore reconstructed in this software.

Free and forced vibration analyzes are performed in both softwares, aiming at identifying critical speeds and vulnerable shaft segments. Further analyzes focus on these frequencies and parts. Calculations of natural frequencies and construction of Campbell diagrams detect critical excitations. Power spectra, evaluating energy levels by use of the WAFO MATLAB toolbox, are used to validate these speeds. The most dangerous resonance speed was found to be 45 rpm. Mode shapes are used to identify stationary points vulnerable towards torsional fracture. Additionally, resulting torque and torsional stress amplitudes help locate critical shaft segments. Five specific shafts were then revealed; the one connecting the damper to the engine, two segments of the crank shaft, the intermediate shaft and the propeller shaft.

Torsional vibrations are not only dangerous because they initiate high peak displacements (ultimate limit state) that could result in fracture, they also increase the risk of fatigue failure especially if the system is subjected to large vibrations loads more often. Calculations of fatigue damage (also by use of WAFO), which requires time domain simulation, are therefore also included in this research. Since forced vibration analysis results from Simpack are not verified, these studies can only indicate triggers of fatigue, not evaluate if failure will occur in the drive train or not. However, they present a general procedure of how to calculate fatigue damage. Both operation at 45 rpm and the MCR condition were evaluated, in addition to elaborate analyzes of the five mentioned shafts. Vibrations with large amplitudes, occurring over long periods, were identified as a source of fatigue. Furthermore, it was observed that shaft dimensions significantly influenced fatigue. A higher level of radius divided by second area moment results in an increased risk of failure.

Vibration reduction is investigated in terms of a sensitivity analysis in Nauticus Machinery, performed by modifying shaft stiffness and damping factors. Decreased levels of torque and torsional stress, in the identified critical segments at resonance speed, is the general indication of reduced vibrations.

Introduction of damping in the intermediate shaft was the most effective modification. By replacing the intermediate shaft with a shaft that has the same properties as the TVD, torque and stress amplitudes were reduced with 70% in shafts after the engine. Unfortunately, a practical solution to implement this change was not found. An increase of hydrodynamic damping, which could be achieved by a controllable pitch propeller, decreased the vibration responses with 30%. Increasing stiffness and adding mass damping in the TVD, which could be obtained by choosing a different design, reduced the levels with about 5%. At last, the thesis addresses that operational profiles also influence damage levels from vibrations.

The author presents and is aware of the major assumptions and simplifications in her work. Introduction of damping through the dynamic magnifier model is one example, and mathematical modelling by the lumped mass approach is another. Nevertheless, the objectives are obtained and all analyzes are presented in such a way that they can be reconstructed by others in the future. Established theory and methods are taken into account throughout the work.

Sammendrag

Shipping-industrien har i nyere tid opplevd en teknisk transformasjon motivert av miljøhensyn og ønsker om å redusere driftskostnader. Skipsmotorer med lavere propulsjonskraft og lavere operasjonelle turtall er to eksempler på dette. Disse modifikasjonene har hatt positiv effekt, men de har også ført til ulemper som økte torsjonale vibrasjoner. Denne masteroppgaven presenterer en tilnærming til vibrasjonsproblemet. Et case-studie, drivverket i et moderne øko-skip, brukes til dette formålet. Skipet i case-studiet drives direkte av en to-takts dieselmotor, med en torsjonsvibrasjonsdemper (TVD) montert på dens frie ende, og propellen har fast pitch (FPP). Detaljer om propulsjonssystemet er levert av DNV GL. Den presenterte metoden er generell og kan derfor overføres til andre fremdriftssystemer. Oppgavens endelige mål er å identifisere vibrasjonsreduksjonstiltak og å vurdere konsekvensene av store torsjonsvibrasjoner.

Alle vibrasjonsanalyser trenger et stabilt grunnlag, her i form av en nøyaktig programvaremodell. Den anvendte matematiske tilnærmingen er lumped mass method med én frihetsgrad i hver node. Massene er modellert som stive, og akslingene er modellert masseløse. Dempning blir videre introdusert ved bruk av the dynamic magnifier model, som definerer dempning som uavhengig av varierende rotasjonshastighet. Nauticus Torsional Vibration, en programvare fra DNV GL, brukes til å simulere i frekvensdomenet. Simpack Multi-Body Simulation Software brukes til å også introdusere tid i simuleringen. To programvaremodeller i de respektive programvarene er konstruert, begge med utgangspunkt i lumped mass modellen av drivverket.

Modellen i Nauticus Machinery er verifisert ved bruk av empiriske data fra DNV GL. Tidsbegrensninger førte til at propelldemping ikke er inkludert i Simpack, og det er i tillegg benyttet en forenklet representasjon av motormomentet i Simpackmodellen. Kun systemets frie og udempede oppførsel blir derfor rekonstruert tilstrekkelig i denne programvaren.

Frie og tvungne vibrasjonsanalyser utføres i begge programmene med mål om å identifisere kritiske hastigheter og utsatte akselsegmenter. Videre analyser fokuserer på disse spesifikke frekvensene og segmentene. Beregninger av egenfrekvenser og konstruksjon av Campbell-diagrammer identifiserer kritiske eksitasjoner. Effektspekter, evaluering av energinivåer ved bruk av WAFO MATLAB Toolbox, brukes til å validere disse hastighetene. Den mest kritiske resonanshastigheten ble analysert til å være 45 rpm. Mode shapes brukes til å identifisere stasjonære punkter som er spesielt sårbare mot torsjonsbrudd. I tillegg benyttes resulterende dreiemoment- og torsjonsspennings-amplituder til å lokalisere kritiske akselsegmenter. Disse metodene lokaliserte fem kritiske akselsegmenter; akselen som kobler torsjonsdemperen til motoren, to segmenter av veivakselen, mellomakselen og propellakselen.

Torsjonsvibrasjoner er ikke kun uønskede fordi de initierer store forskyvninger (ultimate limit state) som kan resultere i brudd, de øker også risikoen for utmatting, spesielt hvis systemet ofte blir utsatt for store vibrasjoner. Beregninger av utmattingsskader (også ved bruk av WAFO), som krever simuleringer i tidsdomene, er derfor også inkludert i denne undersøkelsen. Siden de tvungne vibrasjonsanalyseresultatene fra Simpack ikke er verifisert, kan disse studiene kun indikere utløsende årsaker til utmatting og ikke vurdere om utmattingsbrudd vil oppstå i drivverket eller ikke. Derimot kan studiene brukes som en generell prosedyre for å beregne utmattingsskader. Både operasjon ved 45 rpm og MCR-tilstanden ble evaluert, i tillegg til omstendelige analyser av de fem nevnte kritiske akslene. Vibrasjoner med store amplituder, som forekommer over lange perioder, ble identifisert som en kilde til utmatting. Videre ble det observert at akseldimensjonene betydelig påvirket utmatting. Et høyere forhold mellom radius delt på andre arealmoment resulterer i økt risiko for svikt.

Tiltak for å redusere vibrasjoner undersøkes gjennom bruk av følsomhetsanalyser i Nauticus Machinery. Følsomhetsanalysen ble utført ved å endre stivhets- og dempningsparametere. Reduserte nivåer av dreiemoment og torsjonsspenning i de allerede identifiserte kritiske segmentene ved resonanshastighet er den generelle indikasjonen på reduserte vibrasjoner. Innføring av demping i mellomakselen var det mest effektive tiltaket. Ved å erstatte mellomakselen med en aksel som har samme egenskaper som en TVD, ble dreiemoment- og stressamplituder redusert med 70% i akslinger etter motoren. Dessverre ble det ikke funnet en praktisk løsning for å implementere denne endringen. En økning av hydrodynamisk dempning, som kan oppnås ved bruk av en controllable pitch propeller (CPP), reduserte vibrasjonsresponsene med 30%. Ved å øke stivheten og legge til mer massedemping i TVD, som kan oppnås ved å velge et annet design, ble nivåene redusert med ca 5 %. Til slutt påpeker oppgaven at den operasjonelle profilen til et skip også påvirker skadenivåene fra vibrasjoner.

Forfatteren presenterer og er klar over de store antagelsene som er gjort og forenklinger i hennes arbeid. Innføring av demping gjennom bruk av dynamic magnifier model er et eksempel, og matematisk modellering ved lumped mass-tilnærming er en annen. Til tross for antagelsene og forenklingene, blir målene oppnådd, og alle analyser presenteres på en slik måte at de kan rekonstrueres av andre i fremtiden. Etablerte teorier og metoder tas i betraktning gjennom hele arbeidet.

Table of Contents

Problem Description i

Preface iii

Acknowledgements v

Summary vii

Sammendrag x

List of Tables xiv

List of Figures xv

Abbreviations xvi

Symbols xvii

1 Introduction 1

1.1 Motivation 1

1.2 Research Objectives 3

1.3 Scope of the Thesis 4

1.4 Structure of the Report 5

2 Background 7

2.1 Terminology 7

2.2 State-of-the-Art for Torsional Vibrations 10

2.2.1 Modern Propeller Designs and Torsional Vibration Calculations . . . 10
2.2.2 Quick Passage Through the Barred Speed Range . . . 12
2.2.3 Damping Measures . . . 14
2.2.4 Current Standards and Regulations . . . 18

3 Methodology **21**
3.1 Modelling Methodology . . . 21
3.1.1 Torsional Lumped Mass Systems . . . 22
3.1.2 Nauticus Torsional Vibration . . . 25
3.1.3 Simpack Multi-Body Simulation Software . . . 26
3.2 Torsional Vibration Analysis . . . 27
3.3 Free Vibration Analysis . . . 29
3.3.1 Dynamics of Multi-Body Systems . . . 30
3.3.2 Undamped Free Vibrations . . . 31
3.3.3 Free Vibrations with Damping . . . 35
3.4 Forced Vibration Analysis . . . 37
3.4.1 Harmonic Excitation . . . 38
3.4.2 The Dynamic Magnifier Model . . . 40
3.4.3 Forced Vibration Equations of Motion of a Drive Train . . . 45
3.4.4 Critical Speeds and Campbell Diagrams . . . 47
3.5 Post-Processing Methodology . . . 49
3.5.1 Power Spectra . . . 49
3.5.2 Torsional Shaft Stress . . . 50
3.5.3 Fatigue Analysis . . . 51
3.5.4 WAFO - a MATLAB Toolbox for Analysis of Random Waves and Loads . . . 57
3.6 Case Study . . . 57
3.6.1 Propulsion System Design and Characteristics . . . 58

4 Modelling **65**
4.1 Frequency Domain . . . 65
4.1.1 Modelling in Nauticus Torsional Vibration . . . 65
4.1.2 Load Case in Nauticus Machinery . . . 69

4.2 Time Domain . . . 71
4.2.1 Modelling in Simpack MBS Software . . . 71
4.2.2 Engine Excitation through Co-Simulation in Simpack . . . 74
4.3 Discussion . . . 80
4.4 Introduction to Modelling Verification . . . 80

5 Free Vibration Analysis **81**
5.1 System Characteristics . . . 81
5.1.1 Natural Frequencies . . . 82
5.1.2 Normal Modes and Stationary Points . . . 83
5.2 Verification . . . 84

6 Forced Vibration Analysis **87**
6.1 Critical Speeds . . . 88
6.1.1 Campbell Diagrams . . . 88
6.1.2 Power Spectrum . . . 90
6.1.3 Discussion . . . 91
6.2 Forced Vibration Analysis in Nauticus Torsional Vibration . . . 91
6.3 Forced Vibration Analysis in Simpack . . . 94
6.3.1 Steady State Simulation . . . 94
6.3.2 Variable Reference Speed and Transient Regions . . . 99
6.4 Discussion . . . 100

7 Short Term Fatigue Analysis **105**
7.1 Procedure . . . 105
7.2 Case Studies . . . 106
7.2.1 Constant Speed, Different Shafts . . . 107
7.2.2 Same Shaft, Different Speeds . . . 112
7.3 Discussion . . . 115

8 Study of Vibration Reduction Measures **117**
8.1 Sensitivity Analysis in Nauticus Machinery . . . 118
8.1.1 Modification of Natural Frequency . . . 119
8.1.2 Changing Damping Ratio . . . 120
8.1.3 Discussion . . . 125

8.2 The Significance of Operational Profiles 126

9 Conclusions **129**

9.1 Concluding Remarks 129

9.2 Recommendations for Further Work 130

Bibliography **I**

A Miscellaneous **VII**

A.1 Deriving rotational natural frequency VII

A.2 Calculating propeller damping factor C - Ex. 77 rpm VIII

B TVC Data for the Eco-Ship - Provided by DNV GL **IX**

B.1 Drive train specifications and TVC results X

B.2 Propeller damping table XV

B.3 Engine excitation data XVI

C Attachments to Analyzes in Nauticus Machinery **XVIII**

C.1 Free analysis XVIII

C.1.1 Input data XIX

C.1.2 Natural frequencies and mode shapes XXI

C.2 Forced analysis XXIII

C.2.1 Load case settings XXIII

C.2.2 Explanation of 'synthesis' XXVI

C.2.3 Maximum torque and stress amplitudes XXVII

C.3 Excel sheet for sensitivity analysis XXVIII

D Attachments to Simpack Simulation **XXIX**

D.1 Values of absolute and relative damping in Simpack XXIX

D.2 Example of a Simpack model XXXI

D.3 MATLAB files for variable reference speed XXXI

D.3.1 Simulink setup XXXI

D.3.2 MATLAB function for updating engine torque . . XXXII

D.3.3 MATLAB script for updating reference speed . . . XXXII

D.4 Result file - eigenvalues, eigenvectors and energies XXXIII

E Attachments to Time Domain Post-Processing **XXXVI**
E.1 The WAFO codes XXXVI
E.2 Investigation of power spectra XXXVI
E.2.1 MATLAB script for construction of PSD plots . . XXXVI
E.2.2 Plots of power spectral density XXXVII
E.3 MATLAB script for calculations of fatigue damage XXXIX

List of Tables

3.1 Shaft material properties of alloy steel 16MnCr5 [36] 54
3.2 Main engine specifications 60
3.3 TVD and propeller details 61
3.4 Mass elastic data for the drive train 63

4.1 Selected controller gains 76

5.1 Natural frequencies from Nauticus Machinery 82
5.2 Natural frequencies from Simpack 82
5.3 Natural frequencies from DNV GL 84

7.1 Fatigue damage in shafts at 45 and 77 rpm operation 107
7.2 Fatigue damage in a selection of shafts at different ω 112

D.1 Relative shaft damping XXX
D.2 Absolute mass damping XXX

List of Figures

2.1 Design of a Geislinger damper [22] 16
2.2 Schematic of an active magnetic bearing [33] 18

3.1 Lumped versus distributed mass [6] 23
3.2 Example of a torsional lumped mass system - Discs mounted on a shaft 24
3.3 Modelling of hydrodynamic damping 25
3.4 Decomposition of torsional vibration analysis 27
3.5 Interconnections in a multi-body system [46] 30
3.6 Mode shape for a two-disc torsional system 33
3.7 Comparison of motions with different types of damping [43] . 36
3.8 Vector diagram for forced vibrations 39
3.9 Dynamic response in terms of frequency and damping ratio [49] 40
3.10 Vector diagram at resonance 42
3.11 Absolute and relative damping 43
3.12 Free body diagram of a vessel drive train 45
3.13 Campbell diagram: critical rpm during periodic excitation [41] 48
3.14 Example of power spectral density [23] 50
3.15 Example of an SN curve - Material: UNS G41300 steel [8] . . 53
3.16 Example of an RFC histogram 54
3.17 Illustration of the RFC method [35] 56
3.18 Sketch of the propulsion system 59
3.19 Variable propeller damping curve 62

4.1 Drive train model in Nauticus Torsional Vibration 66
4.2 Defined variable propeller damping in Nauticus Machinery . . 67
4.3 Defining diesel engine data in Nauticus Torsional Vibration . 68

4.4 Model with parameter values 69
4.5 Propeller curve in Nauticus Machinery 70
4.6 Drive train model in Simpack Pre-Processor 72
4.7 Co-simulation - Applying torque in Simulink 75
4.8 Simulink model of PID-controller 77
4.9 Engine curve according to the propeller law 78
4.10 Harmonic engine excitation at 30 rpm 79

5.1 Normal modes from Nauticus Torsional Vibration 83

6.1 Campbell diagram for engine excitations 88
6.2 Campbell diagram for propeller excitations 89
6.3 Power spectrum of intermediate shaft (from torque at 45 rpm) 90
6.4 Results from forced vibration analyzes in Nauticus Machinery 93
6.5 Engine and propeller torque at different speeds (Black=77rpm, Red=45rpm, Blue=30rpm) 96
6.6 Torque levels at 45 rpm operation (Red=T_{eng}, Green=Mass damping, Black=Propeller torque 97
6.7 Internal torque at 77 rpm operation for a selection of shafts (Magenta=CT3, Black=Shaft 9-10, Green=Interm. and Prop. shaft, Red=Shaft 2-3, Purple=Shaft 3-4 97
6.8 Amplitude against frequency ratio 98
6.9 Variations in rotational speed with time 99
6.10 Shaft torque oscillations in transient region (Red=CT3, Black=Shaft 9-10, Green=Interm. and Prop. shaft) 100

7.1 Damage ratio X for constant speeds (D shaft i/Max D) . . . 108
7.2 Intermediate shaft - Plots from fatigue analyzes at 45 rpm . . 110
7.3 Intermediate shaft - Plots from fatigue analyzes at 77 rpm . . 111
7.4 Damage ratio X for constant shaft (D at ω / Min D) 113
7.5 Changes in intermediate shaft torque with speed 114
7.6 Changes in torque at Shaft 9-10 with speed 114

8.1 Results from forced vibration analyzes with two damper stiffnesses 123

8.2 Vibration response and operational profiles 127

E.1 Power spectrum of damper stiffness (from torque at 45 rpm) XXXVII
E.2 Power spectrum of third crank throw (from torque at 77 rpm) XXXVIII
E.3 Power spectrum of Shaft 10-11 (from torque at 60 rpm) XXXVIII

Abbreviations

AMB Active Magnetic Bearing

BRF Body Reference Frame

BSR Barred Speed Range

CPP Controllable Pitch Propeller

DLF Dynamic Limiter Function

DOF Degrees Of Freedom

ECTS European Credit Transfer and Accumulation System

EEDI Energy Efficiency Design Index

eom equation of motion

FEM Finite Element Method

FPP Fixed Pitch Propeller

IACS International Association Classification Society

ISO International Organization for Standardization

LRM Light Running Margin

MARPOL Marine Pollution convention

MBS Multi-Body Simulation

MCR Maximum Continuous Rating

MOI Moment Of Inertia

NTNU Norwegian University of Science and Technology

OMAE International Conference on Ocean, Offshore and Arctic Engineering

PID Proportional-Integral-Derivative (PID-controller)

PSD Power Spectral Density

RFC Rain Flow Cycle counting

RFM Rain Flow Matrix

rpm revolutions per minute

SHOPERA Energy Efficient Safe Ship Operation

TVC Torsional Vibration Calculation

TVD Torsional Vibration Damper

ULS Ultimate Limit State

UR Unified Requirements

Symbols

A Oscillation amplitude [m]

β Angular displacement about y [rad] (Simpack syntax)

C Rotational damping [Nms/rad]

C_{abs} Absolute / External damping [Nms/rad]

C_{rel} Relative / Internal damping [Nms/rad]

D Fatigue damage [-]

e Error [-]

f Frequency [Hz]

I Polar area moment of inertia [m^4]

J Polar moment of inertia [kgm^2]

K Rotational stiffness [Nm/rad]

K_d Derivative gain constant [-]

K_i Integral gain constant [-]

K_p Proportional gain constant [-]

M Dynamic magnifier percent [-]

$\tilde{M}$ Dynamic magnifier number [-]

n_e Engine speed [rpm]

n_p Propeller speed [rpm]

ω Angular velocity/frequency ([rad/s]/[Hz]/[rpm], specified in text)

ω_n Natural frequency ([rad/s]/[Hz]/[rpm], specified in text)

ϕ Phase angle [rad]

r Shaft radius [m]

T Torque [Nm]

t Time period [s]

τ Torsional stress [N/mm^2]

θ Angle of rotation / Angular displacement [rad]

Θ Excitation amplitude [m]

$\dot{\theta}$ Angular velocity [rad/s]

$\ddot{\theta}$ Angular acceleration [rad/s^2]

X Ratio [-]

ζ Damping ratio [-] *or* Percent of critical damping [%]

Chapter 1

Introduction

The research topic of this master thesis is investigation of torsional vibration reduction and fatigue in slow rotating vessel drive trains. The next section will aim at explaining the motivation behind such analyzes, and why it is a timely issue in the shipping industry. Thereafter follows the research objectives and scope of the thesis. Chapter 1 will be concluded by presenting the structure of this report.

1.1 Motivation

The environmental climate changes are one of the world's biggest challenges. Measures to reduce emissions are therefore considered pivotal in future technological development. A consequence has in recent years been the emergence of strict emission regulations, where both national and international agencies pass through new regulations and standards which aim to reduce the impact from human activities on the environment. One example related to marine activities is the Energy Efficiency Design Index (EEDI), launched by the International Maritime Organization (IMO) in 2011. This index is defined as the environmental impact from shipping in terms of carbon dioxide emissions, divided by the transportation work [39]. Regulation 21 in

Chapter 4 of MARPOL Annex VI defines a *Required EEDI*, which is the regulatory limit for this index, determined based on ship type and size [40].

To obtain the required EEDI index and meet the various emission regulations, shipowners have tended to install smaller main engines with reduced power [40]. Furthermore, they tend to operate at lower speeds, called *slow steaming* [28]. It should also be mentioned that the aim of lowered fuel consumption is an incentive for these changes. The result has been a new type of vessels called *eco-ships*, which are operated by a slow rotating direct-drive 2-stroke engine [7]. With these comprehensive adjustments follows consequences that should be addressed and evaluated. This is what happened when the Marine Environment Protection Committee (MEPC) raised concern towards inadequate manoeuvrability in extreme weathers for underpowered ships. A consortium representing the main stakeholders in the maritime industry was put together, aiming at developing new guidelines for the required minimum propulsion power and steering performance to maintain manoeuvrability in adverse conditions [9]. The consortium ended their work in year 2016, and the project is known under the name SHOPERA - the Energy Efficient Safe Ship Operation project.

Poorer manoeuvrability is not the only consequence of reducing the installed engine power. On one side we have the mentioned positive effects of reduced hazardous emissions, including CO_2, and lower fuel consumption. On the contrary, reduced power results in a longer operating time within the engine's range of critical speeds. This range is called the *barred speed range* (BSR), and operation within this window is associated with resonance [7]. Since the BSR traditionally is located at low rpms [54], an engine with reduced power will have problems with passing through it quickly enough, resulting in vibrations.

The torsional vibrations are of special interest for marine propulsion systems as they contain multiple rotating parts. These vibrations can be explained as a twisting motion of a rotor about its own axis of rotation [15]. The rotating propeller, the crank shaft of the engine and the propulsion, and intermediate shaft are examples of components that are affected. In other

words, the drive train is vulnerable towards torsional vibrations, which again will be the focus of this thesis.

Damping is introduced to cope with vibrations and suppress the excitations that are caused. As a consequence, the drive train of a vessel contains several components that act as dampers. The propeller determines the essential part of the mass moment of inertia and subsequently the system damping, called *hydrodynamic damping* [31]. Other examples of measures are individual torsional vibrations dampers and damping through the shafts and inertias.

1.2 Research Objectives

This master thesis will aim at developing a general procedure to evaluate the increased torsional vibrations in eco-ships, and eventually recommend damping measures. The objectives are more specifically to perform dynamic analysis of an eco-ship selected as case study, to evaluate fatigue and thereafter to search for methods of vibration reduction. To achieve these goals, the following steps must be followed:

(1) Create a mathematical formulation of a state-of-the-art slow rotating propulsion system on board an eco-ship

(2) Model the drive train by use of computer software(s)

(3) Verify the software model(s) by use of empirical data from DNV GL

(4) Determine system characteristics and identify critical components and external excitations through free and forced vibration analyzes

(5) Perform post-processing by evaluating torque amplitudes, torsional stress and fatigue life

(6) Test and evaluate torsional vibration reduction measures based on obtained results from point (4)

1.3 Scope of the Thesis

The applied research approach will be presented in relation to, and in the same order as, the objectives above. A selected case study, meaning a propulsion system, will be modelled mathematically in terms of the *lumped mass modelling method*. Damping is further introduced by the *dynamic magnifier model*. Since the focus is on torsional vibrations, modelling only one degree of freedom in each node is sufficient, namely rotation about the shaft. Utilized softwares for computer modelling are Nauticus Machinery - Torsional Vibration and Simpack Multi-Body Simulation Software, where the first is developed and owned by DNV GL. Verification will be performed through comparison to analyzes executed by DNV GL, who in turn have validated their results based on physical drive train measurements. System characteristics will thereafter be determined through vibration studies divided into two categories, 'free' and 'forced'. Traditional vibration theory is the applied methodology in this process. Post-processing is the next step, focusing on investigation of angular displacements, torsional stress and short term fatigue damage. The applied methods related to fatigue evaluation are *rain flow cycle counting* (RFC), the *Palmgren-Miner hypothesis* and the MATLAB toolbox WAFO. Vibration reduction measures will lastly be tested through a sensitivity analysis of stiffness and damping magnitudes.

The investigated propulsion system, from now on referred to as 'the eco-ship', limits the scope of this research. It belongs to an eco-ship owned by one of DNV GL's customers. Torsional vibration behavior will consequently be investigated for direct-drive arrangements exclusively. The power source is further a 2-stroke slow rotating diesel engine, and the propeller is fixed pitch. During executed analyzes in this master thesis, the design of these main components will be more or less untouched. This includes a fixed barred speed range as one example, excluding verification of its limits. Instead, the focus will be on modifications of the propulsion shaft and system design, leaving out inertia characteristics. Even though a specific case study is investigated, the procedure can be transferred to other propulsion systems as well.

1.4 Structure of the Report

This report consists of three parts, divided in nine chapters. They are in brief; background information, executed analyzes and lastly conclusions.

The first part contains the chapters '1 Introduction', '2 Background' and '3 Methodology', setting the stage for the research studies in the second part. Chapter 1 presents the research motivation, the objectives and the approach and limitations of the work. Chapter 2 proceeds with background knowledge including terminology and state-of-the-art for torsional vibrations. Both modelling methodology, theory related to free and forced vibration analyzes, and post-processing theory will be given in Chapter 3. This chapter is concluded by case study specifics, namely the characteristics of the investigated propulsion system in this master thesis.

The second part of the report, chapters 4 to 8, exhibits the performed research studies. Chapter 4, 'Modelling', takes care of software modelling in Nauticus Machinery and Simpack. Both system dynamics and applied external excitations are described. The next chapter, 'Free Vibration Analysis', identifies natural frequencies and mode shapes. They are verified by empirical data from DNV GL. Chapter 6, 'Forced Vibration Analysis' evaluates critical speeds both by use of Campbell diagrams and by plotting power spectral density. Forced vibration analyzes are performed in both softwares, where the main result is identification of vulnerable shaft segments. Section '7.3 Discussion' summarizes the critical speeds and critical shafts which will be focused on in the next two chapters. Chapter 7, 'Short Term Fatigue Analysis', presents calculated fatigue damage through two different case studies. The last chapter in this part of the report, '8 Vibration Reduction', focuses on evaluation and testing of vibration reduction measures. Both a sensitivity analysis and the significance of operational profiles are presented.

Chapter 9, 'Conclusions', forms the third and last part of the report. These pages present concluding remarks in addition to recommendations for further work.

Chapter 2

Background

The aim of the following chapter is providing the reader with information viewed necessary for further understanding. Some crucial terms and concepts will be presented and explained in section 2.1. These definitions will be useful background information for the literature study on torsional vibrations that follows in the second section. The content in the literature review is a continuation of the state-of-the-art study from the associated project thesis 'Dynamic Analysis and Modelling of Slow Rotating Propulsion System' [44].

2.1 Terminology

Drive Train of a Vessel

The drive train of a vessel is a group of components that together deliver thrust to the ship. It consists in the simplest form of an engine and its crank shaft, the reduction gears, an intermediate, or drive shaft, flexible couplings and the propeller shaft with the propeller [41].

Maximum Continuous Rating

The *maximum continuous rating* (MCR) of an engine is the maximum con-

tinuous rated power output as specified in the component's technical file and on its nameplate [3].

Classification of Vibrations

- ***Free:*** Vibrations that occur due to an initial disturbance of the system. No dynamic torque or other external forces are applied [15]. Free vibration analyzes can further be categorized as undamped or damped [49]. The first approach can be utilized to obtain system parameters such as natural frequencies, and the second to find damping ratio as an example.

- ***Forced:*** Occurs when an external dynamic force (for example a torque) is applied to the system, forcing it to vibrate. The oscillations that arise in a diesel engine is an example of harmonic forced vibrations [43]. Analysis under external excitations can reveal the critical components of the system, in addition to addressing hazardous operating speeds.

Torsional Vibrations

Torsional vibration is defined as the motion when a rigid body oscillates about a specific reference axis [43]. The body displacement is in this case angular, not translational. In such torsional vibrating systems, the restoring moment may be caused by introduced elasticity or external disturbances as some examples.

A drive train of a vessel is exposed to a constant turning moment that transmits power from the engine to the propeller. In addition, the system is affected by dynamic torques set up by the propeller and the inertia forces of the crank mechanism of each engine cylinder [41]. Another contribution to the dynamic torques is the time varying gas forces from the piston. They are caused due to the gas pressure of the engine acting through the connecting rod mechanism with varying torque on each crank throw [52]. Summarized; torsional vibrations emerge in a vessel drive train due to these contributing forces.

Natural Frequency

The frequency that a system oscillates at on its own after an initial disturbance (free vibrations), is called the system's *natural frequency*. A vibratory system with n degrees of freedom is found to have n natural frequencies in general [43].

Resonance

If the frequency of an external force coincides with one of the system's natural frequencies, the phenomenon called *resonance* takes place. This condition is recognized by dangerously large oscillations, with the undesired potential result of system failure [43].

Barred Speed Range

The *barred speed range* (BSR) is defined as the engine speed range that can cause harmful torsional vibrations in a drive train [3]. Continuous operation within this range of critical speeds should therefore be avoided to avert potential damage in the propulsion shaft. As a consequence, it is common that a fast passage through the BSR is required in ship rules and guidelines, for example defined by class societies. 'Fast' is in this context normally specified as within seconds [53].

Simulation Domains [16]

- ***Time domain:*** Amplitudes vary with time.
- ***Frequency domain:*** Amplitudes are series of sine and cosine waves where its magnitude vary with frequency.

Fatigue

Fatigue damage is material failure initiated by repetitive stress fluctuations [3]. These loads are generally not large enough to cause material yielding, instead it is their relatively high stress amplitudes applied over a certain number of cycles that cause this type of failure. In other words, to evaluate fatigue life one need to study stress amplitudes and cycles over time, not

peak values.

2.2 State-of-the-Art for Torsional Vibrations

Fuel saving measures and stricter emission regulations have led to the new designs of ultra-long stroke engines, now commonly used in shipping [29]. They are able to generate more power than the traditional designs at low revolutions. However, problem arises when these engines fail to pass quickly enough through the barred speed range, resulting in torsional vibrations. Before studying and evaluating this field, current methods and research should be addressed through a literature review.

The next pages contain a state-of-the-art literature study on the topic of concern. Firstly, how can we model the hydrodynamic damping for modern propeller designs? Recommended changes to the traditional propeller damping models will be presented. Secondly, a quicker passage through the barred speed range of the engine implies reduced torsional vibrations. How to achieve a reduced passage time will be covered. Lastly, an introduction to general damping measures will be presented (including torsional vibration dampers and magnetic bearings), followed by a brief overview of current torsional vibration regulations and standards. Note that not all of the presented research will be accounted for in this master thesis due to the limitations associated with its scope.

2.2.1 Modern Propeller Designs and Torsional Vibration Calculations

High fuel prices and regulations on emissions from combustion are motivators for fuel reduction. In recent years, propeller designs have therefore been optimized to save fuel. The applied changes include larger propeller diameters, more cambered propeller profiles, as well as larger skew and lower blade area ratios [14][31]. These 'new' designs challenge the traditional propeller

damping models. The Torsional Vibration Symposium-conference in 2014 and the International Conference on Ocean, Offshore and Arctic Engineering (OMAE) of 2017, have examined the issue. A summary of their studies and findings will be presented.

Dahler et al. performed a case study with the purpose of comparing models for steady-state torsional vibration calculations with sea trial measurements [14]. A standard oil-tanker with a slow speed main engine and a fuel efficient fixed pitch propeller (FPP) design was the selected subject vessel. The torsional stress responses were calculated for the intermediate shaft for normal firing of the engine. Three methodologies were tested; the Archer methodology, the constant magnifier model (constant percent of critical damping) and the newly developed *variable percent of critical damping-model*.

Comparing calculated torsional behavior under forced vibrations with the measured levels at sea trial, the Archer model yielded a significantly overestimated response at resonance. The constant magnifier methodology was proven non-conservative at resonance speed. Lastly, the revised magnifier model (first proposed by MAN Diesel & Turbo) showed a much better compliance with the measurements. This approach utilizes a percent of critical damping which varies with the rpm, given in percentage of the maximum continuous rating (MCR). The conclusion from these findings is that traditional TVC-models (e.g. the Archer and Magnifier approach) need to be revised and updated, such as the revised method from MAN, to handle modern propeller designs.

The variable percent of critical damping-model gave the most accurate results among the three tested methods in the study above. Krüger and Abels presented a different approach to consider modern screw propeller designs, namely an extension of Schwanecke's and Grim's method [31]. The latter methodology was developed between 1970 and 1980 based on the theory of oscillating airfoils. It aims at computing the hydrodynamic damping of the propeller. However, without any further adjustments it is apparently outdated with regards to modern designs.

Abels and Krüger suggest two major corrections to cope with the modern screw propellers. Firstly, the propeller skew must be taken into consideration. Secondly, the modern propeller designs are more complex than the traditional ones, making a simplification as an airfoil incorrect. Corrections must accordingly be done to include the inflow conditions, where the angle of attack is reduced due to a 3D-flow around the propeller blade. A consequence of the latter, is a reduced effective profile camber. This must also be accounted for in an updated lifting line model.

The above corrections have been applied and tested on a modern controllable pitch propeller (CPP). Where Schwanecke's and Grim's method predicts the hydrodynamic damping and added mass moment if inertia (MOI) for off-design pitch conditions wrongly, the proposed method by Abels and Krüger solves this issue.

The presented studies recommend approaches on how to adjust the traditional hydrodynamic damping models to cope with modern propeller designs. For an FPP, the variable percent of critical damping-model gave most accurate results. Since the relevant research is limited to fixed pitch propellers, only this damping method will be taken into consideration in further work.

2.2.2 Quick Passage Through the Barred Speed Range

Operation within the barred speed range of an engine (see definition in section 2.1) should be avoided to reduce torsional vibrations. Under low loads, the fuel efficient ships tend to have difficulties with accelerating the engine rpm as they lack sufficient torque to do so. The result is relatively long operations within the barred speed range. It takes up to several minutes whereas it should take seconds [53]. This concern demands new measures. Reducing the operation window within the barred speed range, which implies a decrease in torsional vibrations, is desirable.

The barred speed range was until recently placed in the lower end of the rpm range, such that the engine generally had enough power available to pass

fast through it [54]. However, the newer engine designs (motivated by fuel economy and regulations such as the EEDI) tend to have a BSR moved closer to the specified MCR. There is subsequently a trade-off between improving the EEDI by derating the engine, and the negative effect of a slower passage through the BSR which also appears when derating. As a reference, *derating* is achieving a smaller deviation between optimal and operational speed of an engine [51].

To pass the BSR quickly, the engine manufacturer MAN Diesel & Turbo recommends in a market update note from 2015 to increase the propeller light running margin (LRM) [53]. This margin relates the engine speed difference between the service propeller curve and the propeller curve for trial condition at continuous service rating-power to the speed at MCR [57]. Increasing LRM will again increase the power margin within the barred speed range so that the time required for passing the critical range is reduced. However, according to Kim et al. this is not wise as the propeller- and fuel efficiency will decrease [29]. If the latter efficiency is reduced, one miss the initial advantage of utilizing a fuel efficient engine.

A second approach from MAN Diesel & Turbo is the so-called *dynamic limiter functionality* (DLF). This is an engine control system upgrade which increases the torque that the engine can deliver long enough to pass the barred speed range. Further explained, it aims at improving the engine's acceleration capability at low loads by injecting more fuel into the cylinders momentarily [54].

Kim et al. have examined the application of the DLF-approach in a recent article from 2017 [29]. Their results are in line with the specifications from MAN, the time for passing the BSR was significantly reduced. By applying the dynamic limiter function one can therefore reduce the effect from torsional vibrations on the shafting system; DLF accomplishes less time spent with a shaft speed near resonance.

2.2.3 Damping Measures

Utilizing ultra-long stroke engines with reduced power has increased the usage of torsional vibration dampers (TVD) [29]. Details about a steel spring type damper follows in the next subsection. The torsional vibrations can be controlled by tuning the dampers and by introducing tuning and turning wheels on each side of the engine. In 2016 Kim et al. proposed a method to effectively control the torsional vibration stress in a drive train [30]. This could be obtained by adjusting the system parameters according to the optimum damper design theory by Wilson [55] and Bicera [5] for viscous-spring dampers.

One of the most general measures to reduce the influence from torsional vibrations, is selecting the shafting material carefully. As an example, changing from forged steel to alloy steel can in the best case increase the shaft fatigue life to a level where a torsional vibration damper is not necessary anymore. Kim et al. recently performed this experiment by comparing forged steel SF600 to an alloy material [29]. The replacement is however costly, increasing the expenses with as much as about 30%. In addition, they confirmed that designing the fillet part of the shaft with multi radius shape can increase the allowable passing time in the BSR even further.

We can learn a lot by studying how torsional vibrations are avoided in other industries. The offshore wind turbine, and vehicle industry, in addition to oilwell drilling, are three examples that concern rotating machinery. Common measures are damping through control systems or utilizing individual damping components. Examples of research on torsional vibration mitigation in the mentioned fields will be presented beneath.

Zhao proposes in a paper a new method of wave propagation control in oilwell drilling systems [59]. It is accomplished through decomposing the torsional wave in the drilling string into two independent wave forms travelling in opposite directions based on the d'Alembert solution. A speed control is then proposed to reduce the torsional vibrations by reacting to each wave component differently. By implementing this speed control the most com-

mon form of torsional vibrations in drilling, called stick-slip, is prevented. Another example comes from the vehicle industry; by utilizing the material magnetorheological elastomer for an adaptive tuned vibration absorber, the torsional vibrations during transient stage are reduced [45].

The last study is related to offshore wind turbines exposed to external forces such as wind, wave motions and earthquakes. Pitch regulated turbine blades experience torsional vibrations, which is a matter of concern. Zhang et al. recommend to install a novel electromagnetic torsional viscous damper inside the blades to suppress the torsional vibrations in the blade [58].

Steel spring type torsional vibration dampers

A torsional vibration damper is implemented in the design of a propulsion system to reduce torsional vibrations. It protects the shaft segments of a drive line including both crank, intermediate, and propeller shafts. Its working principle and specifications will be explained using a tuned TVD from the Austrian manufacturer Geislinger as an example [22]. Based on the scope of this master thesis, the focus will be on application in 2-stroke engine arrangements.

The Geislinger torsional vibration damper is divided into two sections, one primary (outer) and one secondary (inner). The steel spring packs, with desired stiffnesses, are arranged in between these parts (see illustration 2.1). Chambers where hydraulic oil is added, are created by the springs, intermediate pieces and the secondary section.

According to the manufacturer's recommendations, a TVD should be mounted to the free end of the 2-stroke engine crank shaft. It is the innerstar (see Figure 2.1) that is actually bolted onto the shaft. The inertia of this part is generally low, whereas the outer one is designed with a large magnitude. If the exterior section vibrates relative to the interior section, the springs will bend and pressurized oil will flow from chamber A to B through designed damping gaps (see illustration 2.1). The result is reduced torsional vibrations since the relative motion between the two parts is decreased when this

occurs. The term *tuning* of TVDs is in practice to vary the size of the damping ports and thereby create different rates of torsional damping, which in general are high.

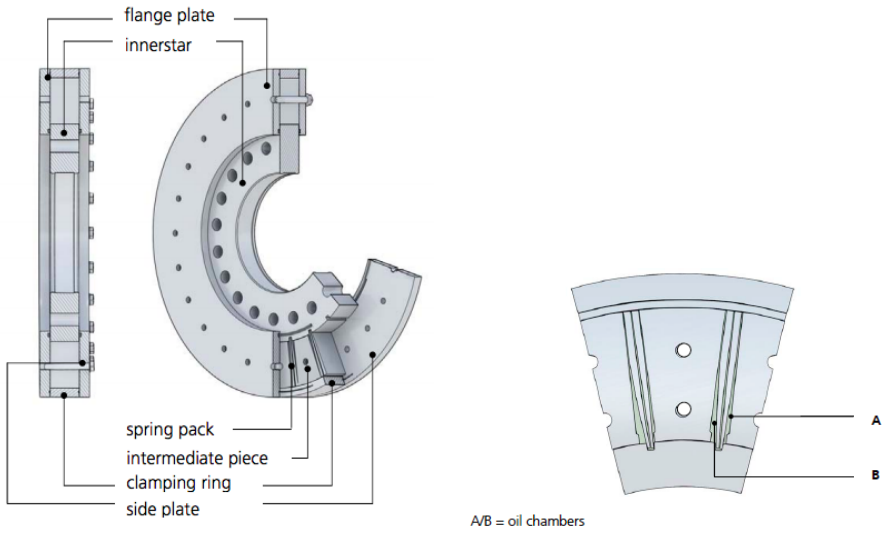

Figure 2.1: Design of a Geislinger damper [22]

The Geislinger TVD has a designation code on the format of 'D 220 /AB'. 'D' stands for damper,'220' for the outer diameter of the biggest single damper part in cm, and lastly 'AB' for its project designation which could be replaced by a number when a damper has been ordered. In the illustration above, 220 cm would be the diameter of the clamping ring.

When selecting a damper for a 2-stroke engine, it is recommended to choose an outer damper inertia equal to 5-25% of the total engine inertia. Furthermore, the damper tuning is performed in line with torsional vibration calculations where stress limits defined by class societies are considered. In 2-stroke propulsion system designs, both counterweights and additional masses can be incorporated into the damper.

Magnetic bearings

A *magnetic bearing* is a free of contact bearing which uses magnetic levitation to support a load [33]. In the case of a vessel drive train, this load is the rotating propulsion shaft. The advantage related to the absence of physical contact between rotor and support is no friction and thereby no mechanical wear, which again removes the need for lubrication. As a result, both the maintenance and operational costs are reduced. For this research project however, the most interesting aspect of this type of bearing is the possibility of vibration control and vibration isolation.

There are two main types of magnetic bearings, the *passive* type and the *active* magnetic bearing (AMB). The passive bearings utilize permanent magnets and as a consequence they have problems with stationary instability. On the contrary, the active magnetic bearing consists of electromagnets with continues power supply and an active control system to ensure a stable magnetic force. Maintaining a stable rotor position is crucial for vibration reduction, and the AMB type is therefore favorable for use in a vessel drive train.

Figure 2.2 presents a schematic of a one degree of freedom active magnetic bearing. An explanation of the closed loop system follows. The rotating shaft is held in position by the magnetic forces from the electromagnets surrounding it. These magnets are fed by the power amplifier which outputs a control current and thereby induces a magnetic field. The gap sensor measures the rotor displacement from the reference position, and sends signals to the controller which in turn controls the power amplifier.

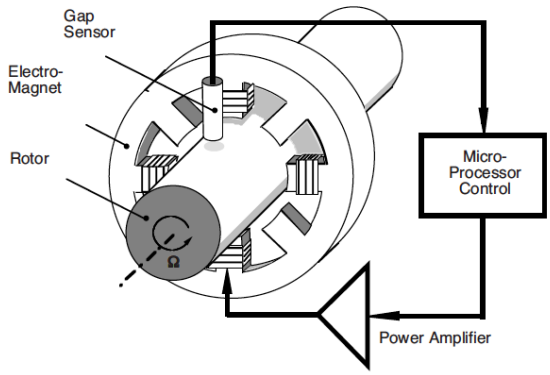

Figure 2.2: Schematic of an active magnetic bearing [33]

The stiffness and damping of the rotor can be adjusted during operation by the controller. It is specifically this option that makes the AMB relevant for vibration reduction.

In the industry at present day, the active magnetic bearing is used to reduce translational vibrations. Wu et al. tested the application of an AMB in a high speed rotor in 2017 [42]. Results revealed that a passage of the first bending critical speed was achieved, and that vibrations were suppressed.

During studies of the literature, no relevant research connecting the magnetic bearing and torsional vibrations were identified. It is however an interesting and relatively 'new' technology with potential, which is why it is presented. Further work could include investigation of active magnetic bearings to reduce angular displacements.

2.2.4 Current Standards and Regulations

The International Association Classification Society (IACS) has defined multiple unified requirements (UR) which should be incorporated into the regulations and practices of all member societies. DNV GL is one of several classifications societies within this association. IACS' UR number M68 defines the limits of the barred speed range as all speeds which exceeds a

certain permissible stress amplitude (in N/mm^2) due to torsional vibrations for continuous operation [26]. The purpose of defining the BSR and requiring a quick passage through it, is thereby to avoid fatigue fracture of the power transmission shaft. With regards to this requirement, IACS proposes guidelines for design of the power transmission shaft, where UR M68 contains one fatigue limit and a reference value for yield stress. Furthermore, the UR number M51 states that when a BSR is required it has to be demonstrated and recorded that the passage time actually is within the approved documentation (if it exists) [27]. This holds for both acceleration and deceleration, in addition to passages in reverse rotational direction.

A unified requirement is only a minimum requirement from IACS, the classification societies are free to implement more stringent rules if desired [25]. DNV GL has in association to IACS UR M68 introduced their own guidelines for evaluating the fatigue life of power transmission shafts. Through their class guidelines DNVGL-CG-0038 [17], they introduce a more detailed calculation than that of IACS, containing a procedure and basic equations for verification of the load carrying capacity for shafts.

A vessel with class needs to meet the associated class society's rules and standards. DNV GL is chosen as an example of a class society since this master thesis is written in collaboration with them. Part 4 of their rules for classification is about rotating machinery, where Chapter 2 to 5 contain the relevant rules with regards to torsional vibrations. Part 4 Chapter 3 Section 1 is as an example about the requirements for torsional vibration dampers on crank shafts and as an auxiliary component [21]. The dampers need to be type or class approved depending on their suppliers. Chapter 2 Section 2 contains the more general rules for torsional vibrations. Torsional vibration calculations are required for both free, forced, time domain and frequency domain vibrations. If any of the results are close to the defined acceptance limit, additional vibration measurements may be necessary.

The last presented example of standards comes from the International Organization of Standardization (ISO). They have several codes related to torsional vibrations. Some examples are the ISO 3046-5:2001 concerning

torsional vibrations in internal combustion engines [38], and the VDI 2039 about calculation, measurements and reduction of torsional vibrations in drive lines [37]. The latter is published by the Association of German Engineers, but it is approved by ISO as an acceptable torsional vibration standard.

Chapter 3

Methodology

Chapter 3 presents the applied methodology and vibration theory. Modelling method involves the selected mathematical approach, in addition to the utilized softwares. This is followed by a presentation of torsional vibration analysis and its sub categories. The theory is further divided into free and forced vibration studies with their associated subjects. Post-processing theory follows afterwards, focusing on torsional stress and fatigue. A presentation of the investigated eco-ship will be given at last, introducing both its design and characteristics.

3.1 Modelling Methodology

A vessel drive train will be modelled as a lumped mass system in this research. Theory regarding the selected modelling approach is presented in the first subsection beneath, including specifics about the elements used to model the propulsion unit. The torsional behavior of a lumped-mass system can be analyzed by hand calculations or by use of computer software. The latter is much faster and more efficient for complex structures, which is why this is the applied approach in the industry. In addition, it is easier to implement changes to a model when utilizing a computer software, and

thereafter simply run the simulation again. Another advantage is the enabling of easy and fast sharing of models and simulation results, which is valuable for company-customer relations.

Two different softwares will been utilized for modelling and to perform dynamic analysis of the investigated propulsion system. They will be introduced shortly in this section, whereas details are described related to the actual modelling in Chapter 4 of this report. *Nauticus Machinery - Torsional Vibration*, a software developed by DNV GL, is used in the first attempt of drive train modelling. The propulsion system is thereafter constructed in *Simpack Multi-Body Simulation Software*. This computer tool uses co-simulation between Simpack and Simulink (MATLAB) to model the applied input torque on the power transmission line. Where Simpack offers time domain simulation, Nauticus Machinery is based on frequency domain analysis.

3.1.1 Torsional Lumped Mass Systems

Systems with a finite number of degrees of freedom (DOF) are called discrete or lumped parameter systems [43]. They typically consists of the following components: lumped masses, springs and dampers, where the latter two are assumed massless [41]. To describe the characteristics of such as system, one can use a beam as an example. The mass of a beam is assumed to be concentrated at specific nodes in a lumped mass system, instead of being evenly distributed over its whole length which is the case for continuous systems on the contrary. These nodes divide the beam into different elements. Figure 3.1 states the same principle.

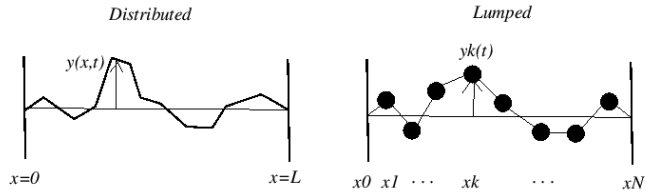

Figure 3.1: Lumped versus distributed mass [6]

It is challenging to simplify a complex physical system into a mathematical representation of it. In this process one need to weigh modelling accuracy against the simplicity of the equations and corresponding computation time. The available analytical methods for continuous systems are limited to a small selection of components [43]. This applies to elements such as uniform beams, slender rods and thin plates. As a consequence, complicated physical systems are often approximated as discrete. Rotating machinery is not an exception, there are in fact long traditions within engineering design departments (including DNV GL) to model them as lumped mass systems [41]. Additionally, a more detailed model such as a finite element method-model (FEM) is not required for typical analysis when there are no problems with boundary conditions [34]. Furthermore, since the focus of this master thesis is on torsional displacements and thereby only modelling one degree of freedom, the lumped mass approach is suitable. The discrete modelling method was selected based on the statements above.

Figure 3.2 depicts a torsional lumped mass system in its simplest form, three discs mounted on a shaft. The masses are assumed rigid with the consequence of excluding the inertias' internal dynamics. These rotating discs each have their own mass moment of inertia J_i, whereas the shaft segments are modelled as rotational springs and dampers with stiffness and damping constants equal to K_i and C_i. External forces are modelled as applied torques T_i, causing the angles θ_i which are the system's degrees of freedom. Vibration theory for torsional multi degree of freedom systems, with and without applied excitations, is covered in section 3.3 and 3.4.

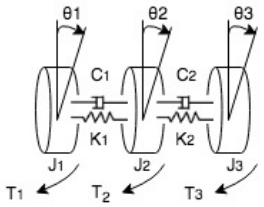

Figure 3.2: Example of a torsional lumped mass system - Discs mounted on a shaft

The drive train of a ship falls under the category *rotating machinery*, a system where the components mainly perform rotating motions [41]. This classification is justified by the system's large shaft stiffnesses and diameters, in addition to its large mass moments of inertia. A propeller can have a mass MOI of sixty thousand kgm^2 as an example, and a propulsion shaft diameter can be one meter. With regards to the dominant rotational motion, a vessel drive train shares resemblance with a torsional lumped mass system. One can therefore model a propulsion system as depicted in the figure above. Additionally, relatively stiff and large shafts defend how the lumped mass modelling approach will assume them as rigid elements instead of flexible.

It is usually sufficient to model a power transmission system with only one DOF in each node [1]. In this thesis it will be the angular displacement about the shaft. Following the same modelling procedure as in Figure 3.2, all rotating masses in the drive train will be represented by inertia elements (discs) described by polar MOI. They are further connected by massless springs and dampers which represent elasticity. The shafts are described in terms of rotational stiffness and *relative* damping, whereas masses contribute with *absolute* damping. Common sources of the latter are gas forces in the diesel engine cylinders and hydrodynamic damping from the propeller [13].

Figure 3.3 shows how the water moved by the propeller can be modelled as a damper element. Parts of the applied engine power will disappear 'into' the water on the right end of the drive train. This specific modelling approach similarly represents aerodynamic drag on the blades of a wind turbine [24].

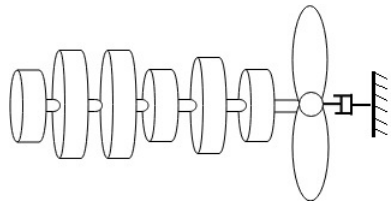

Figure 3.3: Modelling of hydrodynamic damping

Analysis of torsional behavior is most often carried out for the complete drive train instead of individual parts separately [15]. It is advantageous to deal with the system as a whole, because torsional vibrations propagate through the shaft and interfere with the components attached to it. Combining the characteristics mentioned above, a lumped mass model will transform the physical propulsion system into a simplified mathematical representation that can be utilized to study its torsional behavior.

3.1.2 Nauticus Torsional Vibration

DNV GL has developed a series of software modules named Nauticus Machinery. The computer software consists of seven modules with the purpose of handling marine propulsion design and analysis [18]. One of these modules focuses on torsional vibrations, and is consequently a well fitted software for drive train analysis in this thesis. NTNU has an agreement with DNV GL that includes a license key for the software tool Nauticus Torsional Vibration.

According to DNV GL, the torsional vibration module is an 'easy, reliable and effective software for shafting systems' [19]. The tool can identify critical components by analyzing the torsional vibration levels in the system, utilizing the latest available technology. It comprises a graphical user interface for modelling lumped mass systems, in addition to a property grid for input of component parameters such as mass elastic data and acceptance criteria. Moreover, excitation data for the relevant engine can be imported into the software to ensure a reasonable imitation of the physical propulsion

system.

Nauticus Torsional Vibration will in this master thesis be utilized to model the lumped mass version of a vessel drive train. Propulsion system parameters, such as mass elastic data, will be the software input that makes the model of the propulsion unit resemble the physical version of it. Simulations are performed in frequency domain and the equations of motion are solved analytically, giving a fast computation time. Available results from free vibration analyzes are eigenvalues and eigenvectors, and from forced, torsional stress and torque amplitudes as two examples.

3.1.3 Simpack Multi-Body Simulation Software

Simpack is a multi-body simulation (MBS) software, enabling complex multi degree of freedom modelling. The computer tool considers bodies as rigid, connected by complex force elements. According to the software supplier, finite element softwares generally require elastic bodies and do not support the same complicated element interaction as Simpack does [2]. As described in section 3.1.1, the selected modelling approach is the lumped mass method. Simpack is consequently a well fitted modelling environment for a torsional system, due to the fact that lumped masses are categorized as rigid and not elastic. Additionally, the physical shaft stiffness and damping forces can be modelled accurately by the complex force elements and joints in Simpack.

Another advantage with Simpack, is its simple user interface for evaluation of torsional system behavior in time domain. A drawback with introducing this domain, is however relatively long computation time compared to Nauticus Machinery. The software creates the model's equations of motion, and thereafter provides the solutions at a selected sampling rate. Eigenvalue analysis finds natural frequencies and mode shapes, whereas time integration provides torque amplitudes, displacements and modal energy distribution as a function of time. By use of the Simpack post-processing environment, one can study the mentioned results through a user-friendly interface.

The SIMAT interface (Co-simulation with Simulink)

Simpack enables co-simulation with Simulink (MATLAB) through an interface named *SIMAT* [10]. The model of the propulsion system will be constructed in Simpack, whereas the control strategy is defined in Simulink. Results are exchanged simultaneously at a given time step between the two softwares. It is the TCP/IP protocol, commonly used for data communication in computer networks, that facilitates the necessary data transferring.

3.2 Torsional Vibration Analysis

Analysis of torsional vibrations can be divided into two main categories, *free* and *forced* vibration studies. The distinction between them is that the system vibrates on its own under free vibrations, whereas the second term involves oscillations due to applied external torques. In this master thesis, both vibration methodology and the performed analyzes related to a case study, will be separated in the same manner. An explanation of the main tasks within each block follows in the next paragraphs.

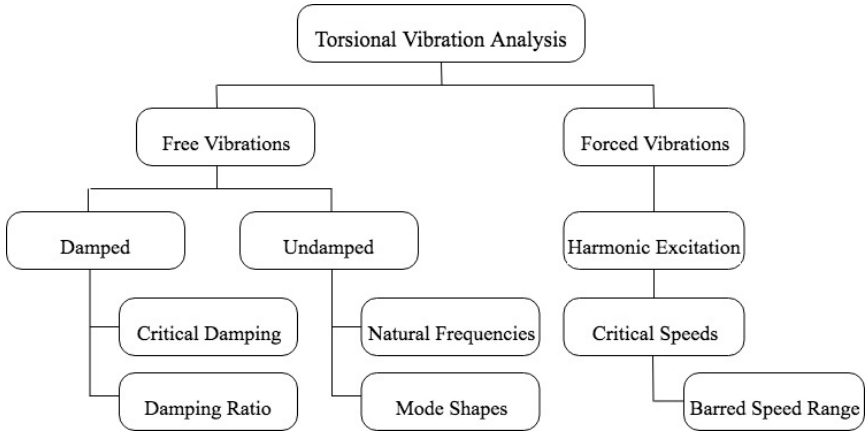

Figure 3.4: Decomposition of torsional vibration analysis

Illustration 3.4 shows an example of further decomposition. The analysis-

tree contains the subjects that will be studied in this research. Free and forced vibration analyzes include however more than the depicted headings, but they have been left out since they are outside the scope.

During free vibrations, system behavior can either be analyzed with or without damping. The undamped case reveals important system characteristics in terms of natural frequencies and mode shapes. Both of these are essential with respect to damage avoidance. Natural frequencies can be utilized to detect potentially dangerous excitations, whereas mode shapes identify critical parts of the system with regards to shaft fractures. Accounting for system damping is the next step. These type of analyzes determine critical damping factors and calculates damping ratios. Acknowledging the form or shapes of the system's damped oscillations is valuable to eventually improve them. The theoretically ideal case is when damping is equal to the critical one, providing the fastest decreasing vibration amplitude possible.

Free vibration analyzes will be performed analytically in this master thesis. A software model of the eco-ship's drive train will be the basis in these studies. However as a reference, the experimental procedure for finding the equivalent parameters is called *modal testing* [43]. The physical machine or structure is in this case excited by a known input force, where the system behavior is transfered into an electrical signal. Before the analyzer (a suitable software) can process the collected data and perform the free vibration analysis, an amplifier must convert the signal into a readable input format.

The second main branch is analysis of forced vibrations. There exist different forms of external excitations, but the focus of the relevant research is harmonic torques. The assumption is based on the fact that propulsion systems on board ships traditionally are driven by reciprocating engines. Internal combustion engines such as diesel engines fall under this category due to its repetitive up-and-down motion of the piston. This type of movement can be simplified as a sinusoidal harmonic function of time [41]. Additionally, the excitation of a vessel propeller is also best represented in the same manner.

Under forced oscillations one can detect the excitations that potentially can

lead to resonance. Frequencies where external torques overlap with a natural frequency are so called *critical speeds*. By averting long operations at these conditions, severe damages from resonance can more or less be avoided. Furthermore, when a vessel drive train is powered by a diesel engine, detection of the barred speed range (BSR) becomes relevant. This is the engine speed interval which is associated with notably large vibration amplitudes. Referring to section 2.2.4, the ranges of this characteristic is verified by evaluating stress levels at different operational frequencies. Since engine characteristics are assumed fixed, the actual verification process is outside the scope of this research.

3.3 Free Vibration Analysis

Free vibrations are oscillations initiated by forces inherent in the system itself, meaning that all external forces are absent [49]. Under free vibrations the system vibrates at a rate equal to one or more of its natural frequencies. These rotational speeds are determined based on the dynamical properties of the system, including mass and elastic characteristics.

The purpose of free vibration analyzes is to identify a system's dynamic properties. Some examples are its motional behavior in terms of equations of motion (eom), its natural frequencies and mode shapes. These attributes are important to identify at an early stage of research, because they can explain the system's reaction to external excitations in the forced vibration analyzes that follow. Furthermore, free vibration analysis identifies the critical states and vulnerable components of the system. Vibration mitigation measures should aim at reducing the stress levels at exactly these parts of the drive train.

This section contains theory on free vibrational motion of multi-body systems. Firstly, the general eom for a damped torsional lumped mass system will be portrayed. Its undamped solutions are called eigenvalues, which are the natural frequencies of the system. A system with n degrees of freedom is said to have n natural frequencies. The next subsection deals with the sys-

tem's eigenvectors, also called mode shapes. Rotation at a natural frequency gives one corresponding displacement configuration. The number of mode shapes is thereby also n. Lastly, taking damping into account again will reveal the critical damping and damping ratio of the mathematical model. These factors are important for understanding the damped behavior of the system.

3.3.1 Dynamics of Multi-Body Systems

A *multi-body system* is a collection of interconnected bodies, either rigid or deformable, where each of them may experience displacements individually [46]. Figure 3.5 illustrates how the bodies can be connected in different ways, e.g. by joints, force elements or control devices. *Dynamics* on the other hand, is the science of studying motion of particles or bodies. As the section title states, this paragraph will consequently describe the motion of multi-body systems. Its behavior will more specifically be described in terms of a mathematical formulation, namely the so called *equations of motion*.

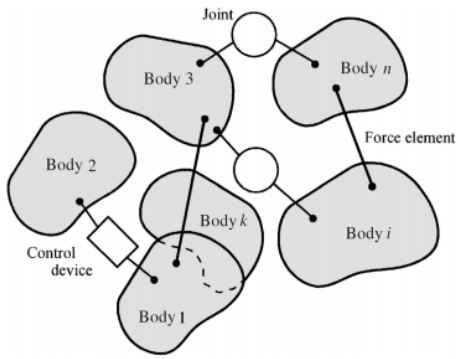

Figure 3.5: Interconnections in a multi-body system [46]

A torsional lumped mass system can be categorized as a multi-body system according to the definition above. The example in Figure 3.2 is composed of multiple rigid bodies, connected by force elements that represent rotational shaft stiffness and damping. Its equation of motion is derived from *Newton's*

second law of motion for rigid bodies, which states that the system's rate of change of momentum is equal to the sum of moments acting on it [43]. The damped lumped mass system dynamics are represented by the left hand side of Equation 3.1. As mentioned in section 3.1.1, lumped mass modelling excludes the inertias' internal dynamics. The right hand side of the eom would be the external excitations. In free vibration analysis however, all outer forces are neglected, resulting in a right hand side equal to zero. Such differential equations are called homogeneous, and its solutions are referred to as complementary functions [49].

J is the rotational mass moment of inertia matrix, followed by C and K, the rotational damping and stiffness matrices respectively. θ is the angular displacement, with angular velocity ($\dot{\theta}$) and acceleration ($\ddot{\theta}$) as its first and second derivatives. The system's number of DOF determines the amount of possible states and consequently the dimensions of the square matrices J, C and K. Going back to the example in section 3.1.1, three discs with one DOF each results in square matrices of dimension 3x3. The system's eom will thereby become three separate differential equations.

$$J\ddot{\theta} + C\dot{\theta} + K\theta = 0 \tag{3.1}$$

3.3.2 Undamped Free Vibrations

Performing analysis of undamped ($C = 0$) free vibrations, also called *modal analysis* [8], gives natural frequencies and mode shapes as result. These two concepts will firstly be introduced, followed by the procedure of how to find them mathematically by calculations. A requirement for their detection is a system in *static equilibrium*, meaning that all torques acting on the system are balanced [43]. The starting point is in both cases the free and undamped equation of motion on matrix form:

$$J\ddot{\theta} + K\theta = 0 \tag{3.2}$$

Natural frequencies

A system will oscillate at the natural frequency (ω_n) under free vibrations without external forces. Each degree of freedom has one corresponding ω_n. Since damping in moderate amounts has little influence on natural frequency, the undamped eom (C-matrix equal to zero) will be utilized to identify them [49]. Solving the undamped eom gives the *eigenvalues* of the system, namely the natural frequencies. The resulting expression, number 3.3, is the square root of rotational stiffness divided by polar moment of inertia. Appendix A.1 derives this formula. When a system is modelled mathematically with free ends (not fixed), the first natural frequency will be zero. This is called the *rigid-body mode* of vibration, characterized by no twisting of the shaft.

$$\omega_n = \sqrt{\frac{K}{J}} \tag{3.3}$$

The natural frequencies are of special interest since resonance will occur here. This well known phenomenon takes place when an external force has a frequency equal to one of the natural frequencies, resulting in severe oscillations. Identifying ω_n is in this way proven to be of importance for further dynamic analysis.

Mode shapes

Mode shapes are spatial shapes of vibration [15]. With every natural frequency follows a specific mode of vibration that visualizes motion over the length of the system under this specific rotational speed. In some points displacement may be absent, whereas others experience large movements. With regards to torsional systems, these modes of vibration are angular displacements deviant from the reference position. Referring to the rigid-body mode ($\omega_n = 0$), the corresponding mode shape is that all inertias rotate together as one single mass.

Torsional vibration amplitudes are calculated for one natural frequency at a

time and for each inertia separately. In mathematical terms, these values are the *eigenvectors* of the system's eom. Mode shapes are finally established by drawing lines between the inertia's respective vibration levels. Some may be positive and others negative depending on the defined axis system. Furthermore, the eigenvectors can be normalized by fixing one displacement to a value of one. The vibration shape is then called a *normal mode*.

A two-component rotational lumped mass system will be used as an example to visualize the theory above. One positive and one negative displacement (A2 and A1 respectively) means in this case that the two discs rotate in opposite directions, or *out of phase*. This statement is illustrated in Figure 3.6. In this example, an intermediate point on the shaft between the two discs will not experience any motion. These points are called *stationary points*, and are of interest as shaft fractures may occur if the opposing torques are high enough. The mode shapes of a system are consequently also valuable to acknowledge.

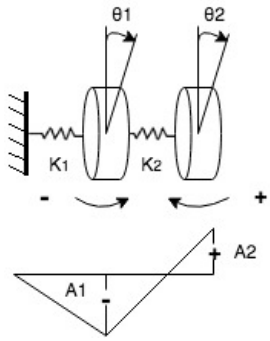

Figure 3.6: Mode shape for a two-disc torsional system

Identifying eigenvalues and eigenvectors

The rotational system in Figure 3.6 will be used to show how natural frequencies and mode shapes are calculated. Newton's balance of moments will result in two differential equations of motion, one for each degree of freedom θ_1 and θ_2. Taking into account the directions of the torques, the eom end

up as:

$$J_1\ddot{\theta}_1 + \theta_1(K_1 + K_2) - K_2\theta_2 = 0 \tag{3.4}$$

$$J_2\ddot{\theta}_2 + K_2\theta_2 - K_2\theta_1 = 0 \tag{3.5}$$

A general solution of both displacements theta 1 and theta 2, is harmonic motion of the same frequency ω. It is given as $A \cdot e^{i\omega t}$, where A is oscillation amplitude. All derivatives of this expression are further inserted into the two equations of motion. Removing the exponential part, since it cannot be equal to zero, leads to the matrix form:

$$\begin{bmatrix} -J_1\omega^2 + K_1 + K_2 & -K_2 \\ -K_2 & -J_2\omega^2 + K_2 \end{bmatrix} \begin{Bmatrix} A_1 \\ A_2 \end{Bmatrix} = \begin{Bmatrix} 0 \\ 0 \end{Bmatrix} \tag{3.6}$$

This equation is satisfied for any A_1 and A_2 as long as the determinant of the first matrix is equal to zero [49]. Omega squared is further defined as a parameter lambda (λ), which then will replace all ω^2-terms. The result is the second-degree *characteristic equation* underneath. Eventually the system's two natural frequencies ω_{n1} and ω_{n2} can be found as the square root of λ_1 and λ_2 (the eigenvalues of the system).

$$J_1J_2\lambda^2 - (J_1K_1 + J_2K_1 + J_2K_2)\lambda + K_1K_2 = 0 \tag{3.7}$$

The ratio between the two amplitudes A_1 and A_2 will be used to determine mode shapes. Either of the two equations formed by the matrices in Formula 3.6 can be selected. It is however convenient to avoid the most complex one, in this case the upper expression. The result when choosing the other is:

$$\left(\frac{A_1}{A_2}\right)_j = 1 - \frac{J_2{\omega_{nj}}^2}{K_2} = Ratio_j \tag{3.8}$$

ω_{n1}, and then ω_{n2}, will further be inserted into Equation 3.8. This gives ratios between the amplitudes, not their magnitudes which then are insignificant. By fixing either A_1 or A_2 equal to 1, the amplitude ratio is said to be 'normalized' with respect to this parameter. The corresponding mode shape is then called a normal mode symbolized as $\phi_j(\theta)$.

One example is letting A_1 be equal to $Ratio_j$. Parameter A_2 will then become 1 and is now the normalized number. The associated normal mode, or eigenvector, becomes consequently:

$$\phi_j(\theta) = \begin{Bmatrix} Ratio_j \\ 1 \end{Bmatrix} \tag{3.9}$$

By following the procedure above for both natural frequencies j, the resulting two vectors can be drawn as mode shapes similarly to Figure 3.6. If $Ratio_j$ ends up as negative, the graph in this illustration would be representative for $\phi_j(\theta)$ above.

3.3.3 Free Vibrations with Damping

The homogeneous equation of motion (Formula 3.1) is referred to as damped free vibrations. By examining this expression, the role of damping becomes more understandable.

The traditional solution to the free vibration eom is on the form $\theta(t) = e^{st}$, where s is a constant [49]. By inserting all forms of $\theta(t)$ into the homogeneous equation of motion, and knowing that e^{st} cannot be zero, the characteristic equation as a function of s becomes:

$$s^2 + \frac{C}{J}s + \frac{K}{J} = 0 \tag{3.10}$$

This second-degree equation has the two roots in Expression 3.11, leading to the general solution given by Formula 3.12. a and b are constants which can be found through evaluation of the initial conditions $\dot{\theta}(0)$ and $\ddot{\theta}(0)$.

$$s_{1,2} = -\frac{C}{2J} \pm \sqrt{\left(\frac{C}{2J}\right)^2 - \frac{K}{J}} \tag{3.11}$$

$$\theta(t) = a \cdot e^{s_1 t} + b \cdot e^{s_2 t} = e^{(-C/2J)t}(a \cdot e^{(\sqrt{(C/2J)^2 - K/J})t} + b \cdot e^{(\sqrt{(C/2J)^2 - K/J})t}) \tag{3.12}$$

The general solution where the two roots are substituted into the equation (right part of Formula 3.12), can further be used to evaluate different forms of damping. The exponential term outside the parenthesis is simply a decaying function of time and does not influence the resulting damping form. It is however the mathematical sign and value of the radical terms that determine the characteristics of damped motion.

All presented states of damping are illustrated in the next figure. *Undamped* motion, meaning damping equal to zero, is intuitively repeated and unchanged oscillations. *Overdamped* vibrations on the other hand, take place when the $(C/2J)^2$-term is larger than K/J. The exponents inside the parenthesis are in this case real numbers and no oscillations occur. When the first exponent-term is less than K/J, the free vibrations are *underdamped*. The exponents are then imaginary numbers and the parenthesis can be rewritten in terms of sine and cosine of time t. The underdamped case is thereby characterized by decaying oscillations.

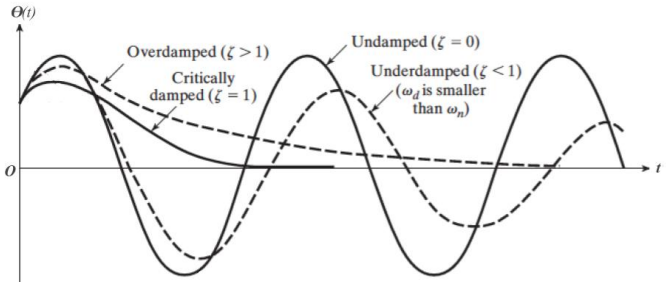

Figure 3.7: Comparison of motions with different types of damping [43]

The fourth and last damping state is called *critically damped* vibrations.

This happens when the terms inside the square roots are equal to each other, resulting in decaying vibrations on the form $e^{-(C/2J)t}(a+b)$. This is the fastest form of vibration mitigation and the associated damping constant is consequently called the *critical damping constant* symbolized as C_c. The parameter is given by Equation 3.13, derived from the initial statement saying that the radical is equal to zero.

$$C_c = 2 \cdot J \cdot \omega_n \tag{3.13}$$

All damping forms can alternatively be expressed in terms of the non-dimensional *damping ratio* ζ. It relates the actual system damping to the critical one, which is shown in the equation below. A damping ratio equivalent to one implies that the system is critically damped, whereas $\zeta = 0$ is the undamped case. Furthermore, overdamped vibrations are described by a damping ratio larger than 1 and underdamped oscillations as $\zeta < 1$. The damping ratio multiplied by 100 gives the ratio in percent, ζ is then called *percent of critical damping*.

$$\zeta = \frac{C}{C_c} \quad [-] \tag{3.14}$$

3.4 Forced Vibration Analysis

Oscillations occurring due to external excitations are called forced vibrations. The system's equation of motion will then have a right hand side equal to the external forces. If the excitation is *periodic*, that means repeated in equal intervals of time, the system will vibrate at the excitation frequency [49].

This section will present the mathematical formulation of external excitations, and introduce how they affect a dynamical system. In relation to this, the utilized method for modelling system damping will be presented. The dynamic magnifier model is the selected approach in this research. Forced

vibration equations of motion will thereafter be constructed for a drive train, followed by a discussion about detection of critical excitation frequencies. An evaluation of the applied forces' energy levels concludes the forced vibration theory.

3.4.1 Harmonic Excitation

The simplest form of periodic motion is *harmonic motion*. A system under these excitations is forced to vibrate at the same frequency as that of the excitation. In the forced vibration eom, Expression 3.15, the right hand side is the applied sinusoidal harmonic force. Common sources are unbalance in rotating machines, forces produced by reciprocating machines, and the motion of the machine itself [49]. For a propulsion system on board a ship, the engine is in general the main source of external harmonic displacement.

$$\begin{aligned} J\ddot{\theta} + C\dot{\theta} + K\theta &= T_0 \; sin(\omega t) \\ &= External \; excitations(t) \end{aligned} \tag{3.15}$$

For simplification in this section, the differential equation will be analyzed for a one degree of freedom system instead of multiple. The procedure is the same when treated as separate equations or expressed on matrix form. The differential eom has two solutions, the homogeneous solution (right hand side equal to zero) and the *particular* one. Reference to section 3.3, the first solution is related to damped free vibrations. The particular solution on the other hand, is assumed to be of the harmonic form beneath. This steady-state oscillation has the same frequency ω as the harmonic force. Θ is the amplitude of oscillation and ϕ is the phase of the displacement with respect to the exciting force.

$$\theta(t) = \Theta \; sin(\omega t - \phi) \tag{3.16}$$

Derivatives of the particular solution yield that the phase of angular velocity (cosine) is 90° ahead of the displacement, and acceleration (sine) 180°

ahead. These relations are used to construct a graphical representation of the differential equation of motion, namely the vector diagram in Figure 3.8. Oscillation amplitude and phase angle can further be expressed directly from this sketch. Tangent to ϕ is the damping vector divided by the stiffness vector minus inertia, leading to Equation 3.17. Furthermore, the Pythagorean theorem can be treated on the right-angled triangle formed by vector T_0 as the hypotenuse, creating the expression for amplitude Θ as in Formula 3.18. To develop the same two equations mathematically, all three forms of the particular solution must be inserted into the initial differential eom.

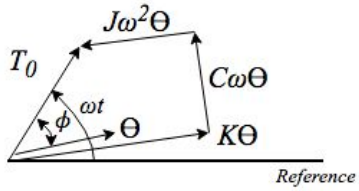

Figure 3.8: Vector diagram for forced vibrations

$$\phi = tan^{-1}\frac{C\omega}{K - J\omega^2} \tag{3.17}$$

$$\Theta = \frac{T_0}{\sqrt{(K - J\omega^2)^2 + (C\omega)^2}} \tag{3.18}$$

The expressions for amplitude and phase angle can also be written on a non-dimensional form. Dividing both numerators and denominators with K, and thereafter use formulations of natural frequency, critical damping and damping ratio from free vibration methodology, leads to the following two relations:

$$\phi = tan^{-1}\frac{2\zeta\left(\frac{\omega}{\omega_n}\right)}{1 - \left(\frac{\omega}{\omega_n}\right)^2} \tag{3.19}$$

$$\frac{\Theta K}{T_0} = \frac{1}{\sqrt{\left[1 - \left(\frac{\omega}{\omega_n}\right)^2\right]^2 + \left[2\zeta\left(\frac{\omega}{\omega_n}\right)\right]^2}} \tag{3.20}$$

Observe that phase angle and amplitude now only are dependent of frequency ratio ω/ω_n and damping ratio ζ. Plotting these against each other reveals illustration 3.9. This figure is constructed for translational vibrations, but since the theory is identical for torsional oscillations it can also be used here. The trend from these graphs is that oscillation amplitude and phase are strongly correlated with damping ratio near resonance ($\omega = \omega_n$). As an example, increased damping factor C can reduce amplitude at resonance quite significantly.

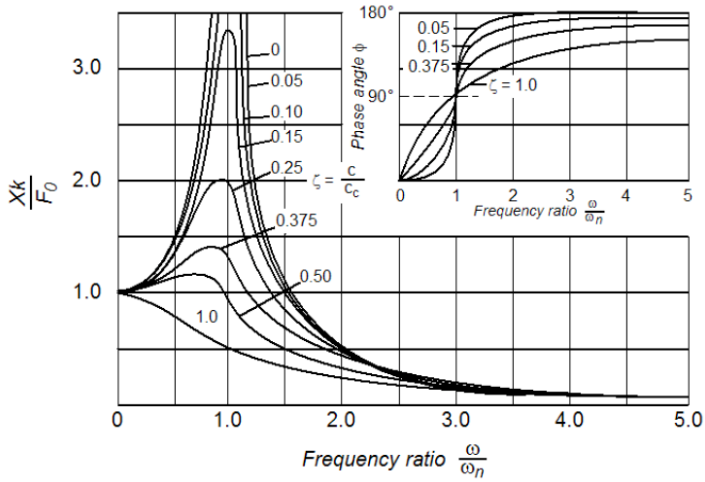

Figure 3.9: Dynamic response in terms of frequency and damping ratio [49]

3.4.2 The Dynamic Magnifier Model

Propulsion system damping is in this thesis introduced by means of the dynamic magnifier methodology, one of the most conventional and valid damping models applied in the industry at present-day [14]. It is a dimensionless approach based on a single mass-spring damper system and for only

one applied excitation source of a given frequency. Percentage of critical damping is further used to define both mass and shaft damping characteristics. The hydrodynamic propeller damping is an exception, it is defined by the variable percent of critical damping-model presented in section 2.2.1. For all other inertias and shafts, the constant magnifier model is achieved by introducing a parameter called the *dynamic magnifier number*, symbolized as $\tilde{M}$. All shafts and masses have one associated magnifier number each, constant with variable rpm. Additionally, the relevant methodology also offers an alternative where component damping is introduced in Nms/rad by damping factor C.

The magnifier approach divides damping into two categories, *absolute* and *relative*. The first one (C_{abs}), 'on masses', is typically initiated by gas compression in the diesel engine cylinders or by the propeller's hydrodynamic damping contribution. The damping constant of the propeller varies with rpm. Relative damping (C_{rel}) on the other hand, 'between masses', can arise from torsional vibration dampers, steel shafts or elastic couplings as some examples. With each of the two forms of damping factors C_i, follows an alternative definition by a magnifier number $\tilde{M}_i$.

Even though the two types of damping come from different sources, the expression for calculating them is the same. It is derived from the forced vibration equation of motion in section 3.4.1. The damping factor C in this expression includes both relative and absolute damping. C can therefore be replaced by either of the two damping factors C_{abs} or C_{rel}, to make one differential equation at a time. They will however become identical, the only difference is the subscript i of parameter C_i.

By making use of the vector diagram for forced vibrations excited by a harmonic force, the peak oscillation amplitude reveals as T_0 over damping times natural frequency. This is trivial as peak amplitude implies displacement at resonance where $\omega = \omega_n$ and the phase angle ϕ is equal to ninety degrees (see Figure 3.9) [49]. The vector diagram consequently becomes a rectangle such that the two vectors on the short sides are equal to each other (see Figure 3.10). Furthermore, static motion yields $\omega \to 0$, which graphically is repre-

sented as harmonic excitation vector (Θ) equal to the stiffness vector ($K\Theta$). The related vibration amplitude thereby becomes T_0 over rotational stiffness K. An expression for the magnifier number as a function of rotational speed ω_n is eventually obtained as Equation 3.21.

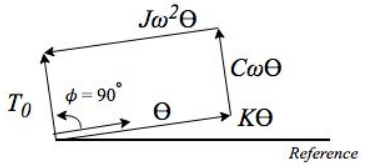

Figure 3.10: Vector diagram at resonance

$$\tilde{M}_i = \frac{\Theta_{peak}}{\Theta_{static}} = \frac{\frac{T_0}{C_i \cdot \omega_n}}{\frac{T_0}{K}} = \frac{K}{C_i \cdot \omega_n} \tag{3.21}$$

Before the final expression for mass and shaft damping in Nms/rad is achieved, one final simplification will be performed. Making use of the definition of natural frequency in section 3.3.2, torsional stiffness can be written as $J \cdot \omega_n^2$. Inserting this into the previous equation finally gives damping as moment of inertia times natural angular velocity, divided by the magnifier number. When calibrating mass damping, C_{abs}, J would be the MOI of the associated mass. Parameter J for relative damping on the other hand, is calculated based on the polar mass moment of inertia of the next mass, the one to the right of the relevant shaft. Formula 3.22 expresses damping in the unit of newton meter second per radian. This is the first out of two possible damping approaches within the constant magnifier methodology.

$$C_i = \frac{J \cdot \omega_n}{\tilde{M}_i} \quad [Nms/rad] \tag{3.22}$$

The direct connection between the magnifier number and the percent of critical damping (ζ in [%]) can now be established. Using this dimensionless approach is the second alternative for defining system damping. By using the formulation of damping C as equal to $\zeta/100$ times C_c, and substituting

critical damping from Expression 3.13 into Formula 3.22, the relation is obtained. Equation 3.23 proves that $\tilde{M}$ is only dependent on the percentage of critical damping, namely what the dynamic magnifier model is based on. It can also be written in terms of the *dynamic magnifier percent* denoted M, which in reality is a dimensionless ratio. M is consequently the same as the damping ratio (Formula 3.14), namely percent of critical damping divided by 100.

$$\tilde{M}_i = \frac{100}{2 \cdot \zeta_i} = \frac{1}{2 \cdot M_i} \quad [-] \tag{3.23}$$

Illustration 3.11 will help to understand the theory presented above. Summarized, the dynamic magnifier model offers introduction of damping either by $\tilde{M}_i$ or C_i, where i represents either masses or shafts. Both approaches will be utilized in this research. The software Nauticus Machinery enables input of both damping parameters, whereas Simpack requires damping in the unit of Nms/rad. Using factor C will result in a total damping torque equal to Equation 3.24. Internal shaft damping is a function of the angular velocity difference between the first and second inertia. The external damping torque however, is only dependent on the respective mass. These two damping contributions can be recognized as parts of the damped equation of motion for a vessel drive train. The next subsection will set up the differential equations for such a system.

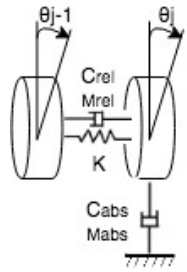

Figure 3.11: Absolute and relative damping

$$T_{damp} = T_{rel} + T_{abs} = C_{rel}(\dot{\theta}_{j-1} - \dot{\theta}_j) + C_{abs} \cdot \dot{\theta}_j \tag{3.24}$$

Discussion

The downside with the constant magnifier methodology becomes visible during vibration analyzes. Both alternatives for introducing damping (using C or $\tilde{M}$) will be calculated based on the maximum natural frequency, namely the most prevalent first mode of oscillations ω_{n1}. The damping coefficients are thereby not following the gradient of the torque characteristics. Instead, they are assumed as constant system parameters, independent of the applied rotational speed. A consequence of this assumption is that torsional responses of multi-mass systems only will be estimated properly at the rpm of the first mode resonance speed [14]. At other rpms the damping model will be less accurate. Assuming damping as independent of the variable rotational speed, and basing the damping model on a single mass-spring damper system, is in this way quite extensive.

An important fact is however the introduction of a propeller damping that varies with speed. The propeller is the main source of damping in a propulsion system [31], making the selected damping approach for this specific component most crucial for TVC results. As a reference, Dahler et al. tested the accuracy of the magnifier model on a drive train with an FPP directly driven by a slow speed MAN-main engine [14]. They found out that the constant magnifier model is non-conservative at resonance speed since it underestimates the associated torsional stress levels. Responses at MCR condition and other speeds were more correct, they were estimated in the vicinity of the measured ones. But more importantly, they proved that the variable percent of critical damping-model showed a much better compliance with measurements. The propeller damping contribution will in this way improve the accuracy of forced vibration analyzes. Anyhow, the less accurate introduction of system damping by means of the constant magnifier model should be addressed during evaluation of results.

3.4.3 Forced Vibration Equations of Motion of a Drive Train

The sketch underneath is a free body diagram of a multi-body torsional lumped mass system, which can be a vessel drive train. For simplification it contains three inertias where the middle part represents the engine and the propeller is located furthest to the right. Regardless of the number of masses included, the procedure would be the same, which is why only a selection of them is accounted for here. The forced vibration equations of motion will now be constructed for this system, using the general subscript *j*.

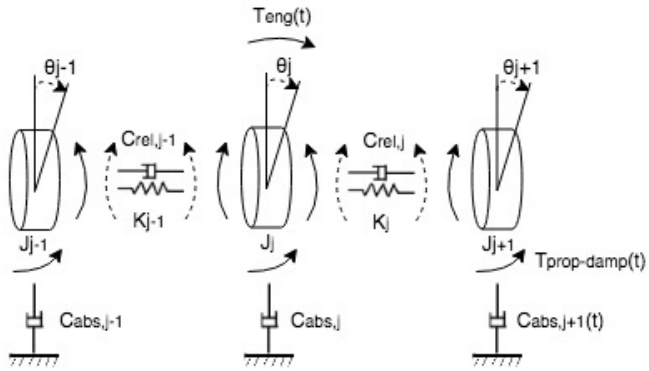

Figure 3.12: Free body diagram of a vessel drive train

As mentioned under free vibrations analysis, Newton's second law of motion is the basis for construction of the differential eom. Starting with disc *j-1*, MOI times torsional acceleration is equal to the forces acting on it. For the valid mass, this involves both absolute and relative damping torques (see Formula 3.24), in addition to the stiffness term. The mathematical sign (plus or minus) is further determined based on the directions of the arrows, whether they rotate with or opposite of the angle θ_{j-1}. Figure 3.12 and Formula 3.25 illustrates these statements.

Continuing in the same manner with the second and third mass, the equations of motion become the next two formulas. External harmonic excitation from the engine ($T_{eng}(t)$) is part of inertia j's right hand side. There are no external excitations effecting the other two masses, only torques due to

rotational damping and stiffness. However, the absolute damping factor for the propeller can be assumed variable with time, resulting in a function $T_{prop-damp}(t)$. The physical explanation for this time dependent parameter is that it represents the propeller's hydrodynamic damping. It can consequently viewed as an external torque.

$$J_{j-1}\ddot{\theta}_{j-1} = -\Big[C_{rel,j-1}(\dot{\theta}_{j-1} - \dot{\theta}_j) + K_{j-1}(\theta_{j-1} - \theta_j)\Big] - C_{abs,j-1}\cdot\dot{\theta}_{j-1} \tag{3.25}$$

$$J_j\ddot{\theta}_j = T_{eng}(t) + \Big[C_{rel,j-1}(\dot{\theta}_{j-1} - \dot{\theta}_j) + K_{j-1}(\theta_{j-1} - \theta_j)\Big] - \Big[C_{rel,j}(\dot{\theta}_j - \dot{\theta}_{j+1}) + K_j(\theta_j - \theta_{j+1})\Big] - C_{abs,j}\cdot\dot{\theta}_j \tag{3.26}$$

$$J_{j+1}\ddot{\theta}_{j+1} = \Big[C_{rel,j}(\dot{\theta}_j - \dot{\theta}_{j+1}) + K_j(\theta_j - \theta_{j+1})\Big] - T_{prop-damp}(t) \tag{3.27}$$

It is mathematically easier to solve the set of differential equations when they are written on matrix form. The result is shown underneath, which again can be recognized as the forced vibration equation of motion in Formula 3.15. Torsional behavior of the drive train is then equal to the external excitations that vary with time.

$$\begin{bmatrix} J_{j-1} & 0 & 0 \\ 0 & J_j & 0 \\ 0 & 0 & J_{j+1} \end{bmatrix} \begin{Bmatrix} \ddot{\theta}_{j-1} \\ \ddot{\theta}_j \\ \ddot{\theta}_{j+1} \end{Bmatrix} + \begin{bmatrix} C_{rel,j-1} + C_{abs,j-1} & -C_{rel,j-1} & 0 \\ -C_{rel,j-1} & C_{rel,j-1} + C_{rel,j} + C_{abs,j} & -C_{rel,j} \\ 0 & -C_{rel,j} & C_{rel,j} \end{bmatrix} \begin{Bmatrix} \dot{\theta}_{j-1} \\ \dot{\theta}_j \\ \dot{\theta}_{j+1} \end{Bmatrix} + \begin{bmatrix} K_{j-1} & -K_{j-1} & 0 \\ -K_{j-1} & K_{j-1} + K_j & -K_j \\ 0 & -K_j & K_j \end{bmatrix} \begin{Bmatrix} \theta_{j-1} \\ \theta_j \\ \theta_{j+1} \end{Bmatrix} = \begin{Bmatrix} 0 \\ T_{eng}(t) \\ -T_{prop-damp}(t) \end{Bmatrix} \tag{3.28}$$

It should be mentioned that parameter K could be a so called *equivalent spring constant* K_{eq}. This is applicable if for example shaft segment $j-1$ in Figure 3.12 contains multiple shafts in series, each with different stiffness magnitudes in Nm/rad. These types of segments are called *step shafts*. The resulting expression for K_{j-1} would then be equal to K_{eq} in the formula underneath [43]. i is the number of stiffnesses in series. There also exists an equivalent stiffness constant for shafts in parallel. In terms of propulsion systems, this would be valid for modelling of gears. However, since this master thesis focuses on direct-drive, parallel K_{eq} do not need further notice.

$$\frac{1}{K_{eq}} = \sum_i \frac{1}{K_i} \quad \Rightarrow \quad K_{eq} = \frac{\prod_i K_i}{\sum_i K_i} \tag{3.29}$$

The set of differential equations in Formula 3.28 can be solved for the unknown angular displacements, velocities and accelerations. Traditional theory of differential equations is the applicable approach. For a complex drive train with more than three masses, this could be a time consuming process, such that computer softwares are preferred. Simpack MBS software will solve the eom continuously over a time period t, at the rate of a selected sampling frequency, which should be chosen very carefully. Discussion about this affair can be found in section 6.3. Since Nauticus Machinery simulates in frequency domain, this software will solve the differential equations for one rotational speed at a time. The right hand side of the eom is then the magnitude of external torques at the associated frequency. Both computer tools solve the differential equations with help from embedded algorithms.

3.4.4 Critical Speeds and Campbell Diagrams

According to Friswell et al., *critical speeds* of a shaft line are rotational speeds at which the machine behaves poorly due to the large vibrations that occur [15]. In other words, they are excitation frequencies that will cause the system to vibrate at one of its natural frequencies, leading to resonance. During this event, the stresses might be dynamically magnified

to many times their values when the same load is applied statically [56]. If a propulsion line is run continuously at a critical speed, failure may take place quite quickly. Locating them is therefore of the utmost importance, and will consequently be identified for the investigated drive train in this master thesis.

A *Campbell diagram* is a tool utilized to determine critical speeds. Engine speed is located on the x-axis in the unit of revolutions per minute, whereas the system's rotational frequency is given on the y-axis in hertz. Both external excitations and natural frequencies of the system will be plotted in the diagram. Figure 3.13 shows an example where periodic excitations are the tilted lines and ω_n is plotted horizontally. The critical engine speeds (n_c) are eventually found at the intersection points with their rpm-values given on the x-axis.

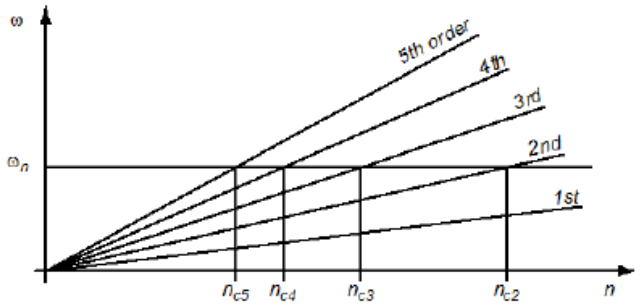

Figure 3.13: Campbell diagram: critical rpm during periodic excitation [41]

The external excitations in a vessel drive train mainly originate from the engine and propeller. The non-uniform character of the engine torque initiates a series of frequencies that are integer multiples of the working cycle [56]. A two-stroke engine with a working cycle that occupies one crankshaft revolution, will therefore have engine excitation frequencies f_e as given in Equation 3.30. When creating the Campbell diagram, they can be recognized as the oblique excitation orders (see diagram above).

$$f_e = \frac{n_e}{60}, \frac{2n_e}{60}, \frac{3n_e}{60}, \frac{4n_e}{60}, \frac{5n_e}{60}... \tag{3.30}$$

The second series of external excitations are initiated by the propeller when water is passing its blades. These frequencies are consequently integer multiples of the number of propeller blades. A five-bladed propeller will as an example cause the frequencies f_p in Equation 3.31 beneath. Campbell diagrams can be created for propeller excitations in the same manner as for the engine. The only difference is that the resulting critical speeds are dangerous excitations from the propeller, not the engine. Additionally it should be noted that in a direct-coupled drive line, these two inertias experience the same rotational speed, namely $n_e = n_p$.

$$f_p = \frac{n_p}{60}, \frac{5n_p}{60}, \frac{10n_p}{60}, \frac{15n_p}{60}, ... \tag{3.31}$$

3.5 Post-Processing Methodology

Torsional stress can be calculated from both time and frequency domain simulation results. The needed information is internal shaft torque and shafting parameters, provided by both of the utilized softwares. Fatigue analyzes on the other hand, require time series of torsional stress, which only is available in Simpack. Furthermore, so called power spectra will be used to evaluate critical speeds, also by use of time series. Both studies will be performed in this thesis, facilitated by the WAFO MATLAB toolbox.

Torsional stress levels and fatigue damage are normally restricted by standards and regulations. The first by acceptance limits defined by class as one example [20], and the latter by e.g. IACS' unified requirement number M68 [26]. These two examples support the importance of investigating stress and fatigue as part of post-processing.

3.5.1 Power Spectra

A *power spectrum* of a time series, also called *power spectral density* (PSD), describes the distribution of power into frequency components composing that signal [48]. A plot of the PSD function, symbolized as $S(\omega)$, has power on the y-axis against frequency on the other. The illustration underneath shows an example of spectral density.

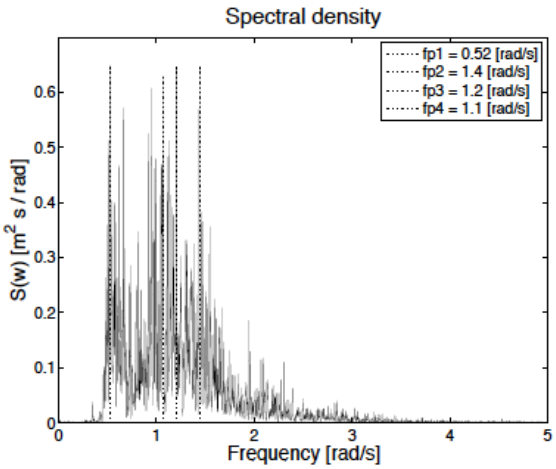

Figure 3.14: Example of power spectral density [23]

These type of diagrams can identify frequencies containing high levels of power, and thereby energy. In the example above, this applies to operation between approximately 0.5 and 1.5 hertz. The energy level is noticeably reduced at higher speeds.

In this master thesis, PSD will be used to evaluate critical speeds. Campbell diagrams are helpful to detect them, but they cannot imply whether they really are dangerous or not. To identify the 'real' critical speeds, energy levels must also be accounted for. By use of power spectra one can distinguish a potential critical speed from an actual threat.

3.5.2 Torsional Shaft Stress

Internal shaft torques from forced vibration analyzes can be evaluated in terms of torsional stress. Nauticus Machinery calculates stress automatically, whereas Simpack only outputs shaft torque. Time domain results from the second software, will therefore be investigated in a separate post-processing study (see Chapter 7).

Torsional stress is produced when a twisting moment is applied about the axis parallel to the length of the shaft, the same as shear stress. Its definition is internal torque times shaft radius (outer), divided by the polar area moment of inertia I_{shaft} [15]. The propulsion shafts will be simplified as either circular or hollow solid cylinders. They consequently have a second moment of area equal to one of the expressions in Formula 3.33 [41]. Both outer and inner shaft diameters are used in the hollow case. During class approval as an example, the internal torque can be replaced by maximum allowable moment, which then result in τ_{tors} as the limiting torsional stress.

$$\tau_{tors} = \frac{T_{internal} \cdot r}{I_{shaft}} \tag{3.32}$$

$$I_{shaft,circular} = \frac{\pi}{32} \cdot d^4 \quad or \quad I_{shaft,hollow} = \frac{\pi}{32} \cdot ({d_{out}}^4 - {d_{in}}^4) \tag{3.33}$$

The parameter $T_{internal}$ is the *internal shaft torque* initiated by rotational stiffness and damping. In other words, it is the moment that acts on the relevant shaft section. It can further be recognized as the terms inside the square brackets of Equation 3.25 to 3.27, or as specified in the next formula. This torque is part of the equations of motion and represents the propulsion system's internal dynamics.

$$T_{internal} = K\Delta\theta + C\Delta\dot{\theta} \tag{3.34}$$

3.5.3 Fatigue Analysis

Fatigue damage occurs due to repeated or fluctuating stresses [8]. Note that maximum stress levels might be well below the ultimate strength of the material, even below the yield strength. It is however the very large number of times the stress levels are repeated that cause fatigue. Compared to statical damage, which can be detected before the actual fracture occurs (by large deflections when yield strength has been exceeded), fatigue failure gives no warning which makes it very dangerous. Analyzes of torsional stress cycles and amplitudes over time will therefore be part of Simpack post-processing.

Determination of fatigue damage over a selected time period, requires material properties in terms of the so called *SN curve*, in addition to time series of torsional stress. The latter is divided into different stress ranges, and the number of cycles within each level are counted by use of the *rain flow cycle counting method* (RFC). Eventually, the total damage is calculated based on the *Palmgren-Miner hypothesis*, comparing actual stress levels to the material's strength. All steps of this procedure will be explained in detail underneath.

The SN curve

The SN-curve, also called a *Wöhler curve*, is utilized in fatigue analyzes to determine a material's number of cycles until failure (N) at a certain stress level (S) [35]. Parameters of the curve are calibrated from fatigue tests, subjecting specimens of the material to repeated forces until destruction [8].

Figure 3.15 shows a typical SN curve plotted on semilog paper. Number of cycles are given on the x-axis, and stress levels on y. The material in this example is UNS G41300 steel. S_{ut} is the ultimate strength of the material, a stress level that only requires one cycle until failure. The yield strength causes the first bend (from the left) in the curve, pointing out the transition from plastic to elastic region. S_e is eventually the endurance limit, if all

stress amplitudes are below this level, no fatigue failure will occur. This part of the curve is consequently defined as 'Infinite life' on the upper axis of the diagram.

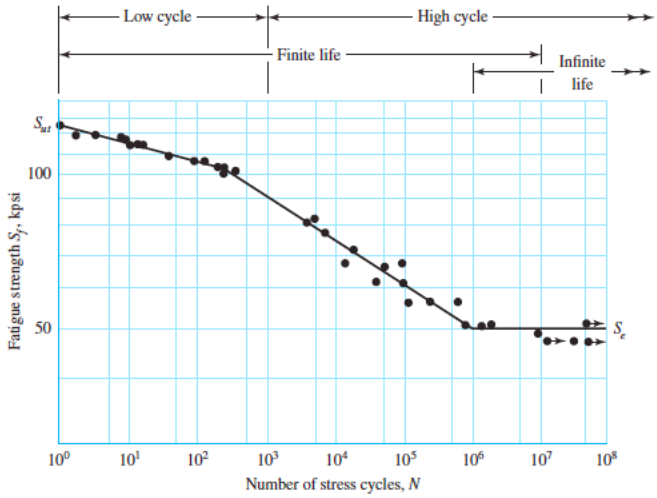

Figure 3.15: Example of an SN curve - Material: UNS G41300 steel [8]

The first equation underneath is the expression for the SN curve, where K_c and m are the material's characteristic location parameter and slope parameter respectively. As mentioned, these parameters are obtained from fatigue tests. Characteristic K is typically 97.7% probability of exceedance [35]. Formulated in terms of mean (μ) and standard (s) deviation of $log_{10}(N)$ for a Gaussian distribution, this corresponds to Formula 3.36.

$$N = K_c \cdot S^{-m} \quad or \quad log_{10}(N) = log_{10}(K_c) - m \cdot log_{10}(S) \tag{3.35}$$

$$log_{10}(K_c) = \mu - 2s \tag{3.36}$$

The selected shafting material for this research is the alloy steel 16MnCr5. This is utilized in wind turbine gears as an example, and can be transferred to ship propulsion systems. Parameters of this steel are given in Table

3.1, where K_c became 23.613 according to Formula 3.36. An SN curve for 16MnCr5 can easily be constructed in the same manner as illustrated above.

Table 3.1: Shaft material properties of alloy steel 16MnCr5 [36]

Symbol	Description	Value	Unit
S_y	Base material yield strength	850	[N/mm^2]
S_{ut}	Base material ultimate strength	1200	[N/mm^2]
μ	Mean deviation of location parameter	24.753	[N/mm^2]
s	Standard deviation of location parameter	0.57	[N/mm^2]
$log_{10}(K_c)$	Characteristic location parameter	23.613	[N/mm^2]
m	Slope parameter	6.225	[-]

Rain flow cycle counting

As mentioned in the introduction to fatigue analyzes, the rain flow cycle counting method determines the number of cycles (n) within different stress ranges (S) of a time series [35]. A stress range is in this context the torsional stress at a peak (or valley), minus the value at the 'next' valley (or peak). The RFC method defines the 'next' valley or peak according to Figure 3.17, which will be explained underneath. Note that this approach thereby studies half and not whole cycles. The results from rain flow counting are normally presented as a histogram with cycles against stress levels on the two axes, depicted in Figure 3.16.

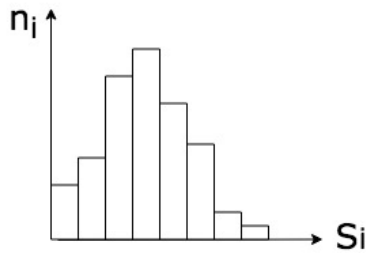

Figure 3.16: Example of an RFC histogram

The algorithm considers time series of torsional stress with the time axis pointed downwards. Connections between peaks and valleys now resemble pagoda roofs. Imitating that rain fall flows down over the roofs has given the name to the method and will be used to count half cycles. The general rules are [35]:

- All rain flows begin at either the start of the time series or at the inside of a peak or valley
- A rain flow drops down until it reaches a peak more positive (or a valley more negative) than the starting point
- Rain flows also end when they meet a rain flow from a roof above
- All rain flows must terminate at the end of the time series
- The stress range of a rain flow, counted as a half cycle, is equal to its horizontal length from the time axis (see the upper horizontal axis)

An example of this procedure is given in the illustration beneath. Beginning at time zero, rain flow 1 drops down until 4 because the next valley (number 5) is more negative than the starting point at 1. Half cycle 1-2-4 has now been identified. The end of the time series (point 10) is counted as a peak, terminating for example rain flow 4-5-7. Both rain flow 2', 5' and 8' are ended since they meet the rain flow from a roof above. In this example there are nine half cycles, each with their own stress range. These magnitudes can further be used to determine fatigue damage.

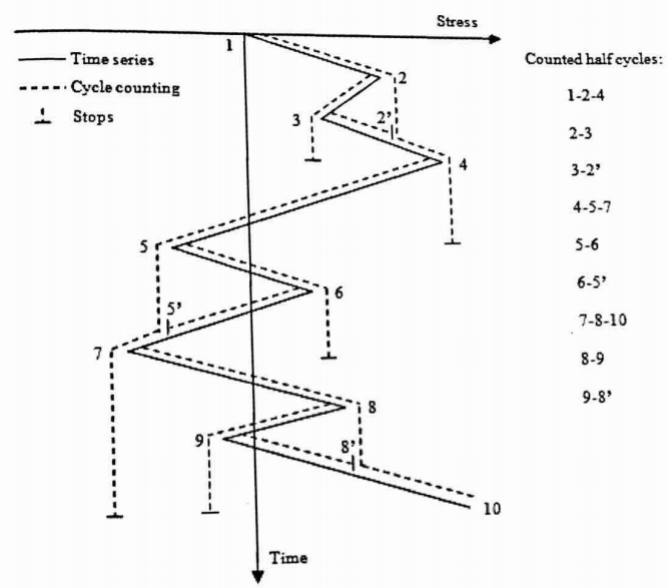

Figure 3.17: Illustration of the RFC method [35]

Fatigue damage

Fatigue damage can be calculated when the material's SN curve is known, and the RFC method has been applied on the relevant time series of stress. The Palmgren-Miner hypothesis formulates accumulated damage over a time period t as [8]:

$$D(t) = \sum_i \frac{n_i}{N_i} \tag{3.37}$$

Parameter n_i is the time series' number of cycles at stress level S_i, and N_i is the material's number of cycles to failure at the same stress level. The material represents fatigue resistance, whereas torsional stress is the fatigue loading. $D(t)$ equal to one implies fatigue fracture. The acceptance criteria for fatigue damage during service life is normally between 0.1 and 1 for marine structures as a reference [35].

3.5.4 WAFO - a MATLAB Toolbox for Analysis of Random Waves and Loads

WAFO is a toolbox of MATLAB routines for simulation and statistical analysis of random waves and loads [23]. It is a free software, developed by Lund University in Sweden, that can be downloaded online[1] and implemented in MATLAB as an additional analysis toolbox. It covers subjects such as fatigue analysis, sea modelling, statistics and numerics.

In this master thesis, the WAFO toolbox will be utilized for time domain post-processing. This includes development of power spectral density plots, and to perform rain flow cycle counting and calculations of fatigue damage based on defined material properties. The utilized WAFO codes and scripts are delivered together with this master thesis in DAIM, see Appendix E.1. Only MATLAB scripts written by the author are added as attachments to this report. See Appendix E.2.1 for power spectra and Appendix E.3 for fatigue calculations.

The necessary input in WAFO is time series of torque and torsional stress, in addition to material parameters. Time series of internal shaft torque are outputs from simulation in Simpack, which can easily be transformed to stress using Formula 3.32. Information about the shaft material can be found in Table 3.1. WAFO only needs torque series to create its associated power spectrum. RFC results are presented as histograms by the toolbox, similar to illustration 3.16. It thereafter calculates the accumulated fatigue damage according to Palmgren-Miner's hypothesis. Further details are described in association to the actual analyzes in Chapter 6 and 7.

3.6 Case Study

The research objectives, presented at the beginning of this report, will be achieved through a case study. In search of a test unit, the cooperation with

[1] WAFO can be downloaded from link: http://www.maths.lth.se/matstat/wafo/

DNV GL was convenient as they could provide necessary propulsion system characteristics and parameters. Furthermore, it was vital to select a drive train that is actually affected by the torsional vibration issue addressed in section 1.1.

The case study eventually became a slow rotating two-stroke engine, direct-coupled, fixed-pitch-propeller arrangement. This system is a power transmission line on a real life eco-ship. Details about the drive train, provided by DNV GL, will be given below. The system damping has been introduced through the presented dynamic magnifier model.

3.6.1 Propulsion System Design and Characteristics

The investigated propulsion system consists of a conventional two-stroke five-cylinder MAN diesel engine, connected to a five-bladed fixed-pitch propeller (FPP) through direct-drive. All components of the drive line are connected by shaft segments.

In the system layout (Figure 3.18) one can recognize the propeller at the leftmost end, followed by a flange, a turning wheel and thereafter the engine on the opposite side. The purpose of the turning wheel is to counteract the forces set up by the diesel engine. There is no gearbox involved, making the engine and propeller rotate at the same speed. Outside the sketch, after the engine, follows a torsional vibration damper (TVD) that reduces angular displacements. This element is composed of a damper stiffness in terms of a shaft segment, in addition to an inner and outer torsional vibration damper inertia. According to the manufacturer Geislinger, the TVD should be mounted to the free end of the crankshaft, which is the case in this drive line [22].

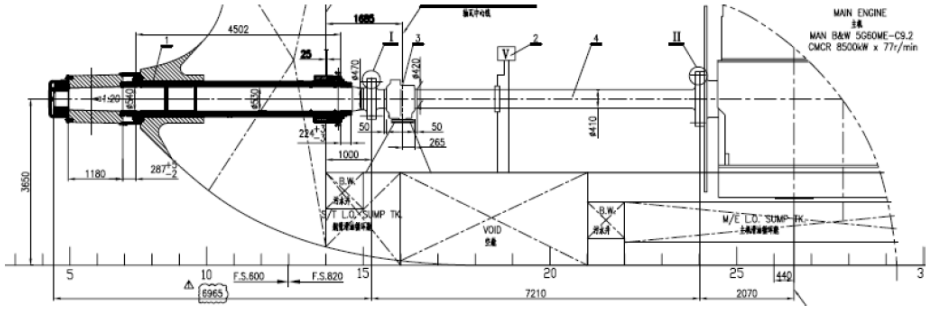

Figure 3.18: Sketch of the propulsion system

The shaft segments of the drive train can be divided into three categories: the crank, intermediate and propeller shaft. All inertias that are part of the engine are connected to the crankshaft. The intermediate shaft connects the engine to the propeller flange, before the propeller shaft eventually connects the propeller to the associated flange. Lengths of these two shafts are known as 7.21 and 6.69 meters respectively.

Some of the damping measures mentioned in the performed literature study (section 2.2.3), are applied in the design of this propulsion system. The implementation of a tuned torsional vibration damper is one of them. Furthermore, both sides of the engine have an inertia that counteracts and suppresses its supplied torques. These components can be recognized as the TVD (at the free end) and the turning wheel (before the intermediate shaft).

Table 3.2 and 3.3 present specifications of the main engine, the propeller and the torsional vibration damper. Detailed features of these three inertias will firstly be presented, followed by a more general description of the additional masses afterwards. All parameters, as well as the system layout above, are provided by DNV GL and attached in Appendix B.

Table 3.2: Main engine specifications

Parameter	**Value**	**Unit**
Manufacturer	MAN Diesel & Turbo	
Engine type	B&W 5G60ME-C9.2	
No. of cylinders	5	
Firing order	1 4 3 2 5	
Gas harmonic	T248078 (*See App. B.3*)	
Max. continuous output	8500	kW
Max. continuous speed	77	rpm
Barred speed range	40-51	rpm
Cylinder bore	600	mm
Stroke	2790	mm
Reciprocating mass	6278	kg/cyl.
Ratio of connecting rod	0.5	-

The main engine is under the low speed-B&W brand of MAN Diesel & Turbo. 5G60ME-C9.2 is the name or ID of the engine, where '5' stands for five cylinders, 'G' means a stroke-to-bore ratio of type 'Green' Ultra long, and '60' is the diameter of the piston in centimeters [52]. 'ME' implies that the engine functions are electronically controlled, such as fuel injection and exhaust valves. The engine is compact ('C'), its release number is '9', and its version is number '2'. The engine excitation data for normal firing is attached in Appendix B.3 by means of gas harmonics of family number '248078'. Normal firing means that all cylinders fire identically, without any imbalance [11]. The barred speed range for normal firing is defined as in between 40 and 51 revolutions per minute.

As previously mentioned, the torsional vibration damper is produced by the manufacturer Geislinger. It is a tuned TVD with steel springs and hydrodynamic oil damping [22]. More details about its working principle and design, can be found in the literature review regarding torsional damping

measures. Relevant characteristics during lumped mass modelling of the eco-ship are torsional stiffness, rotational shaft damping and inertia. The outer inertia of the TVD is in this case about 20% of the total engine inertia, in line with the recommended 5-25% from Geislinger (reference to section 2.2.3).

Table 3.3: TVD and propeller details

Parameter	Value	Unit
Torsional vibration damper		
Manufacturer	Geislinger	
Type	D280/FL, steel springs	
Torsional stiffness	17	MNm/rad
Relative damping	295000	Nms/rad
Outer inertia	20400	kgm^2
Inner inertia	1480	kgm^2
Propeller		
Type	Fixed pitch	
No. of blades	5	
Diameter	7.15	m
Physical damping (@ all rpms)	Variable (*See App. B.2*)	
Physical damping (@ MCR)	5.5	% critical
Power at MCR	8500	kW
Speed at MCR	77	rpm

The fixed pitch propeller has five blades with a blade span equal to its diameter. Physical damping is further defined as variable with rotational speed and expressed in percent of critical damping. This can be recognized as the mentioned variable percent of critical damping-model. Plotting data from the propeller table in Appendix B.2 gives the trend in Figure 4.2. The damping factor is increasing with speed close to linearly, until a certain

knuckle point is reached. This is the point where the curve flattens out and damping is assumed constant with increasing rotational speed [47]. The defined damping at the higher range of rpms, equal to 5.5%, is conservative [14]. For this propeller, the knuckle point is 40 rpm as illustrated beneath.

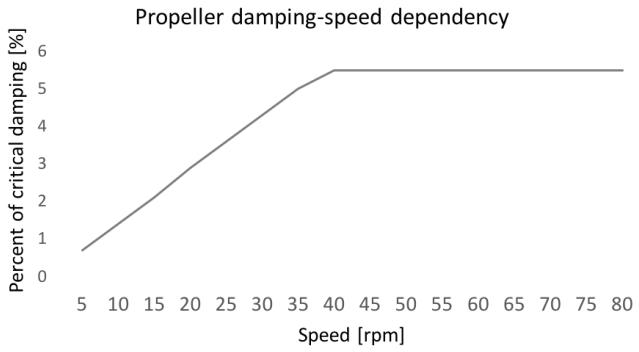

Figure 3.19: Variable propeller damping curve

The complete system consists of thirteen masses and twelve shaft segments. Each shaft has its own stiffness, and both masses and shafts have damping. The main inertias (beginning from the opposite side of the propeller) are the TVD's outer and inner inertia, the five engine cylinders, the thrust actuator, the turning wheel, a flange and lastly the propeller. Table 3.4 contains the mass elastic data for the drive train, which will be the basis for modelling and torsional vibration calculations in this thesis. An explanation of the table content will be given in the next paragraphs.

Column two to four contain information about the masses. Their respective mass moment of inertia are defined, as well as external damping. The latter is absolute damping (reference to section 3.4.2), and is associated with diesel engine cylinder damping (gas compression) and propeller damping (hydrodynamic damping). These values are given in percentage of critical damping, also referred to as the dimensionless dynamic magnifier model (see Equation 3.23). Once again, the critical damping occurs when the damping ratio ζ is equal to one, in other words when the system does not oscillate [15]. The firing angle of the cylinders are lastly defined in degrees.

The three columns on the right are data connected to shaft segments in between two adjacent inertias. Torsional flexibility is defined in the unit of nano (10^{-9}) radians per newton meter, which can easily be transformed into torsional stiffness in the unit of Nm/rad. Outer and inner shaft diameter follows. The right most column specifies the relative damping in the shaft, either in Nms/rad or in percentage of critical damping. The dynamic magnifier model thereby applies for both masses and shafts.

Table 3.4: Mass elastic data for the drive train

Mass ID/Description	**Firing angle** [deg]	**Mom. of inertia** [kgm^2]	**Mass damping(M)** [%]	**Tors. flex.** [nrad/Nm]	**Diameter outer/inner** [mm]	**Relative damping(M)** [Nms/rad] or [%]
1/TVD outer		20400	0			
				58.824	9999/0	295000
2/TVD inner		1480	0			
				0	820/150	1%
3/MomentCompnstr1		4140	0.85			
				0.423	820/150	1%
4/1st cylinder	0	20030	0.85			
				0.490	820/150	1%
5/2nd cylinder	216	20030	0.85			
				0.498	820/150	1%
6/3rd cylinder	144	20030	0.85			
				0.499	820/150	1%
7/4th cylinder	72	20030	0.85			
				0.474	820/150	1%
8/5th cylinder	288	20030	0.85			
				0.358	820/150	1%
9/Camdrive+Thrust		5590	0.85			
				0	820/150	1%
10/MomentCompnstr2		1830	0.85			
				0.258	820/150	0
11/Turning wheel		9377	0.5			
				30.788	410/0	0
12/Flange		354.7	0			
				9.381	530/0	0
13/Propeller		58905	5.5			

Chapter 4

Modelling

The propulsion system will be modelled by the lumped mass approach in two different softwares. Preparing models for simulation from 1 rpm up to the maximum continuous rating of 77 rpm, is the general goal. Nauticus Machinery gives a frequency domain model that can be utilized for studies of vibration reduction measures. Simpack MBS Software on the other hand, provides time domain results which can detect fatigue damage in addition to transient behavior. In this research, both models each have their own purpose.

This chapter is divided in two, one section for each software. They are again split into definition of inertia and shaft characteristics (including damping), and application of external excitation. Discussion and an introduction to modelling verification conclude Chapter 4.

4.1 Frequency Domain

4.1.1 Modelling in Nauticus Torsional Vibration

Nauticus Machinery will be utilized to model a lumped mass version of the selected vessel drive train in section 3.6. Its propulsion system parameters

will be the software input. Figure 4.1 shows the propulsion system in the format of the graphical user interface of Nauticus Torsional Vibration. The elements with green circles are the inertias, whereas the arrows represent torsional force elements. The numbers on top of the masses can be recognized as the inertias' respective ID numbers, given in the leftmost column of Table 3.4.

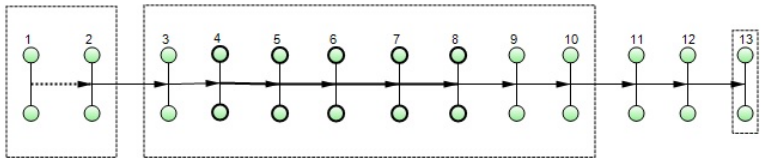

Figure 4.1: Drive train model in Nauticus Torsional Vibration

Beginning from the left, the first frame is the steel type torsional vibration damper which is attached to the free end of the diesel engine crankshaft. Mass 1 represents the outer inertia and mass number 2 the inner. The TVD is included to protect the propulsion shaft by converting mechanical vibrations into heat [12]. Power loss is consequently measured as dissipated heat in the unit of watts.

The dotted box that frames mass number 3 to 10 is the diesel engine, where element 4-8 are the five cylinders. Mass number 3 and 10 are flanges in terms of moment compensators, whereas mass number 9 is the camdrive that represents the thrust actuator. The turning wheel (ID 11) is located after the engine, recognized as a connection flange between the crank and intermediate shaft. The last two masses on the right are a flange (number 12) and the main fixed pitch propeller (mass number 13).

Shaft elements are modelled as arrows pointing in the direction of the torque flow. As can be seen in Figure 4.1, the arrows in between the five engine cylinders are thicker than the others. These four arrows represent crank throws, which is the radial distance from the centre line of a crankshaft to the centre of a crankpin [3]. In the software tool they are handled in the

same way as the shaft stiffnesses (the thinner arrows), the only difference is their representation in terms of a thicker line [47]. The dotted arrow, connecting the inertias of the TVD, is a damper stiffness with a relatively large damping factor (see Table 3.4). Since shafts are assumed massless in the lumped mass modelling approach, their lengths relative to each other are insignificant.

All parameters of the eco-ship are inserted into the software according to the mass elastic data in Table 3.4. Stiffness is introduced as torsional flexibility, and damping as dynamic magnifier percent M. Nauticus Machinery directly transforms these parameters into torsional stiffness and dynamic magnifier number $\tilde{M}$. The variable propeller damping is a special case due to the fact that it is defined by its knuckle point in the software. As described in section 3.6 the knuckle point of the propulsion system is 40 rpm. In percentage of the MCR-speed, which is the required format of the variable percent of critical damping-model and in Nauticus Torsional Vibration, this is equivalent to $40/77 = 0.52$. Inserting this into the software, results in the variable propeller damping curve beneath. This graph is identical to Figure 3.19, as it should be.

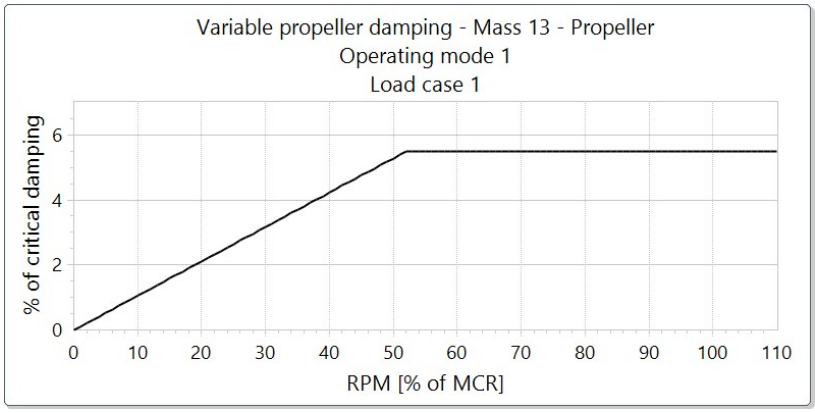

Figure 4.2: Defined variable propeller damping in Nauticus Machinery

The next illustration shows an example of the software's graphical user interface where characteristics are defined. The selected preview is the diesel

engine, defining parameters such as the firing order, the MCR condition and the barred speed range. The engine excitation data in Appendix B.3 is added into the 'Nauticus Engine library' and selected as the 'NormalFiring-DataPath'.

Diesel engine data	
CrankThrow	**FSB245000**
EfficiencyMechanical	**0,9000**
EngineType	**Inline**
ExcitationMethod	**Harmonics**
ExcitationData	
NormalFiringDataPath	**W:\temp\a615700b-7bf3-4b54-83b3-6b42784**
NormalFiringContent	Click to show normal firing data
MisfiringDataPath	
MisfiringContent	Click to show the misfiring data
FiringInterval	Even
FiringOrder	**1-4-3-2-5**
FiringPhase	0-72-144-216-288
FiringType	**Consecutive**
NumberOfStrokes	**2**
PhaseAngle	**0,000 deg**
PowerMCR	**8500,0 kW**
SpeedMCR	**77 rpm**
MaxBarredSpeed	**51 rpm**
MinBarredSpeed	**40 rpm**
NominalTorqueMCR	1,054E+003 kN*m
V-angle	**0,000 deg**

Figure 4.3: Defining diesel engine data in Nauticus Torsional Vibration

Modelling in Nauticus Torsional Vibration offers two node styles, either the *simple* version (Figure 4.1) or the *advanced* (Figure 4.4) [47]. The second alternative shows damping in terms of the dimensionless dynamic magnifier number $\tilde{M}$, in addition to torsional stiffness ([Nm/rad]) and polar mass moment of inertia ([kgm^2]). This preview makes it easy to check if all input data have been defined correctly. Note that the advanced model clearly demonstrates the difference between absolute (mass) and relative (shaft) damping.

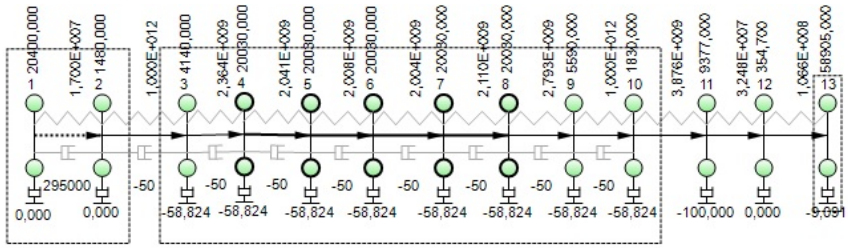

Figure 4.4: Model with parameter values

4.1.2 Load Case in Nauticus Machinery

To prepare the drive train model for forced vibration analyzes, external engine torques must be implemented. In Nauticus Torsional Vibration, this is enabled through defining an *operating mode* with an associated *load case* (reference to user manual sec. 2.7 [47]).

The operating mode defines MCR power, load percent and thereby actual power for both the engine and propeller. An assumption is made where the two components have a load percent of 100, reflecting that the actual power equals the one at MCR. The maximum continuous output is 8500 kW, referring to section 3.6.1 of this report.

A load case will further determine settings such as speed interval and engine firing. All five cylinders are given a firing percent of 100 and their firing status is set to 'normal', meaning not misfiring. The minimum speed is 1 rpm and the maximum is 77 (the MCR speed). The load case is thereafter defined by an embedded type named 'Propeller law-full pitch'. Since the propeller is fixed pitch, full pitch is evident. The propeller law determines how much power the propeller receives at a certain speed. This magnitude will be equal to the total power delivered from all engine cylinders at this specific frequency. The theoretical explanation follows beneath.

The *propeller law* is the relation between delivered power to the propeller (P_p) and its speed (n_p) [57]. Equation 4.1 shows that power is proportional to the cube of propeller speed, where C is a constant. Knowing that power is

equal to torque times angular velocity, the propeller law can be rewritten in terms of T_p. The propeller torque then becomes proportional to the square of n_p. Remember that the direct-drive arrangement makes the propeller and engine rotate at the same frequency, such that $n_p = n_e$.

$$\begin{aligned} P_p &= C \cdot {n_p}^3 \\ P_p = T_p \cdot \omega_p \quad &\Rightarrow \quad T_p = C \cdot \tfrac{60}{2\pi} \cdot {n_p}^2 \end{aligned} \tag{4.1}$$

Nauticus Machinery uses the established MCR point, 8500 kW at 77 rpm, to calculate the unknown constant C. The result is a value of 0.01862, which gives the *propeller curve*, namely speed versus power according to the propeller law. This characteristic, presented in Figure 4.5, is part of the model's 'load case settings'. A similar power-speed relation for the engine is given in Appendix C.2.1, but listed as power per cylinder. The trend is the same. By multiplying power per cylinder with five, an *engine curve* reveals. This graph is identical to the propeller curve since $n_p = n_e$, in addition to the fact that engine and propeller share the same power at MCR.

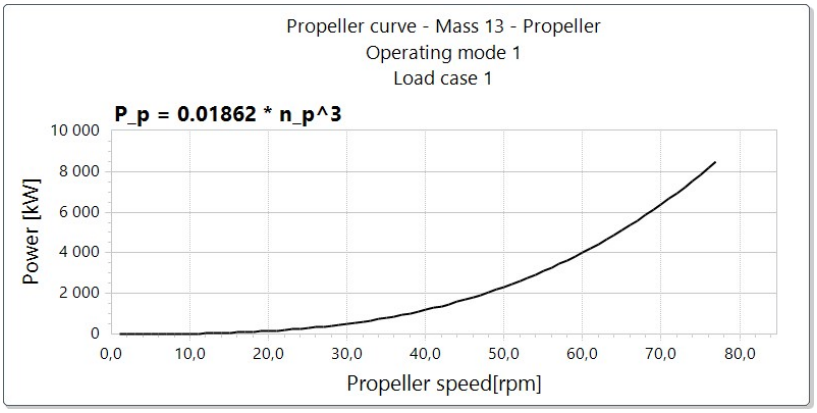

Figure 4.5: Propeller curve in Nauticus Machinery

Propeller damping factors (in Nms/rad) are also part of the load case settings in Appendix C.2.1. These values are equal to parameter C of the dynamic magnifier model, referring to Equation 3.22. Using percentage of critical damping from the variable propeller damping curve (Figure 4.2), will give

the same values as those in the mentioned attachment. Operation at 77 rpm is used to exemplify this calculation in appendix number A.2.

4.2 Time Domain

4.2.1 Modelling in Simpack MBS Software

Simpack defines a six-step modelling approach that should be followed to ensure best possible use of the software features and solver capabilities. These steps will firstly be presented, followed by the actual modelling of the case study system. The latter is part of the fourth step called pre-processing.

The Simpack modelling approach

According to the Simpack Reference Guide there are six steps in the *Simpack modelling approach* [2]. Step 1 to 3 have already been accomplished outside the software interface, but a description follows for information. The first step is 'problem definition', which in this case would be to model the selected vessel drive train. Building a model is necessary to achieve the research objectives. The second one is the 'development of a mechanical model', meaning to establish the structure of the system by dividing it into bodies and force elements connecting them. Choosing to model the propulsion unit as a torsional lumped mass system, see section 3.1.1, has already covered this part of the Simpack approach. The third step is 'provision of the model parameters'. All necessary system characteristics were provided by DNV GL, and have been presented in the previous chapter of this report.

The last three steps of the Simpack modelling approach will be performed within Simpack. Step number 4 is 'pre-processing', more specifically to perform the actual building of the drive train and to enter model data into the software. Such data includes defining body and force element parameters, introducing applied forces and excitations, in addition to the selection of

solver settings. The fifth step is 'Simpack calculations'. This involves automatic generation of the system's eom based on the input data, and thereafter finding its solutions by use of the 'system analysis module' [2]. Last but not least, step 6 presents the results in the post-processor. Multiple forms are available, including 2D line plots, 3D animations and utilizing mathematical algorithms such as Fast Fourier Transforms. This will be valuable when studying and evaluating the torsional behavior of the slow rotation propulsion system.

Among the three steps performed in Simpack, only pre-processing relates to the actual software modelling. As a consequence, only this procedure will be presented in the paragraphs to come. Solving the eom and post-processing of the results, are treated in the next two chapters.

Building the drive train

The propulsion system is built in Simpack on the same principles as used in Nauticus Machinery, namely by the lumped mass approach. However, the main changes are that the Simpack-model is constructed in 3D and that damping is introduced in the unit of newton meter second per radian instead of percentage of critical damping. Other differences are the method used to apply engine torque, and that time limitations resulted in a lack of introduced propeller damping. Furthermore, this software uses so called *markers* to define connection points between elements and local coordinate systems. Multiple versions of the final Simpack model are made to simulate time domain behavior at different operational speeds. One example is attached in the zip-file together with this report in DAIM, see Appendix D.2.

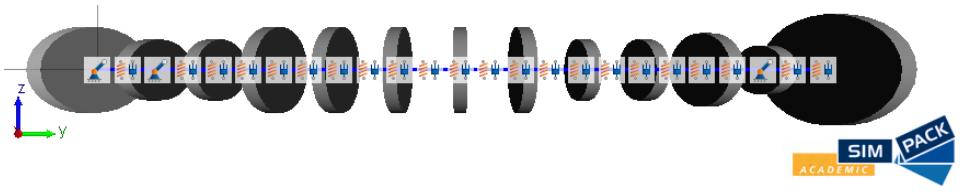

Figure 4.6: Drive train model in Simpack Pre-Processor

Similarly to Nauticus Machinery, the propeller is located furthest to the right and the TVD at the leftmost end. Figure 4.6 illustrates the three-dimensional drive line where inertias are modelled as 1 DOF-discs with a mass density of 7850 kg/m^3, corresponding to conventional steel. The cylinder diameters are selected with respect to their mass moment of inertia relative to each other (see column three in Table 3.4). This parameter is insignificant during lumped mass modelling and simply added to obtain a proper scaling of the components.

Centers of the bodies are defined by joints with single axis rotation about y, causing the angles beta (β). The longitudinal position of the joints is given by local reference frames, whereas rotation will be modelled by body reference frames (BRF) that move with the discs. The first frame is fixed, whereas the axes of the second one move during torsion. In terms of markers and joints, the 'From Marker' is the reference frame, and 'To Marker' is the BRF. All foreign expressions in this section are part of the Simpack syntax (see software manual [10]).

As illustrated above, inertias are connected by force elements symbolized as a spring next to a damper. These building blocks, called a 'Bushing Cmp' in the Simpack language, represent shaft segments with rotational stiffness and damping in y-direction. They are connected by their body reference frames, such that the 'From Marker' is the BRF of the inertia to the left, and the 'To Marker' is the BRF of the next mass. Magnitudes of torsional stiffness (in Nm/rad) are calculated directly from torsional flexibility given in section 3.6.1. Finding rotational damping in Nms/rad on the other hand, is not that straight forward. Assumptions in terms of the dynamic magnifier model will therefore be made to simplify the procedure.

Shaft damping is transformed from percentage of critical damping to relative in Nms/rad by use of Formula 3.22. The torsional vibration damper is an exception since its value already is known. The dynamic magnifier model is also used to calculate absolute mass damping, but the modelling element differs. External damping is introduced in Simpack through a force element called 'Spring-Damp Rot State Inp Cmp'. Linear damping is applied in one

rotational direction between two markers, the masses' reference frames and their BRFs. Calculated damping values are attached in Appendix D.1. As mentioned, the hydrodynamic propeller damping has unfortunately not been implemented in the Simpack model. Further research would include this external damping torque as it is an essential characteristic of a propulsion system's dynamics.

4.2.2 Engine Excitation through Co-Simulation in Simpack

This section will cover modelling of applied engine torque and the system's response to this load. The external excitation is simplified as a harmonic sine function oscillating with simulation time t. The dynamical response of the drive train, described in terms of delivered torque to the propeller, will be modelled by use of a controller. This magnitude should be lower than the input load due to internal shaft dynamics and mass damping.

A *controller* is a system that monitors and physically alters the operating conditions of a dynamical system. It will in this master thesis be utilized to reach a desired operating speed as quickly and accurately as possible. Achieving a rotational speed of 77 rpm, would as an example become the same simulation as in Nauticus Torsional Vibration, namely operation at the drive train's MCR condition. The set point value is then a constant rotational speed, ω_{ref}. It is also interesting with a time varying reference value. Longer periods with *transient* simulation would then be achieved. This is the period in between two reference speeds, before the drive train has stabilized at the new ω_{ref}.

Simulations using the two approaches, a constant reference value and a variable, will be attempted in Chapter 6. The next pages will present quite similar modelling procedures for enabling both. By weighting controller design complexity against corresponding response time, it was decided to implement a Proportional-Integral-Derivative (PID) controller.

Controller algorithms are implemented in Simulink and connected to the Simpack model by use of the SIMAT interface (reference to section 3.1.3).

Illustration 4.7 shows the interconnections during co-simulation with constant reference speed. A separate Simpack block connects the two softwares. The torque is updated by the controller until set point is reached. Only a few adjustments are required to enable a variable reference speed. Further details follow underneath.

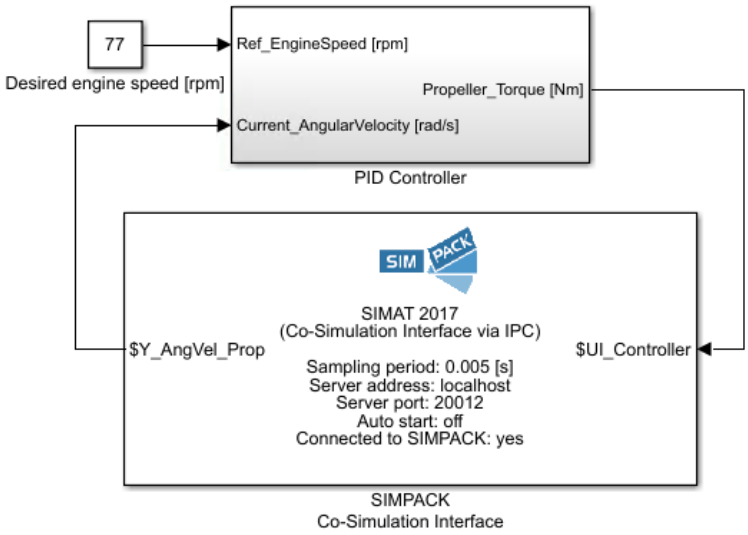

Figure 4.7: Co-simulation - Applying torque in Simulink

The PID-controller

The classical formulation of a PID-controller is given in Equation 4.2. It consists of a proportional, integral and derivative term in that specific order[4]. The controller calculates an error value continuously, namely the difference between desired set point and measured input parameter. Error e is used to update the output value. Since the goal is reaching a predefined rotational speed, the input value will be the measured angular velocity of the drive train. Remember that the eco-ship has direct-drive and that rotational speed consequently is the same for all components. The input parameter can therefore be measured at all thirteen inertias. Equation 4.3 is the error function $e(t)$, more specifically the measured rotational speed of the propeller

(randomly selected) minus set point value ω_{ref}.

$$T_{PID} = K_p \cdot e(t) + K_i \int_0^t e(\tau)d\tau + K_d \cdot \frac{de(t)}{dt} \tag{4.2}$$

$$e(t) = \omega - \omega_{ref} \tag{4.3}$$

The PID-regulator determines a correction of the propeller torque (T_{PID}) based on the proportional, integral and derivative terms. An error equal to zero, implies that set point speed is reached. All three controller terms contribute with a value, but based on different aspects of the error. The P-term accounts for its present value, whereas the I-term uses past values by integrating the error over time t. Lastly, the D-term accounts for future trends of the error by studying its derivative. K_d, K_i and K_p are the gain constants. Their purpose is determining to which extent the P, I and D terms will contribute to the output. Choosing their magnitude, a process called *tuning*, is important in the development of a PID-controller. After trail and error, the selected gains became the magnitudes in Table 4.1.

Table 4.1: Selected controller gains

Parameter	**Value [-]**
K_p	100 000
K_i	50 000
K_d	1 000

Figure 4.8 shows the implementation of the regulator in Simulink. Both set point speed and current angular velocity are inserted in the lower left corner. Since angular velocity is measured in radians per second, the engine speed in rpm needs to be converted to the same unit before the error can be calculated. The error is further treated according to Equation 4.2. The upper branch is the proportional part, the middle one represents the integral term and the lower arm is the derivative contribution. Summing up all three

terms gives the updated controller output, namely the propeller torque at the relevant rotational speed.

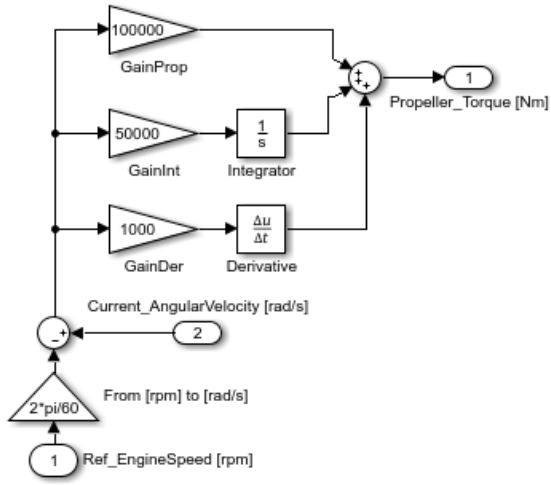

Figure 4.8: Simulink model of PID-controller

The PID-controller can also be recognized as the grey substructure in illustration 4.7, having the same input and output ports as the Simulink model above. Updated propeller torque is sent into the Simpack-block and measured angular velocity is sampled from the drive train so that the error can be calculated by the regulator. Lastly, one can recognize the definition of reference speed ω_{ref}, in the upper left corner. In this example it is a constant gain of 77 rpm.

Harmonic engine excitation

Similarly to the load case in Nauticus Machinery, the harmonic engine excitation will be an input in Simpack. The selected modelling element is an 'Excitation' that reads data from an external text file (see software manual[10]). This document contains engine torque at different times t (in seconds) at a rate equal to a selected time step. Furthermore, the engine excitation is applied at the joint of the first cylinder for simplification. When modelling in Nauticus Machinery, the engine excitation was available as a function of

variable mean indicated pressure (Appendix B.3). In Simpack on the other hand, the engine is modelled by simple inertias. Characteristics such as pressure are therefore not accounted for. The consequence is implementation of engine torque as a traditional sine function instead.

In Nauticus Machinery, the engine excitation was applied according to the propeller law. As mentioned in section 4.1.2, the engine curve will be identical to the propeller curve for direct-drive arrangements. Letting the propeller law construct the relation between engine torque and rotational speed, the result becomes Expression 4.4 and Figure 4.9. Time domain simulation in Simpack requires an engine torque that varies with time. This is where the harmonic sine excitation comes in handy.

$$T_0 = 177.79 \cdot {n_e}^2 \tag{4.4}$$

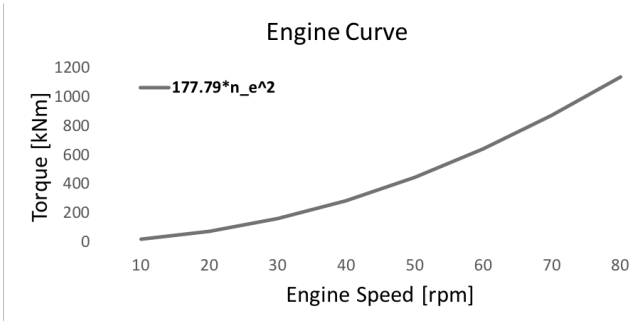

Figure 4.9: Engine curve according to the propeller law

$T_{eng}(t)$ is the selected input function format of applied engine torque in Simpack. The baseline of the harmonic wave is found in the engine curve above. The harmonic torque oscillates around T_0 with a half amplitude of 7.5% of the same value. Simulating drive train operation at 30 rpm ($=\omega_{ref}$) as an example, would give $T_0 = 160$ kNm. Illustration 4.10 shows an applied engine torque which oscillates around this value with $0.075 \cdot 160 = 12$ kNm plus or minus to the top and bottom respectively. This graph is taken from the 'Excitation properties'-window in Simpack MBS Software.

$$T_{eng}(t) = 0.075 \cdot T_0 \cdot sin(\omega_{ref} t) + T_0 \tag{4.5}$$

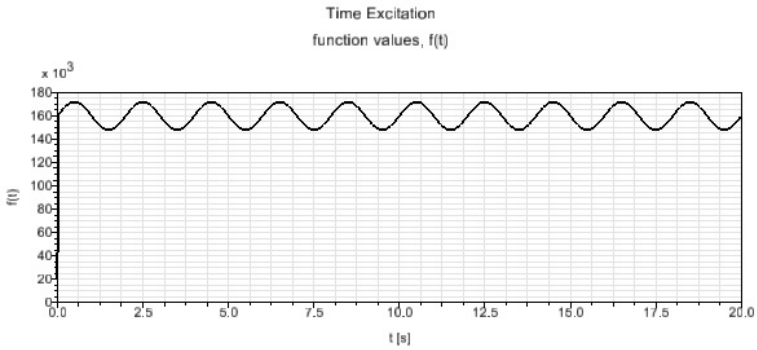

Figure 4.10: Harmonic engine excitation at 30 rpm

The utilized time step t, is 5 hertz. In practice this corresponds to an input file with engine torques specified at every 0.02 seconds, which Simpack reads from. As an example, the text document for input torque running at 70 rpm will contain around forty data points within one oscillation period. The selected time step is more than sufficient enough to create a continuous sine function.

Variable reference speed

During this type of Simpack simulation, a MATLAB script modifies the reference speed multiple times within the same run. A sketch of the applicable Simulink setup is attached in Appendix D.3, together with the mentioned script. Furthermore, the engine torque is updated continuously according to the engine curve in Figure 4.9. For simplification, the applied engine load is introduced as a constant value taken from this curve, not as a harmonic function.

4.3 Discussion

One of the main differences between modelling in Nauticus Machinery and Simpack, is that propeller damping has not been implemented in the second software. If more time was available, the author would use the damping torque in the load case settings from Nauticus Machinery to define different damping factors at each of the simulated engine speeds. Reference to propeller settings column five in Appendix C.2.1, operation at 45 rpm would as an example have a force element 'Spring-Damp Rot State Inp Cmp' with a damping factor C_{abs} equal to 30530 Nms/rad. Adjusting the constant propeller damping at each speed, would resemble the variable propeller curve used in Nauticus Torsional Vibration (see Figure 4.2).

The engine torque is also modelled differently. Where Nauticus Machinery uses the engine curve and expresses the load as a function of pressure, Simpack simplifies the external excitation into a time dependent harmonic sine function. Variations in introduced propeller damping and engine torque make the two models quite different. It implies that only free vibration analysis results will be identical, since they share the same undamped dynamics. Remember also that Nauticus Machinery only enables frequency domain simulation, whereas Simpack can give results in time domain. The latter enables transient studies among others.

4.4 Introduction to Modelling Verification

Before the models can be used to test vibration reduction measures and evaluate fatigue damage in the drive train, they have to be verified. This is performed through comparison to empirical data from DNV GL. They have executed similar simulations and used real measurements to justify their studies. Free and forced vibration analysis results, from the two models, will consequently be the basis for verification. The actual comparisons are presented together with these analyzes in the next two chapters.

Chapter 5

Free Vibration Analysis

Free vibration analysis involves determination of natural frequencies and mode shapes, aiming at identifying critical parts of the system. Referring to the last chapter, these results should be similar in both softwares as they share the same dynamics. Identified system characteristics from each computer tool will therefore be presented and discussed together, not separately. The free vibration models are compared to results from DNV GL in the last section.

5.1 System Characteristics

When external excitations are not applied, the system characteristics of interest are natural frequencies and mode shapes. As long as dynamic properties have been added to the drive train models, the softwares can calculate these parameters. Free analysis results can be extracted in terms of pdf-reports in both Nauticus Machinery and Simpack. However, only the most interesting data will be presented and compared in the pages that follow. The rest of the results are attached in Appendix C.1 and D.4.

5.1.1 Natural Frequencies

Nauticus Torsional Vibration and Simpack calculate natural frequencies in the same way as explained in section 3.3.2 of this report. There are thirteen different ω_n, one for each degree of freedom. However, since the first modes generally contain the highest energy levels, only these will be evaluated. A verification of this statement is given in section 6.1. Note that the free ends of the propulsion system give a natural frequency equal to zero. This is in reality the first ω_n, but it has not been accounted for as the focus is on detection of critical parts in the drive train.

Table 5.1 and 5.2 present the obtained first three modes of natural frequencies. The correlation between the two softwares is acceptable. A maximum difference of 0.06 hertz (or 3.6 rpm) is negligible compared to their magnitudes.

Table 5.1: Natural frequencies from Nauticus Machinery

Mode no.	**Parameter**	**Cyclic frequency**	
		[Hz]	[rpm]
1	ω_{n1}	3.70	221.93
2	ω_{n2}	5.10	306.18
3	ω_{n3}	26.16	1569.74

Table 5.2: Natural frequencies from Simpack

Mode no.	**Parameter**	**Cyclic frequency**
		[Hz]
1	ω_{n1}	3.75
2	ω_{n2}	5.04
3	ω_{n3}	26.13

5.1.2 Normal Modes and Stationary Points

Mode shapes are given directly as part of the free vibration analysis results in both softwares. These reports are attached in Appendix C.1.2 and D.4. Based on the same principles as for natural frequencies, only the first three normal modes are presented in Figure 5.1. Vibration amplitudes in these diagrams are taken from the mentioned Nauticus Machinery-report, but results from Simpack would give the same trends (again see attachment D.4). ID numbers of the masses according to Table 3.4 are given on the x-axis. Angular displacements are further normalized with respect to the large inertia of the outer part of the torsional vibration damper, meaning that mass number 1 always have a y-axis value equal to one. The TVD is chosen arbitrarily, any of the thirteen inertias could have been used.

Remember that the first normal mode in reality is the rigid-body mode where all inertias rotate together as one single mass. This shape of vibration however, is not associated with twisting of the shaft. It is therefore left out since it would not help detecting critical segments.

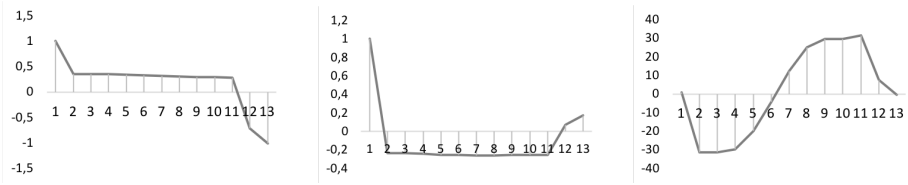

(a) 1st mode (b) 2nd mode (c) 3rd mode

Figure 5.1: Normal modes from Nauticus Torsional Vibration

The shapes of all three normal modes will now be discussed chronologically. Starting with the first mode, one can observe that the left of the drive line is rotating in opposite direction of the flange and the propeller (mass ID 12 and 13). It is said that these two parts are moving *out of phase* relative to each other. On the contrary, the second mode shows that the two ends of the propulsion system are *in phase*, rotating in the same direction. In the last and third mode, half of the drive line rotates together, whereas the rest

is moving in opposite direction.

Stationary points are exposed where motion between adjacent inertias shifts from in phase to out of phase. Depending on the magnitude of displacement, these points will be treated as either hazardous or not that vulnerable towards torsional fracture. Studying the three normal modes above, only the third mode shows significant sign of weakness. With a displacement ratio difference of over sixty between the torsional vibration damper (ID 2) and the turning wheel (ID 11), the associated stationary point inside the engine should be given special attention. It is located in between the third and fourth engine cylinder, namely at crank throw number three. Additionally, the intermediate shaft (between mass 11 and 12) should be investigated. This segment contains a stationary point both in the first and second mode shape.

5.2 Verification

At this stage of the research process, the software models will be verified based on the calculated natural frequencies. Since only dynamic properties have been investigated so far, and not the influence from external excitations, correlating ω_n will be a sufficient basis for verification. As mode shapes are based on natural frequencies, there is no need to verify both results. The actual comparison will be performed by comparing the results in section 5.1.1 against DNV GL's identical calculations. Their studies lead to the cyclic frequencies in Table 5.3, extracted from Appendix B.1.

Table 5.3: Natural frequencies from DNV GL

Mode no.	**Parameter**	**Cyclic frequency**	
		[Hz]	[rpm]
1	ω_{n1}	3.699	221.96
2	ω_{n2}	5.104	306.28
3	ω_{n3}	26.219	1573.11

The two software models will be compared to DNV GL's calculations one at a time, beginning with Nauticus Machinery. Looking at the rpm-column in Table 5.1, the correlation is especially good for the first two mode numbers, whereas the third mode is slightly underestimated in the executed research. However, the deviation is small with a maximum underestimation of 0.2% for the third mode.

Natural frequency is dependent on rotational stiffness and mass moment of inertia according to its definition (Formula 3.3). In other words, differences in calculated ω_n must emerge from definitions of these two parameters. The provided mass elastic data from DNV GL (Appendix B.1) was occasionally difficult to read, and can therefore be a likely cause of the small error.

Deviations are more present when comparing natural frequencies in Simpack (Table 5.2) to DNV GL's results. The first mode is overestimated by Simpack, whereas the second and third are underestimated. A maximum difference of 1.4% (overestimation of ω_{n1}) is however viewed acceptable.

The values of stiffness and MOI, taken from mass elastic data, are defined identically in the two softwares. However, the way stiffness is introduced through their associated shaft elements differs. Simpack defines stiffness K through force elements where rotational stiffness is introduced about the body reference frame axis of the 'previous' inertia. Previous is in this context the inertia to the left of the shaft (see Simpack model in Figure 4.6). Nauticus Machinery on the other hand, does not define markers, joints or body reference frames in the same way as Simpack does. Instead it uses simple shaft elements with parameter 'torsional stiffness' without any further explanation in its manual [47]. Differences in the two softwares' calculated natural frequencies are in this way expected.

At last follows a summary of the modelling verification. The relatively small deviations in calculated natural frequencies, for both softwares, are within acceptable levels. Furthermore, their causes have been justified and accepted, resulting in a successful verification outcome for both models after free vibration analyzes.

Chapter 6

Forced Vibration Analysis

Critical speeds are revealed in Campbell diagrams by the natural frequencies from Nauticus Machinery. Since Simpack gives almost the same magnitudes of ω_n, it will not be performed twice. An investigation of power spectra will further evaluate the detected critical speeds. Since time series are required to make plots of PSD, results from Simpack will also be used.

Vibration analyzes under external excitations in both softwares will be presented afterwards. A brief introduction to transient simulation will also be included. Results from Nauticus Machinery will be verified by comparison to studies by DNV GL. Simpack on the other hand, cannot use the same approach since both engine torque and variable propeller damping differs. However, since the undamped dynamic properties are identical, the same resonance speed should be detected in Simpack.

The final goal from these studies is detection of critical components and dangerous excitation frequencies. Results from free vibration analyzes will be taken into account in this evaluation.

6.1 Critical Speeds

Campbell diagrams identify critical speeds, but they cannot imply which of them that are most dangerous. Power spectra are useful in this process, as they investigate energy levels at different frequencies. Plots of PSD can consequently reveal the 'real' resonance conditions.

6.1.1 Campbell Diagrams

As presented in the methodology chapter, section 3.4.4, it is the natural frequencies and external excitations that determine critical speeds of a propulsion system. Results from the free vibration analyzes in Nauticus Machinery, in terms of parameter ω_n, will be used in this process. Critical engine frequencies will be investigated first, followed by an evaluation of the propeller's influence.

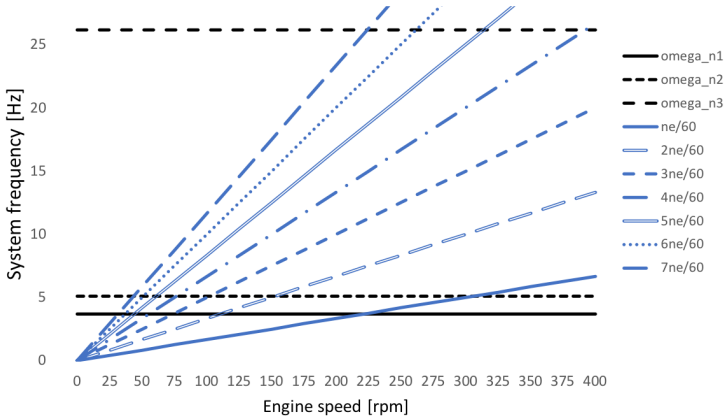

Figure 6.1: Campbell diagram for engine excitations

Repeating the construction of a Campbell diagram, natural frequencies are plotted as horizontal lines and external excitations as tilted. The first three modes of ω_n are taken from Table 5.1, and engine excitations have been assumed as multiples of its working cycle according to Equation 3.30. Crit-

ical speeds reveal at the intersection points. Since they are associated with resonance and thereby natural frequencies, one should be able to recognize all ω_n in rpm on the x-axis vertically down from these spots.

The first natural frequency, of around 222 rpm, can be found at the intersection between ne/60 and ω_{n1}. 306 rpm on the other hand, is caused by the first order engine excitation and ω_{n2}. The x-axis in Figure 6.1 is limited to the operational window of the drive train, such that the third natural frequency (1570 rpm) is not depicted. All frequencies in Table 5.1 have now been identified in the Campbell diagram as critical speeds caused by the first order engine excitation (ne/60).

Higher excitation orders reveal critical speeds other than the natural frequencies. These revolutions cannot be detected by studying eigenvalues alone, which proves the importance of the Campbell diagram.

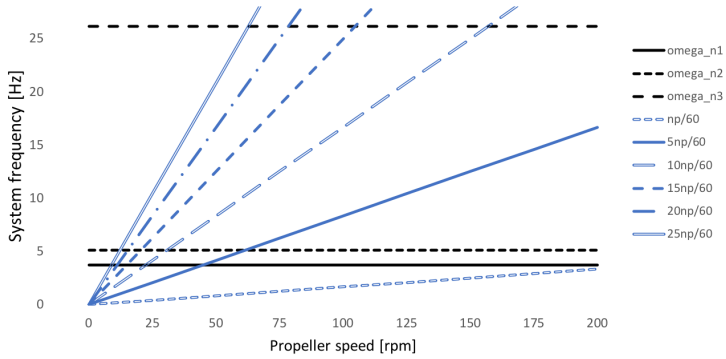

Figure 6.2: Campbell diagram for propeller excitations

Since engine and propeller speeds are equal in a direct-drive arrangement, excitations from these components will overlap at certain orders. Figure 6.2 shows the Campbell diagram based on Formula 3.31. The second order FPP-excitation (5np/60) is identical to the engine's 5ne/60, and so on. At these specific loads, there is reason to expect large vibration amplitudes, overlapping excitations from both of these sources increase responses. The first overlap between np/60 and ne/60 is not accounted for here as the as-

sociated rpm of 222 is outside the operational window of the drive train.

According to the illustrations above, there are potentially multiple excitations that can harm the propulsion system. Being able to separate them from each other requires analyzes of energy levels. Power spectral density is therefore studied in the next section.

6.1.2 Power Spectrum

Power spectrum is constructed from time series of torque at resonance speed in this analysis. Since torque is input, the unit on y-axis is $(\mathrm{Nm})^2/(\mathrm{rad/s})$, normalized with respect to angular velocity. The WAFO toolbox makes plots of function $S(\omega)$, facilitated by the MATLAB script in Appendix E.2.1.

Figure 6.3 shows the power spectrum of the intermediate shaft. Similar plots were made for other segments, and at different speeds, attached in Appendix E.2.2. They are left out since they prove the same points as the presented example.

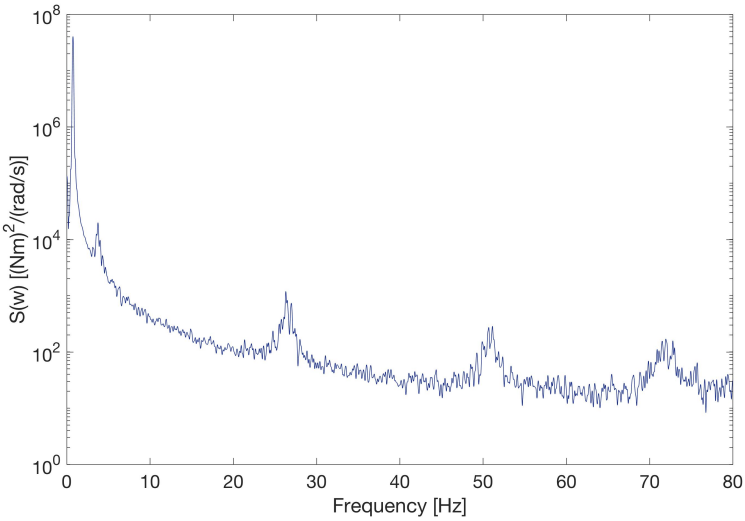

Figure 6.3: Power spectrum of intermediate shaft (from torque at 45 rpm)

Function $S(\omega)$ displays energy levels in the intermediate shaft at different frequencies in hertz. It clearly implies that the segment is subjected to the highest energy levels at around 3 Hz, the first natural frequency in Table 5.1. Power spectral density thereafter decreases with higher frequencies. The most dangerous resonance conditions are those initiated by ω_{n1}, thereafter ω_{n2} (5 Hz) and ω_{n3} (26 Hz), according to this plot. The trend supports representation of only the first three natural frequencies in Chapter 5.

6.1.3 Discussion

The power spectrum of the intermediate shaft indicates that the first natural frequency contains most energy. In further analyzes, only critical speeds caused by ω_{n1} will then be evaluated. Looking back at the two Campbell diagrams, the critical speeds of interest are now reduced to a manageable amount. Moreover, by neglecting engine speeds outside the operational window (MCR = 77 rpm), the number is reduced even further.

Special attention should be given to the critical speeds where propeller and engine excitations overlap. Fifth order engine excitation (5ne/60) equals to the second order propeller torque (5np/60) as one example. This results in a significant load at 45 rpm operation, which verifies the engine's barred speed range (between 40 and 51 rpm). The same will hold for 10np/60 and 10ne/60, associated with around 22 rpm. In further forced vibration analyzes, one should expect noticeable displacements at these specific resonance speeds.

6.2 Forced Vibration Analysis in Nauticus Torsional Vibration

The system's torsional behavior, under the applied load case, is presented in terms of torsional stress and torque amplitudes in the shafts. They are calculated based on expressions from section 3.5.2. All results are plotted

against speed (due to frequency domain simulation) in Figure 6.4. Maximum magnitudes of torque and stress are attached in Appendix C.2.3.

The term 'synthesis' here describes vector sum. Presented plots from the software are consequently maximum amplitude at a given speed over one revolution. The angular displacement is then the average of extrema during this specific rotation. View attachment C.2.2 for further explanation.

Beginning with torque amplitudes in Figure 6.4, there are significant peaks at around 22.5 and 44.4 rpm. They are caused by the first natural frequency with the highest level of energy. Furthermore, they are initiated by the mentioned overlap between engine and propeller excitations. Due to the latter, these critical speeds are especially prominent. Observe also that torque levels generally are highest in the crank shaft and segments after the engine. All parts before them are better protected by the damper.

Torsional stress is proportional to internal shaft torque, and therefore shares similar characteristics over the frequency range. However, due to their dimensions, the intermediate and propeller shafts experience highest stress levels. Referring to the definition of torsional stress in Equation 3.32, it is dependent on both shaft torque and dimensions. The latter term, radius divided by second moment of area, is what causes the differences. The magnitude of the damper stiffness is almost zero, also based on this statement.

Another important discovery is that the maximum values of shaft torque and stress takes place within the barred speed range of the diesel engine. It verifies the fact that this speed range should be avoided and passed fast through, which is indeed the definition of the term.

Last but not least, the dissipated heat from the TVD shows that this component is most active at speeds over 45 rpm. This corresponds to a higher power loss from the damper during operation within this range.

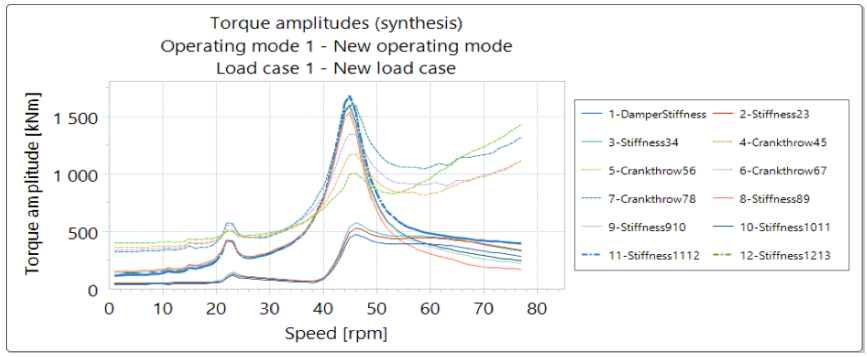

(a) Torque amplitudes [kNm]

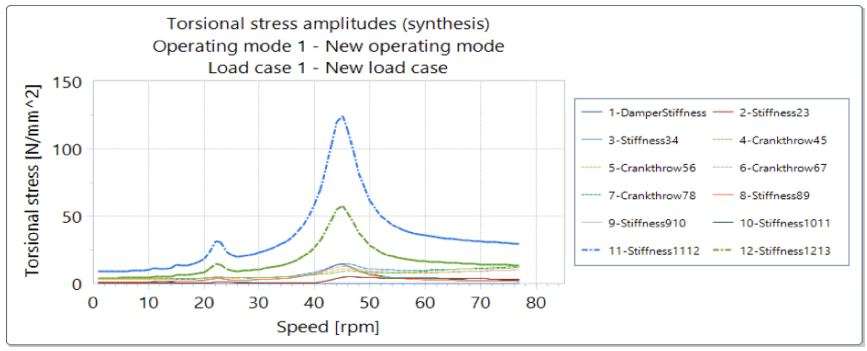

(b) Torsional stress amplitudes [N/mm^2]

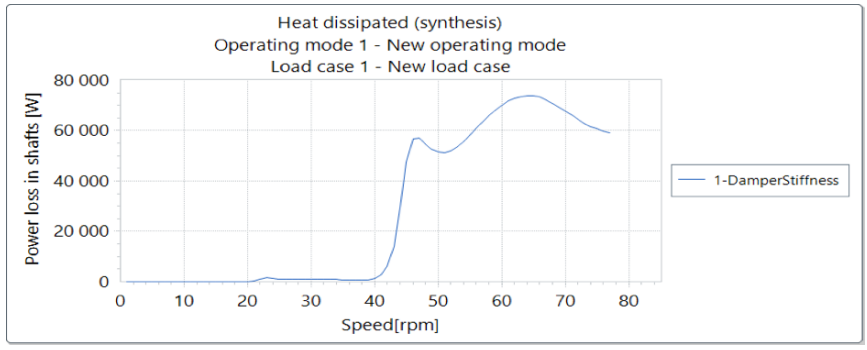

(c) Dissipated heat from TVD [W]

Figure 6.4: Results from forced vibration analyzes in Nauticus Machinery

Presented results in this section show similar trends as graphs from DNV GL in Appendix B.1. The constructed Nauticus Machinery model is thereby verified, and can now be used to evaluate vibration reduction measures.

6.3 Forced Vibration Analysis in Simpack

An important feature during time domain simulation is selecting an appropriate sampling rate. According to the *Nyquist rate*, it must be at least two times the maximum frequency of the signal that should be investigated [32]. If this criterion is not followed, information might be lost. Referring to results from free vibration analyzes of the drive train, the third and highest mode evaluated is 26.13 hertz. The selected sampling rate should consequently be at least 53 Hz. In the forced vibration analysis that follows, a solver frequency of 200 Hz was used. This is within the Nyquist requirement such that all three natural frequencies should be detected in the results, or in other words can be reconstructed from the sampled data.

The applied time integration method is named 'SODASRT 2' by the Simpack syntax. It solves the full set of equations of motion over time, and is the default and recommended integrator of the software [10]. Forced vibration simulation is firstly performed for one operational speed at a time, namely steady state analysis. Thereafter follows an attempt where the reference speed is changed during one run to study transient behavior. Before each simulation it has been checked that the system is in static equilibrium. If this is not fulfilled, the software cannot solve the eom. Time domain results will be used to study fatigue damage in the drive train in the next chapter.

6.3.1 Steady State Simulation

Propulsion system operation is simulated for 75 seconds each at the followings speeds: 10, 20, 30, 45, 50, 60, 70 and 77 rpm. 45 and 77 revolutions per minute were selected since they are the first natural frequency and maximum continuous rating in that order. The body angular velocity, measured at e.g. the propeller joint, should stabilize at the relevant speed in radians per second to know that the simulation went well.

Each run should give a magnitude of the propeller torque that is smaller than the applied engine load. Parts of the external excitation are lost due to

the dynamics of the system. Furthermore, the engine and propeller torque should have opposite mathematical signs. The latter is negative and represents the system's resistance to the applied load. Mentioned trends are visualized in illustration 6.5, where the positive values are engine torque and the negative are magnitudes of the propeller.

During simulation it was shown that the utilized approach for introduction of engine torque, by using the propeller law, is not valid at the two lowest speeds of 10 and 20 rpm. In these two cases, Simpack outputs a propeller torque larger than the engine load. The approximated baseline of harmonic T_{eng}, taken from the engine curve, is too low to actually reach the reference speed. By studying the left part of Figure 4.9, this becomes understandable. The engine curve estimates very low torque magnitudes at 10 rpm and 20 rpm compared to other speeds. The explanation is the mathematical behavior of a square function, which is the form of the assumed baseline T_0. The result is underestimated engine torques at low speeds. To compensate for the lack of external excitation, the PID-controller increases the magnitude of the propeller torque. 10 and 20 rpm operation are therefore left out in further research where the Simpack model is used.

The diagram below shows engine and propeller torque at three different operational speeds. Harmonics of T_{eng} are the positive sine functions, whereas the controller outputs are the negative time series. The oscillations in propeller torque during the first 40 seconds are a result of the controller tuning process. This is the period where the PID-regulator works to stabilize the system at desired reference speed. The response time is acceptable. Further reduction of oscillations and stabilization time would require modified controller gains. Notice that magnitudes of both engine and propeller torque decrease quite remarkably with reduced operational speed. Due to the selected introduction method of applied engine load, this is as expected (reference to section 4.2.2).

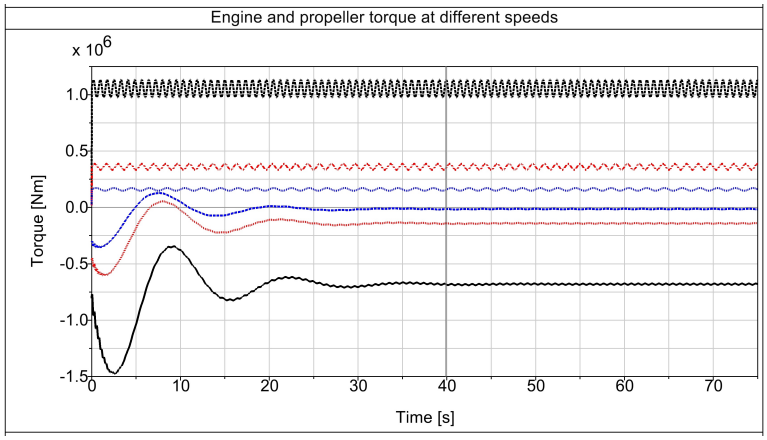

Figure 6.5: Engine and propeller torque at different speeds (Black=77rpm, Red=45rpm, Blue=30rpm)

The performed simulations aim at studying steady state behavior in terms of torque. Since it takes about 40 simulation seconds until the rotational speed has stabilized, only results from the last 35 seconds will be investigated and discussed further. This is symbolized by the vertical line in Figure 6.5.

Illustration 6.6 is a zoom in on the stable region of 45 rpm operation. Mass damping torque ($C_{abs} \cdot \dot{\theta}$) are the green lines. According to the eom from forced vibration theory (section 3.4.3), the propeller torque will be the applied engine harmonics minus system dynamics including stiffness and damping.

The next figure contains internal shaft torque in a selection of propulsion system segments. They are caused by rotational stiffness and damping according to Formula 3.34. Oscillation characteristics differ quite a lot depending on which shaft that is being investigated. Observe that the red and black time series, shaft 2-3 and 9-10, oscillate with large amplitudes and rapid turn overs. The torques in the other shafts are periodic and much calmer.

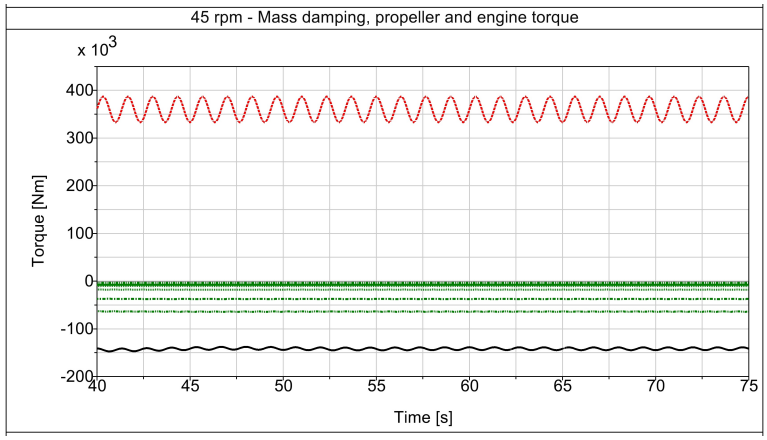

Figure 6.6: Torque levels at 45 rpm operation (Red=T_{eng}, Green=Mass damping, Black=Propeller torque

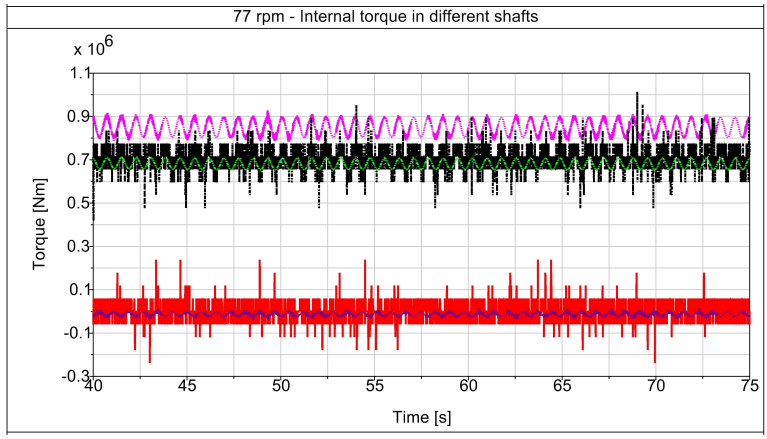

Figure 6.7: Internal torque at 77 rpm operation for a selection of shafts (Magenta=CT3, Black=Shaft 9-10, Green=Interm. and Prop. shaft, Red=Shaft 2-3, Purple=Shaft 3-4

Verification of resonance speed

Resonance can be detected by higher relative oscillation amplitudes between response and applied engine torque. Referring to the non-dimensional ampli-

tude ratio in Formula 3.20 and its associated figure, ratio X_{ampl} underneath should be highest at resonance speed. The numerator is the amplitude of internal shaft torque from Simpack, and the denominator is the amplitude of harmonic engine torque.

$$X_{ampl} = \frac{\Theta_{response}}{2 \cdot (0.075 \cdot T_0)} \tag{6.1}$$

Amplitude ratios have been calculated for a selection of shafts. Their internal torque amplitudes ($\Theta_{response}$) are found by use of similar plots as those in illustration 6.7 above. T_0 is calculated from the engine curve, and must be multiplied by two since $0.075 \cdot T_0$ is a half-amplitude.

X_{ampl} is plotted against frequency ratio ω/ω_{n1} underneath. The graphs look similar to the ones in illustration 3.9, where amplitude ratio generally is lowest at higher frequencies. All four shafts have peaks at the critical speed, justifying that operation at 45 rpm leads to resonance. This again verifies the undamped dynamics of the Simpack model. However, remember that torque levels in Simpack cannot directly be compared to Nauticus Machinery results.

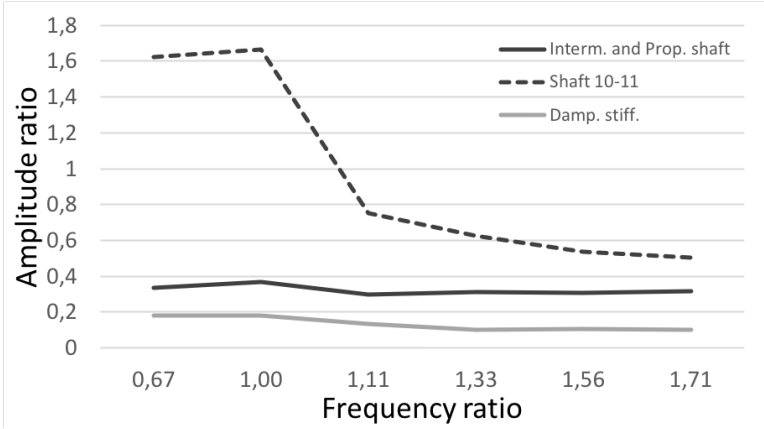

Figure 6.8: Amplitude against frequency ratio

6.3.2 Variable Reference Speed and Transient Regions

By use of the MATLAB script in Appendix D.3.3, the controller's reference speed has been updated seven times during one simulation. These speeds are multiples of eleven, up to 77 rpm. The graph of the propeller's angular velocity, shows how the propulsion system stabilizes at these values one at a time. The interesting regions during this case study is the transient parts in between two reference speeds.

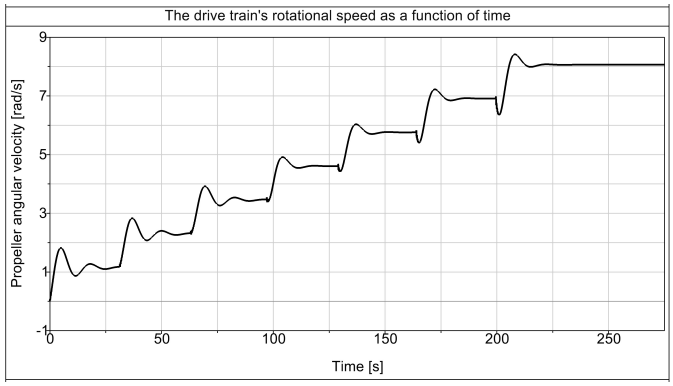

Figure 6.9: Variations in rotational speed with time

Figure 6.10 depicts the behavior of shaft torque when rotational speed shifts from 33 to 44 rpm, after around 100 seconds. It is evident from the graphs that these transient regions contain dangerous oscillations. Their magnitudes at these peaks are also higher than when the speed has stabilized, which can pose a risk towards ultimate limit state. Their rapid turn overs on the other hand, should be addressed with regards to fatigue.

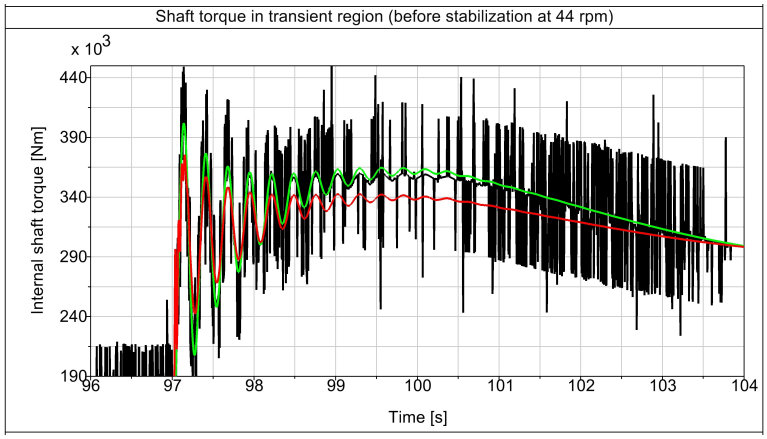

Figure 6.10: Shaft torque oscillations in transient region (Red=CT3, Black=Shaft 9-10, Green=Interm. and Prop. shaft)

Transient regions have not been studied further, but this case study proves the importance of their attention and detection. The illustration above clearly shows that they are dangerous, both towards maximum peaks and thereby torsional fracture, but also with respect to sudden fatigue failure. In the physical drive train, transient regions are typically a concern during engine start-up and stop.

6.4 Discussion

The two software models have in this chapter been tested with applied load cases. A drawback with Nauticus Machinery is that simulation only is available in frequency domain. Nonetheless, this software enables a good representation of the drive train's engine and propeller, probably the most vital components of the drive train. During modelling in Simpack on the other hand, the hydrodynamic propeller damping was not implemented, in addition to a quite simple representation of the engine torque. Despite these deficiencies, Simpack MBS Software introduces the aspect of time.

Using either of the two softwares is in this way associated with both downsides and advantages. The gain in having the two, is that they enable one post-processing study each. Since the model in Nauticus Machinery best represents the physical drive train, it will be used in studies of vibration reduction for the system. Due to Simpack's time domain results, it is also possible to study fatigue damage and transient behavior. These investigations however, cannot precisely detect hazards because the forced vibration results have not been verified by real measurements, which is the case for Nauticus Torsional Vibration. On the other hand, since the Simpack simulations are conservative, they could potentially be useful. As an example, the torque amplitude in the intermediate shaft at MCR has a magnitude of around 700 kNm in Simpack (see figure 6.7), against 400 kNm in Nauticus Machinery (see figure 6.4a). Taking into account that steady state simulations in the DNV GL-software are 'worst case', it presents peak values, the Simpack model could potentially be used in a rough estimate of fatigue life evaluation. What is more certain, is that the results can exemplify the process of fatigue detection and identify causes of this phenomenon, which is approached in the next chapter.

One should also keep in mind the drawbacks when using the constant magnifier model to introduce relative shaft and absolute mass damping. Only responses at the first natural frequency, which was used to calculate the constant damping factors, are estimated properly for a multi-mass system by use of this approach. However, these results may be non-conservative at resonance speed according to Dahler et al. [14]. One should generally be careful to anticipate that the model is valid for non-resonance speeds as well. This implies uncertainty for utilization of these results in further post-processing analyzes.

At the same time, the actual ratio of the shafts' and masses' contribution (excluding the propeller) in the total damping of the system is important in this evaluation. According to the literature, the propeller is the main source of damping in a drive train [14] [31]. Furthermore, the propeller's variable percent of critical damping-model is conservative at high speeds. This could indicate that the results might be used more generally than for

the speed used to calculate the constant damping factors. In further work, this assumption would enable an evaluation of the physical drive train, for example a comparison to regulatory limits for approval. Another example is testing of additional damping efforts, which will be attempted in Chapter 8 of this report. Obtained damping will then be measured as reduced vibration responses at resonance speed.

After free and forced vibration analyzes, it is time to summarize the detected critical speeds and vulnerable parts of the propulsion shaft. Being most critical means for a rotational speed that it will cause the most severe damages, and for a shaft segment that it will fail first. Vibration levels and fatigue damage should therefore be evaluated at these specific revolutions and at these parts of the drive train.

The Campbell diagram revealed several critical speeds. However, after an investigation of power spectrum, around 22 and 45 rpm are viewed most dangerous. Since the second is located within the barred speed range, and gave the highest response peaks in Nauticus Machinery, only this will be evaluated in further analyzes. The specific fuel consumption of an engine is lowest at around 80% of MCR power [50] [57]. Using the drive train's engine curve, this corresponds to an operational speed of 71 rpm. To save fuel, this speed is assumed as 'normal operation', applicable for sailing at open sea. For simplification, since 71 rpm is in close vicinity of MCR condition, the MCR condition will also be evaluated in further analyzes. The rotational speeds of interest are then:

- *45 rpm (the most severe resonance speed)*
- *77 rpm (MCR condition, close to 'normal operation')*

Based on peaks in torque and torsional stress amplitudes, analyzes in Nauticus Machinery point out the intermediate, propeller and crank shafts. Simpack also adds the aspect of oscillations over time, and thereby addresses shaft 2-3 and 9-10, which are located before the engine and in between the camdrive and second moment compensator respectively. Accounting for mode shapes from free vibration analysis (same for both softwares), the

shafts with stationary points are the intermediate shaft and the third crank throw. As a result of these findings, the shafts underneath will mainly be focused on in the next chapters. Segments are given names according to their two associated inertias on each side. The masses and their IDs are displayed in Table 3.4, under specifics about the drive train.

- *Shaft 2-3*
- *Crank throw 6-7 (no. 3)*
- *Shaft 9-10*
- *Intermediate shaft (11-12)*
- *Propeller shaft (12-13)*

Chapter 7

Short Term Fatigue Analysis

Torsional vibrations are not only associated with ultimate limit state (ULS), they also affect fatigue. This chapter aim at presenting the link between vibrations and fatigue. Time domain simulation is the basis in these studies since it is the number of cycles, not peak amplitudes in ULS, that cause the phenomenon. The Simpack model will therefore be utilized, not Nauticus Machinery which perform steady state frequency domain simulation.

Two different case studies are selected to investigate the fatigue life of the propulsion system. The first of them involves investigation of all shafts with the speed kept constant. The second study on the other hand, evaluates one shaft at a time, comparing fatigue damage at different speeds. Investigated revolutions per minute and shafts with special attention, are selected based on results from free and forced vibration analyzes in previous chapters.

7.1 Procedure

Calculating fatigue damage is the final goal of this chapter. The procedure and required steps to get there are as follows:

(1) Create time series of torsional stress based on shaft torque results from

Simpack time domain simulation

(2) Determine the shafting material's parameters from its unique SN curve

(3) Count cycles at different stress levels by use of the rain flow cycle counting method

(4) Calculate accumulated fatigue damage over the investigated time period t

Simulations in Simpack were run for 75 seconds each, but only the last part can be used since this is when the set point speed has stabilized. The investigated time period is thirty seconds, namely $t = 30$ s. Fatigue analyzes in this research are consequently *short term* studies, not long term.

The first step above will be performed by exporting torque series from Simpack post-processor as text files. Since the sampling rate is 200 Hz, these time series will give torque magnitudes at every 0.005 seconds. A MATLAB script (attached in Appendix E.3) will transfer these magnitudes into torsional stress $\tau(t)$ according to Equation 3.32.

Step number two of the procedure is already clarified. The selected shafting material is the alloy steel 16MnCr5, with properties given in Table 3.1. The third and fourth tasks are completed by use of the WAFO toolbox (reference to section 3.5.3), accessed and ran in MATLAB by use of the script in Appendix E.3.

7.2 Case Studies

Mode shapes from free vibration analyzes, in addition to results from time domain simulations, helped determine the investigated load cases. They revolve around shaft 2-3, the third crank throw, shaft 9-10, the intermediate and propeller shaft. Stationary points are normally associated with torsional fracture, but if the shaft is subjected to fatigue as well, the risk of damage increases. The engine speeds of interest are further 45 and 77 rpm, a reso-

nance speed and the MCR condition respectively. All mentioned speeds and shaft segments will be investigated in the two case studies to come.

7.2.1 Constant Speed, Different Shafts

Table 7.1 presents fatigue damage at each shaft over a time period of 30 seconds. Load case 1 is a critical speed, whereas load case 2 is MCR condition. In relation to the shafts' overall lifetime, the investigated period is very short. This can explain the very small fatigue damages in Table 7.1. Consequently, one cannot conclude based on these results whether the shaft will fail due to fatigue or not. Nevertheless, the results can imply damages in each shaft relative to each other. This is also valuable knowledge.

Table 7.1: Fatigue damage in shafts at 45 and 77 rpm operation

Shaft	**D at 45 rpm** $[\cdot 10^{20}]$	**D at 77 rpm** $[\cdot 10^{20}]$
Damp. stiff.	1.4E-31	1.54E-29
Shaft 2-3	6.2E-01	1.60E-01
Shaft 3-4	2.6E-06	5.55E-07
CT1	3.9E-05	1.35E-03
CT2	4.9E-05	7.63E-04
CT3	4.2E-05	3.66E-04
CT4	4.0E-05	1.90E-04
Shaft 8-9	5.0E-05	1.10E-04
Shaft 9-10	2.94	4.10E-01
Shaft 10-11	5.8E-05	1.02E-04
Interm. shaft	1.0E-03	1.31
Prop. shaft	1.8E-05	1.15E-02

As expected, the damage is generally high in shaft 2-3 and 9-10. This can be justified by high torque amplitudes and many oscillations compared to in the other parts (see Figure 6.7). What is more surprising, is that the intermediate shaft experiences the largest fatigue damage at 77 rpm

operation, even though the torque amplitudes are not the highest (reference to Figure 6.7). This shaft is subjected to fatigue partly due its dimensions. Shaft 2-3 and 9-10 are hollow with an outer diameter of 820 mm, whereas the intermediate shaft is circular with half of this diameter. Larger fatigue in the intermediate shaft is consequently justified by its relatively high magnitude of the torsional stress term r/I_{shaft} (73.9 against 9.3 for the hollow shafts). Looking back at the definition of torsional stress (Formula 3.32), proves the importance of this value related to fatigue. This can also explain the almost negligible damage in the torsional vibration damper.

Ratios X_ω, damage in shaft i divided by the maximum damage, are plotted in Figure 7.1 to show the levels relative to each other. This graph visualizes the peaks at the mentioned shafts even better. Observe that 45 rpm gives higher fatigue damage than MCR for shaft 2-3 and 9-10, which is reasonable as the first speed is associated with resonance and large oscillation amplitudes.

$$X_\omega = \frac{D_{shaft,i}}{D_{max}} \tag{7.1}$$

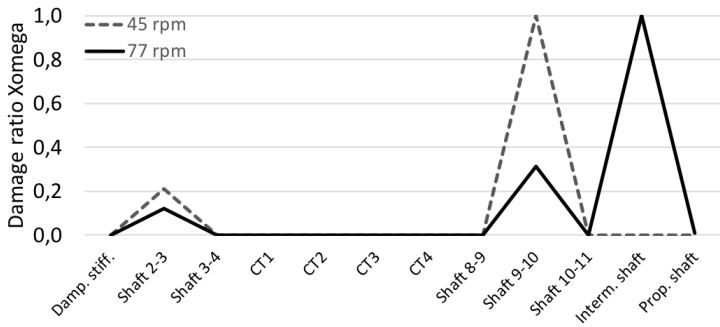

Figure 7.1: Damage ratio X for constant speeds (D shaft i/Max D)

Studying Table 7.1 further, shows a large increase in fatigue damage from operation at 45 to 77 rpm at the intermediate and propeller shaft. Damage is increased with a factor of around 10^3, instead of being decreased when

resonance speed is avoided. Remember that even though critical speeds lead to higher relative increase in amplitudes (see section 6.3.1), the oscillations might actually be larger and more rapid at other revolutions per minute, namely what initiates fatigue. The next two figures can explain this trend by showing plots from fatigue analyzes of the intermediate segment.

Both illustration 7.2 and 7.3 are divided into three sub figures. (a) shows the so called *rain flow matrix*, denoted RFM. With maximum stress level on the y-axis, against minimum on the x-axis, this plot displays the distribution of peaks and valleys of the half-cycle rain flows. Reference to section 3.5.3, a rain flow begins at a peak ('Max stress') and terminates at a valley ('Min stress'), or opposite. The square in the upper left corner of Figure 7.2a for example, is a rain flow with a peak equal to 11.2 MPa, which terminates at a valley of around 9.7 MPa. This single rain flow corresponds to a stress range of 1.5 MPa, visualized as the almost unrecognizable bin in sub figure (b). More squares in close vicinity to each other means a higher number of cycles in the RFC histogram at these stress ranges. The rest of the squares at max 11.1 and min 9.8 create the bins around stress level 1.3 in Figure 7.2b.

The last sub figure is a graph of torsional stress against simulation time. Both RFM and RFC plots are created and calculated based on this respective time series according to fatigue theory and the WAFO toolbox. Axes of the rain flow matrix plot can be recognized from the oscillating stress function. All three sub figures are in this way closely related to each other. Comparing them at critical and MCR operation, will reveal why fatigue damage in the intermediate shaft increases with higher ω.

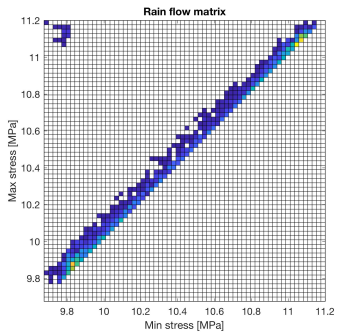

(a) Rain flow matrix

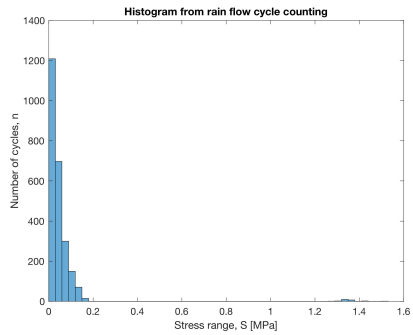

(b) RFC histogram

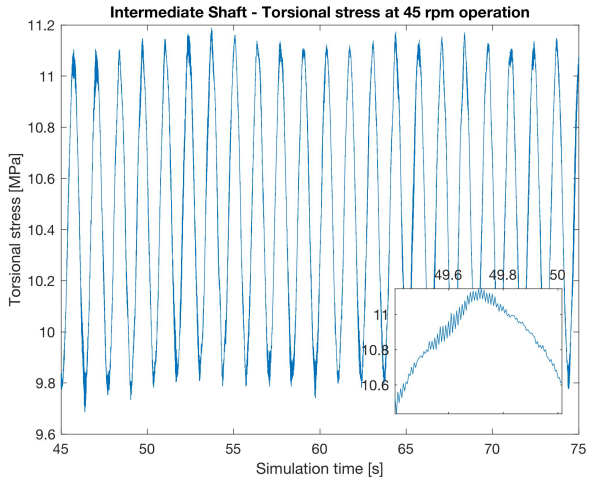

(c) Torsional stress

Figure 7.2: Intermediate shaft - Plots from fatigue analyzes at 45 rpm

First of all, time series of stress shows that the average amplitude at 77 rpm is higher than at 45, around 3.7 against 1.3 MPa. This alone implies that fatigue damage most likely is higher at MCR speed. Furthermore, more rapid oscillations suggest a higher number of cycles which provokes fatigue. However, zooming in on the graphs can show crucial oscillation properties. It can be the case that the number of half cycles with maximum amplitude is larger at 45 rpm compared to 77. If so, fatigue damage can be larger at critical speed even though its maximum stress range is lower. This

comparison should be addressed.

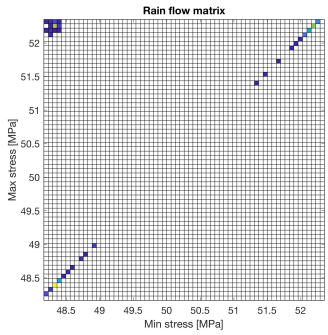

(a) Rain flow matrix

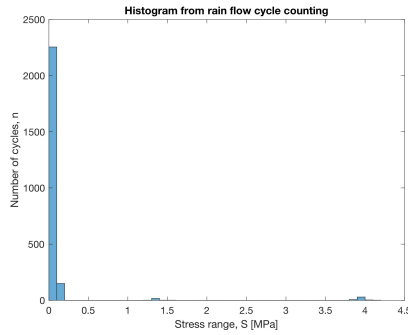

(b) RFC histogram

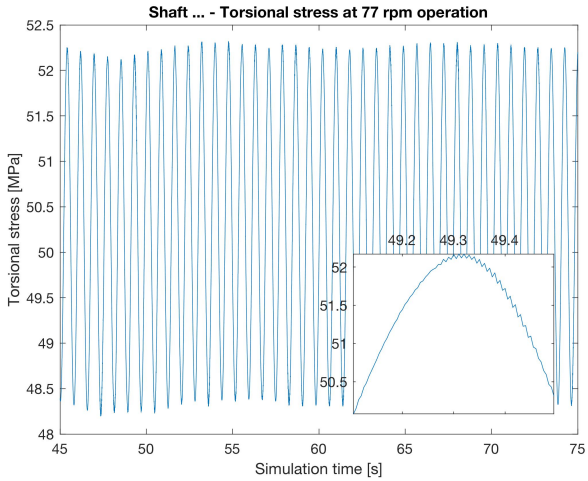

(c) Torsional stress

Figure 7.3: Intermediate shaft - Plots from fatigue analyzes at 77 rpm

Sub figure (c) for 45 rpm, displays that torsional stress generally oscillates continuously over the whole simulation time, caused by resonance. MCR condition on the other hand, shares the same characteristic only close to peaks and valleys, explaining the symmetric RFM in Figure 7.3a. The statement in the previous paragraph is therefore not applicable for this specific case study. More chops in the resonance stress function decrease the number of half cycles with maximum stress range. Furthermore, the two RFC

plots are quite similar at low levels of stress, such that the main and crucial difference is the number of cycles with high stress range. They are around 50 at resonance speed against 200 at MCR. A larger fatigue damage in the intermediate shaft at 77 rpm, see Figure 7.1, is thereby justified.

7.2.2 Same Shaft, Different Speeds

This case study investigates short term damage (still $t = 30$s) at a careful selection of four shafts during operation at 30 rpm to MCR. The reason why lower speeds are neglected, is explained during forced vibration analyzes in Simpack.

Table 7.2 shows two general trends: damage in shaft 2-3 and 9-10 decreases with increased speed, while the crank throw and intermediate shaft experience more fatigue when ω goes up. These patterns can also be displayed by plotting ratio X_{shaft} for each shaft, the damage at a speed divided by the minimum magnitude. Due to highest relative changes for the intermediate shaft, ratios for this segment are plotted in a separate diagram (to the right in Figure 7.4).

$$X_{shaft} = \frac{D_\omega}{D_{min}} \tag{7.2}$$

Table 7.2: Fatigue damage in a selection of shafts at different ω

Speed	**Fatigue Damage**			
$\boldsymbol{\omega}$	**Shaft 2-3**	**CT3**	**Shaft 9-10**	**Interm. shaft**
[rpm]	$[\cdot 10^{20}]$	$[\cdot 10^{20}]$	$[\cdot 10^{20}]$	$[\cdot 10^{20}]$
30	5.91	6.02E-05	1.27E+01	1.03E-05
45	6.23E-01	4.24E-05	2.94	1.01E-03
50	9.39E-01	4.04E-05	2.92	3.73E-03
60	7.10E-01	3.93E-05	4.91E-01	3.67E-02
70	5.83E-01	1.62E-04	7.33E-01	3.51E-01
77	1.60E-01	3.66E-04	4.10E-01	1.31

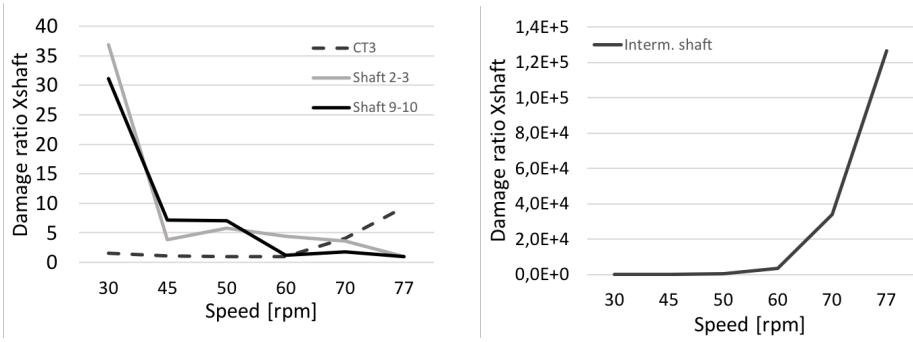

Figure 7.4: Damage ratio X for constant shaft (D at ω / Min D)

Some of the results in this case study overlap with the previous. Again it is clear that the shafts in first and third column have the highest damages over all. Furthermore, as already commented, the intermediate shaft experiences a noticeably large increase in fatigue at speeds over 60 rpm. This time the torque results from Simpack simulation will be used for justification. The illustration beneath shows torque in the intermediate shaft at all investigated speeds. The black curve on the bottom is 30 rpm, and the one on top is the highest speed of 77. It illustrates that there is a distinction between torque oscillations at the three lowest and three highest rpm, in line with Figure 7.4. A torque plot with similar characteristics can be made for the crank throw segment (CT3), proving that fatigue increases with higher speeds for these two shafts.

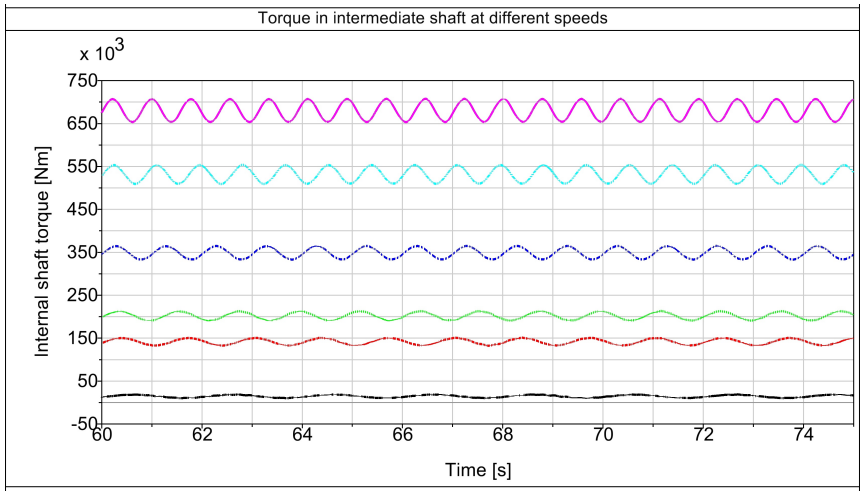

Figure 7.5: Changes in intermediate shaft torque with speed

The opposite development is the case for shaft 2-3 and 9-10, oscillations decrease when speed is increased. Plotted time series of torque at shaft 9-10 depicts that oscillations are calmer at 77 rpm (purple) than at 60 (blue) and 30 (black). This trend is also applicable for shaft 2-3. Fatigue damage calculations are consequently in line with time domain results from Simpack.

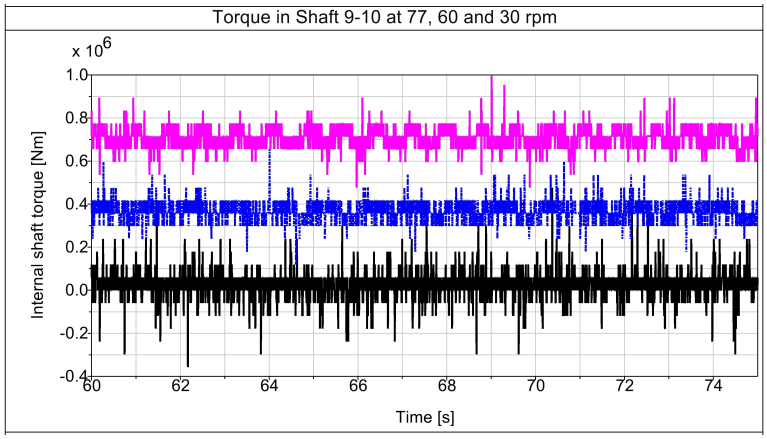

Figure 7.6: Changes in torque at Shaft 9-10 with speed

Rain flow matrices and histograms where utilized in the first case study to

prove initiation of fatigue. This has not been approached in the second, since it was desirable to show that also time series of torque can prove damage trends. Internal shaft torque is the same as torsional vibrations, namely angular displacements deviant from reference position.

7.3 Discussion

Each of the two case studies from Simpack post-processing have revealed different types of triggers leading to fatigue damage. The first case study compared fatigue levels at all propulsion shafts at a constant speed. Operation at 45 rpm, a resonance speed, showed that shaft 2-3 and 9-10 generally had the highest levels of fatigue. This proves that high torsional stress amplitudes and many cycles with large stress ranges (namely high levels of torsional vibrations), which is the case for these two shafts, provoke this type of failure. Running thereafter at MCR condition implied that not only dangerous oscillations play a role, but also shaft dimensions through the r/I_{shaft}-term of torsional stress. Higher magnitude means larger torsional stress and therefore increased risk of fatigue. Lastly it was addressed that oscillation properties, such as a broken graph, can affect the number of cycles with maximum stress range. If time series of stress are not smooth, this number will decrease.

The second case study treated one shaft at a time (from a careful selection) running at speeds from 30 to 77 rpm. It was shown that the third crank throw and the intermediate shaft experience largest fatigue damage at high revolutions. Referring to free vibration analyzes and normal modes, these two shaft segments contain stationary points as well. Adding fatigue damage to this load is a dangerous combination which should be addressed. MCR condition is in fact close to normal sailing speed (71 rpm), a condition which occupies large parts of the vessel's operational profile.

The other investigated parts, before the engine (shaft 2-3) and at the end of it (shaft 9-10), showed an opposite trend where damage decreases when the speed is raised. These two segments are subjected to the highest torque

oscillations in general, referring to forced vibration analyzes in Simpack. For the overall damage in the system, it is therefore positive that fatigue goes down with increased speeds in these specific shafts.

Analyzes in this chapter have identified both shafts and speeds associated with noticeable fatigue damages. The highest detected damage level, with a magnitude of 10^{-19}, takes place between the camdrive and the second moment compensator (shaft 9-10) at 30 rpm. Based on that result, this shaft will fail first due to fatigue. However, it should be repeated that only short term damage has been calculated. Furthermore, the applied engine torque and propeller damping are not identical to the input in Nauticus Machinery, which makes it questionable whether the findings can be transferred to fault detection in the physical propulsion system. Anyhow, the two case studies showed connections between drive train properties, torsional stress and fatigue. Since stress is proportional to shaft torque amplitudes, where the latter can be viewed as vibrations, these studies also showed the link between torsional vibrations and fatigue damage. In later work, with a correct representation of applied engine torque and propeller damping, the same procedure can easily be conducted over again.

Referring to the literature review from section 2.2.4, IACS recommends a fatigue limit through their unified requirement number M68. This limit could have been suitable for evaluation of the calculated fatigue damages. However, since the analyzes above only assess short term failure, this is not applicable in this master thesis.

Chapter 8

Study of Vibration Reduction Measures

The drive train model in Nauticus Torsional Vibration is selected to perform a sensitivity analysis, which aim at studying the influence from system parameters on torsional vibrations. In this research, the focus is on shafting characteristics such as stiffness and damping factors, in addition to individual damping elements. Testing changes in engine or propeller design is outside the scope. There are consequently two main alternatives to reduce vibrations, either by changing natural frequency or by influencing the damping ratio. Both methods will be approached in this chapter. An explanation of how vibrations are effected by these parameters, and how they can be changed, follows in the next section.

Forced vibration analyzes in Nauticus Machinery detected stationary points and highest torque and stress levels in the following shaft segments: crank throw number 3, the intermediate shaft and propeller shaft. Vibration reduction in these parts of the drive train will consequently be in focus. The damper stiffness will also be added to this list since the TVD is important for the total system damping. Furthermore, mainly reductions in peak values (at resonance speed) will be discussed. These magnitudes are in general associated with greatest risk towards system failure.

In addition to modifications of system parameters, the significance of operational profiles will be discussed. A custom plan of operation might also reduce the impact from torsional vibrations on the propulsion system.

8.1 Sensitivity Analysis in Nauticus Machinery

A *sensitivity analysis* is studying how changes in an input parameter influence the output. With regards to vibration reduction, the output will be torque amplitudes and torsional stress levels. The input parameters on the other hand, are variables that affect natural frequency and damping ratio. Results from sensitivity analyzes in Nauticus Torsional Vibration are treated in an Excel sheet (see Appendix C.3). Only a selection of the results will be discussed, the rest are attached in the zip-file together with this report in DAIM.

Shifting the natural frequency region can reduce torsional vibrations in a propulsion system. If these critical speeds are moved outside the operational window of the drive train, resonance (and thereby severe vibrations) can be avoided. Referring to the theory of undamped free vibrations (section 3.3.2), the natural frequency of a torsional lumped mass system is defined as the square root of stiffness divided by moment of inertia. Natural frequency can therefore be influenced either by changing rotational stiffness or polar mass moment of inertia. The masses of the system are however assumed fixed, resulting in K to be the parameter that can be modified.

Damping ratio ζ is the actual damping factor of the system divided by the critical one. Parameter C can consequently change the value of this ratio. Repetition of the theory of free vibrations with damping can explain how this approach can influence vibration reduction. Looking back at Figure 3.7, either the critically damped ($\zeta = 1$) or overdamped case ($\zeta > 1$) are theoretically best. These are the two vibration forms without oscillations. However, obtaining damping ratios equal to or larger than one, is not realistic for the eco-ship. The shafts' percent of critical damping is currently only 1% (reference to Table 3.4). Anyhow, increased damping ratio in general

is advantageous according to illustration 3.9. The vibration amplitude will decrease with increased ζ, or in other words with higher damping factor C.

The existing link between ω_n and ζ is also interesting. Damping ratio is dependent on critical damping $(2 \cdot J \cdot \omega_n)$, and thereby the natural frequency. Lowering the latter implies higher damping ratio (ζ) and thereby reduced amplitude ratio, especially at resonance (see Figure 3.9). Additionally, a lowered ω_n results in higher frequency ratio (ω/ω_n) for a certain operational speed, which is associated with lower vibration amplitudes in general. This is visualized by moving further to the right, along the x-axis, in Figure 3.9. Remember further that shaft torque is proportional to torsional stress. A decrease in vibration amplitude is then the same as lowered stress level.

If not specified differently in the next sections, all mentioned reductions in torque and stress levels are the average decrease in torque and stress amplitudes at resonance speed in the following four segments on average: the damper stiffness, the third crank throw, the intermediate shaft and the propeller shaft.

8.1.1 Modification of Natural Frequency

Increased shaft stiffness

According to its definition (Equation 3.3), natural frequency will increase with increased parameter K. The next analysis will aim at shifting the natural frequency region outside the operational window of the propulsion system. This is obtained by increasing stiffness, or in Nauticus Machinery to reduce the inverse, namely torsional flexibility (unit nrad/Nm).

The torsional flexibility of a shaft has been reduced with 10%, testing one segment at a time. In terms of torsional stiffness in Nm/rad, this corresponds to an increase of 11.1%. The performed sensitivity analysis revealed a maximum increase in natural frequency of 5% (ω_{n2} from 5.1 to 5.34 Hz), resulting from a single modification in the damper stiffness. This small increase corresponds to an operational speed of around 64 rpm, still within the

rpm range of the drive train. Stiffness was thereafter increased with 11.1% for both the damper stiffness, intermediate and propeller shaft at once. The result was a five percent increase in both the first and second natural frequency, which still is too low. It is not realistic to increase the stiffness with more than 11.1%, both with regards to economy and design-wise. Increasing parameter K is consequently not effective enough, the natural frequency region is still inside the operational window.

Decreased shaft stiffness

Referring to the mentioned connection between natural frequency and damping ratio, a decreased shaft stiffness can potentially reduce vibrations. The torsional flexibility is then increased, resulting in a decreased stiffness. It is now expected that torque amplitude, and thereby stress, should decrease. For explanation, see the last paragraph under the section title of section 8.1, the introduction to sensitivity analysis. The torsional flexibility is increased with 10% for one shaft at a time. Again, it is modification in the damper stiffness that gives largest changes. Both torque amplitudes and torsional stress levels at resonance speed decrease with around 6% due to an increased damping ratio ζ. In this process, the four shaft segments mentioned in the chapter introduction were studied. Natural frequencies were not decreased significantly, only by a magnitude of 5% as in the previous case study, and therefore need no further attention. Design modifications of the torsional vibration damper is relatively easy to obtain. One can select another steel spring pack for the Geislinger-TVD (reference to section 2.2.3), or alternatively choose a different design or manufacturer. Decreasing TVD stiffness can therefore be a feasible measure to reduce responses from torsional vibrations.

8.1.2 Changing Damping Ratio

It is intuitive that more damping in the system, or higher damping ratio, implies reduced vibrations. This is also showed in Chapter 3 of this report.

In practical terms, this is achieved by increasing the damping factor C, or by adding more damper elements. In Nauticus Machinery, the first approach is obtained if either mass or relative damping are given higher magnitudes of the dynamic magnifier percent M. The damper stiffness is an exception, since it is defined by damping in Nms/rad. Note that damping does not change natural frequency. All peak values of torque amplitude and stress therefore appear approximately at the initial resonance speed of around 45 rpm. Increased damping factors will firstly be approached for shafts, and then for masses, modifying one element at a time.

Modification of shaft damping

Beginning with the damper stiffness, relative shaft damping was first doubled to 590000 Nms/rad. This analysis revealed decreased torque and stress levels in the elements before the engine, a reduction of about 20%. However, it did not apply for segments inside the engine or after, vibrations were increased with around 11%. A damping factor of this magnitude tends to counteract the engine torque only locally, and actually worsens the conditions elsewhere. In total, the damper is consequently less 'active', which can be recognized as a 21% decrease in its dissipated heat (in watts) at resonance. The damping factor of the TVD was further multiplied with 0.8 and 1.5, but neither of the two analyzes improved system responses globally. Modification of damping in the torsional vibration damper is consequently not recommended.

Increased damping in the other shafts was also approached. The segment between the TVD and the engine, shaft 2-3, gave no interesting results. The dynamic magnifier percent was increased to as much as 1 ($C = C_c$), but still it only influenced the responses before the engine. Changing M in the crank shaft, from 0.01 to 0.02, was also not noticeable. After the engine however, modifications were significant. These shaft segments are initially free of damping, namely $M = 0$ (see Table 3.4). Introducing a magnifier percent of 0.01 at the intermediate shaft, decreases both torsional stress levels and torque amplitudes with about 10% inside and after the engine. A similar introduction at the propeller shaft gave lower reductions. Compared to all

other shaft segments of the drive train, the intermediate shaft is consequently the most effective place to modify damping.

Modification of mass damping

Absolute mass damping has also been increased, for one inertia at a time. The general trend from these studies was low reductions in torque and stress levels. Some inertias were even given a damping factor equal to the critical one, but it did not decrease vibration levels significantly. There are however two exceptions, the outer inertia of the TVD and the propeller.

Introducing mass damping in the TVD (M from 0 to 0.05) decreases torque responses after the engine with around 4%. This modification could be achieved by changing damper design. The constant part of the variable propeller damping curve (see Figure 4.2), was thereafter increased from 5.5% to 10%. This reduced the torque amplitudes and torsional stress, in the four investigated shafts, with as much as 29% on average! Whether a hydrodynamic damping factor of $M = 0.1$ is realistic for an FPP or not, should be investigated. At the same time, it is well known that one of the advantages with a controllable pitch propeller is facilitating increased propeller damping. Replacing the fixed pitch propeller with a CPP, can thereby potentially decrease vibration responses significantly.

Additional damping in the intermediate shaft

Studies above have shown that the most effective place to increase shaft damping is after the engine, or more specifically in the intermediate shaft. The next analysis will aim at increasing damping in this area. The relevant segment will be replaced by a Geislinger damper stiffness, similar to the one located before the diesel engine.

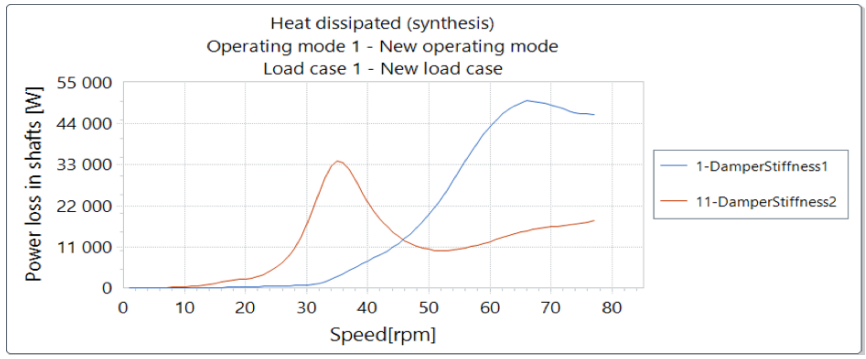

(a) Dissipated heat from damper stiffnesses [W]

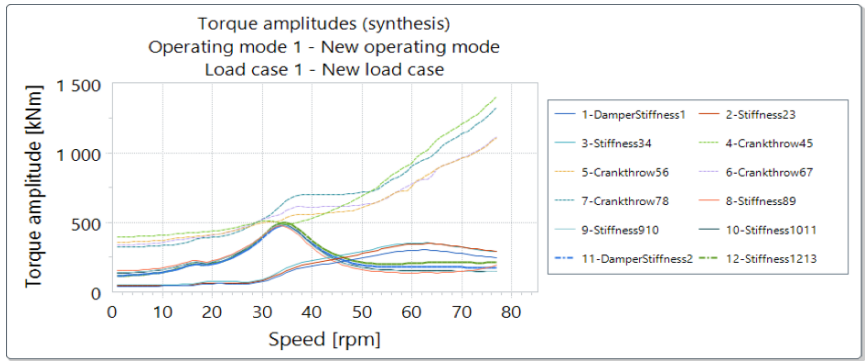

(b) Torque amplitudes with two damper stiffnesses [kNm]

Figure 8.1: Results from forced vibration analyzes with two damper stiffnesses

The old shaft had a torsional flexibility of 9.381 nrad/Nm and a dynamic magnifier percent of zero. The damper stiffness on the other hand, has a torsional flexibility of 58.824 nrad/Nm and a damping factor of 295000 Nms/rad. Replacing the old shaft thereby modifies both natural frequency and damping ratio. An increased torsional flexibility means lowered stiffness and therefore reduced resonance speed. The first two natural frequencies are now rotations at 35 and 60 rpm, earlier 45 and 61 (reference to section 6.1). In Figure 8.1a, the dissipated heat from the damper stiffnesses illustrates these critical speeds. The new damper stiffness (DamperStiffness2) peaks at the first natural frequency, whereas the old TVD (DamperStiffness1) is most active around the second. Furthermore, the peak of the original damper

stiffness is reduced with 32%, simply because the work load now is split in two.

The second sub illustration presents updated torque amplitudes when both damper stiffnesses are active. Similar results with only the original TVD can be found in Figure 6.4a. For simplification, torsional stress is not presented since it is proportional to torque. Values at resonance speed, caused by the new ω_{n1} of 35 rpm, are generally reduced for all shafts. This trend can be explained by the increased damping ratio. Peak values in the intermediate and propeller shafts are actually reduced with as much as 70%! Inside the engine on the other hand, a decrease of around 20% reveals. In comparison, the reductions at higher speeds are not that significant. This can be explained by studying the power loss in the damper stiffnesses. Looking back at illustration 8.1a, the new element is not that active at speeds over 50 rpm. Additionally, it has been mentioned that the dissipated heat from the original element is reduced with around thirty percent. The total damping contribution from both shafts is thereby close to the previous case, resulting in almost unchanged torque amplitudes after 60 rpm.

Results from this investigation implies that the second damper stiffness was a positive modification. It is however doubtful that this element can be implemented into the design in practice. The TVD manufacturer suggest installation of the component at the free end of the crank shaft, since the engine will supply the necessary oil. The latter is a problem since the intermediate shaft is as long as seven meters. Furthermore, the shaft dimensions of the damper stiffness are not realistic for a seven meter long segment. Its diameter is namely approximately one meter. The presented study is consequently not realistic, but it still shows the very positive effects of increased damping in the intermediate shaft. In further work, practical approaches to obtain this should be investigated. A suggestion, which potentially could be promising, is a an active magnetic bearing. Referring to the literature review in section 2.2.3, it has only been used for reduction of translational vibrations until today. However, it would be interesting to study whether torsional displacements also could be influenced.

8.1.3 Discussion

The link between torsional stress and increased parameters K and C should be discussed. Torsional stress is proportional to the internal shaft torque, whereas this again is dependent on the mentioned two parameters. Equation 3.32 and 3.34 illustrates this dependency. An increase in K and C would consequently imply increased torsional stress, which contradicts that e.g. more damping reduces torsional vibrations. In this evaluation however, decreases in angular displacement and velocity must also be taken into account. More damping and higher stiffness namely reduce $\Delta\theta$ and $\Delta\dot{\theta}$. The chicken or the egg dilemma thereby applies for this connection. However, it is generally positive with decreased torque amplitudes and torsional stress levels, which is why this has been focused on in the performed analyzes. The study of short term fatigue damage exemplifies this statement, reduced stress decreases the risk of fatigue failure.

A summary of findings in the sensitivity analysis will now be presented, beginning with the ineffective system modifications. The attempted increase in shaft stiffness (of 11.1%) was not able to move the natural frequency region outside the drive train's operational window. In general, increased damping factors in both shafts and masses were also not successful. Some exceptions however, which will be described below, gave positive results. If not specified differently, all mentioned reductions in torque and stress levels are the average decrease in torque and stress amplitudes at resonance speed in the following four segments on average: the damper stiffness, the third crank throw, the intermediate shaft and the propeller shaft.

An increase in propeller damping from 5.5 to 10% decreased torque and stress levels with around thirty percent. Furthermore, introduction of damping in the intermediate shaft ($M = 0.01$) had the same outcome, but at a magnitude of approximately 10% reduction. The first modification can potentially be obtained by installation of a controllable pitch propeller. The second approach was extended into an analysis with two damper stiffnesses in total, replacing the intermediate shaft. This revealed decreases in torque and stress amplitudes of up to seventy percent, achieved in the segments

after the engine. A practical approach for introduction of damping in this area however, was not found. Some interesting suggestions that could be investigated are the active magnetic bearing and modification of the shaft material.

A decrease in shaft stiffness (of 11.1%) also gave positive outcomes. Vibration responses were reduced with about six percent in this case, which might be enabled by replacing the steel spring packs of the Geislinger TVD or by choosing a different damper design. A new type of damper could also introduce mass damping in the outer part of the TVD. This case study revealed a 4% reduction in torque after the engine.

In conclusion, among the identified system modifications with success, replacing the intermediate shaft by a damper stiffness was most effective. However, no practical design solutions to obtain this were found in this research. At the same time, feasible modifications such as a CPP, a less stiff torsional vibration damper, or a TVD with mass damping in the outer part, tend to improve resulting responses. The sensitivity analysis has thereby been able to identify some achievable measures for vibration reduction. Additionally, one specific segment has been pointed out for further investigations, namely the intermediate shaft.

It should be mentioned that the damped natural frequency has not been accounted for in this thesis. A system with a lot of damping would in reality experience resonance at this damped natural frequency. However, this magnitude is normally very close to the natural frequency [49], which is why it has not been mentioned in this research.

8.2 The Significance of Operational Profiles

The vessel's operational profile can also impact the resulting strain from torsional vibrations, not only propulsion system design. Holding drive train dynamics fixed, including its resonance speeds, the experienced levels of vibrations can be reduced through a carefully considered operational profile.

Figure 8.2 illustrates the connection between vibration responses and two different operational profiles. Since the operating conditions of the eco-ship are unknown, a fictional case was constructed to prove the importance of operation. The upper graph shows amplitude against frequency ratio of the fictive vessel. Resonance speed is ω_{n1}, and the MCR condition is marked in the diagram. Notice that the x-axis displays operational speed in all three plots. An rpm value on the graph in the middle, will have the same magnitude vertically upwards in the first diagram.

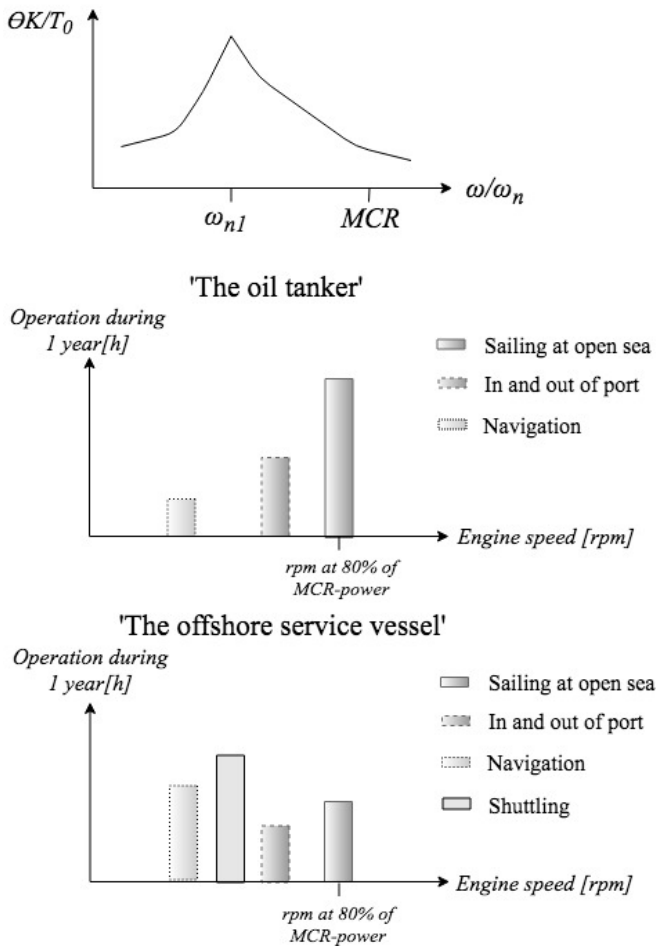

Figure 8.2: Vibration response and operational profiles

The other graphs are two examples of possible operational profiles, if the ship was an oil tanker or an offshore service vessel (OSV) respectively. Engine speed is located on the x-axis, and sailing time in hours during one year on y. Operation is further divided into different categories. Sailing at open sea, associated with high speed, is generally viewed as 'normal operation'. The specific fuel consumption of an engine is lowest when propulsion power equals 80% of the MCR power [50] [57]. To reduce operational costs, the speed at sailing will consequently be the rpm that corresponds to this power magnitude. Sailing in and out of port, or other trafficked areas, require less propulsion and lower speeds. The same holds for 'navigation', which in this case covers e.g. preparations for anchoring and sailing into dock or a platform. This category is thereby situations with very low power requirements. A special case for the offshore vessel is 'shuttling'. In this context, it means sailing back and forth between other service vessels or platforms, also associated with relatively slow pace.

According to the illustration above, the offshore service vessel will experience more vibrations than the tanker. Operation at shuttling speed, which occupies a substantial part of the OSV's operational profile, is close to resonance condition. The oil tanker on the other hand, mostly sailing at open sea, operates at an rpm range with much lower vibration amplitudes (see the upper graph).

The presented vessel types are not really important in this study. They just exemplifies two different cases of operation. Alternatively, they could be the profiles of a single ship under different freight contracts. As an example, the OSV profile could be shipment of cargo on a route with a lot of narrow straits, and customers in many different ports. The analysis is consequently more general than at first glance. Ship owners should have in mind that various practices may subject the vessel to quite different vibration loads. It could be advantageous to include an evaluation of operational profile in route and mission planning.

Chapter 9

Conclusions

9.1 Concluding Remarks

This research has addressed a new type of problem related to environmental friendly and fuel efficient engines in the maritime industry. New propulsion designs in eco-ships are associated with operation within the barred speed range and thereby large torsional vibrations.

The master thesis has attacked this issue in a systematic manner, by use of a case study, the drive train of an eco-ship. DNV GL provided system characteristics and data for modelling verification. The author's contribution was a general approach on how to proceed in the attempt of evaluating and reducing vibration levels in drive trains. Established vibration theory and methods were applied on a new type of problem in a timely context.

A vital foundation in vibration analyzes is the construction of an accurate dynamic model of the system. Two softwares were used to facilitate both frequency and time domain simulations, which thereafter were verified by empirical data. Detection of critical speeds and vulnerable shaft segments was performed to identify the most crucial areas regarding system failure. The aspect of power spectral density was introduced to validate the critical components.

Through the lifetime of a vessel, the operation period at critical speeds is relatively short. In addition to studies of ultimate limit state (ULS), namely evaluating peak values of angular displacement towards torsional fracture, fatigue damage was therefore addressed. The latter reduces component lifetime due to relatively large oscillations over time, not only due to the short operation periods at critical speeds. A contribution to field of study was combining ULS and fatigue analyzes in evaluation of eco-ships. Reducing torsional vibrations will also reduce the risk of fatigue, which could be essential since a ship might fail due to fatigue before torsional fracture.

Specific recommendations for torsional damping were obtained through a sensitivity analysis. Due to limitations in the scope, the relevant modifications were shaft stiffness, shaft and mass damping, and additional damper elements. The successful changes were as follows: New vessel designs can take advantage of larger hydrodynamic damping by installing a controllable pitch propeller. Existing ships would benefit from TVD designs with more shaft stiffness and mass damping in its outer part. However, the most effective modification was introduction of shaft damping in the intermediate shaft, but no practical approaches to obtain this were identified in the literature. Furthermore, it was addressed that also operational profiles affect the vibration loads on a propulsion system.

9.2 Recommendations for Further Work

System modelling contained major assumptions in this thesis. Suggestions for creation of a more complex model are flexible shafts and thereby FEM analyzes, and a more accurate representation of damping which varies with rotational speed. By better accounting for diesel engine dynamics and hydrodynamic damping in time domain simulations, results could be compared to regulations and standards. Two examples are comparison to fatigue limits and acceptance limits for ultimate limit state, which have not been approached. ULS is normally associated with peak values. This again can be connected to transient regions, which then should be investigated more

thoroughly.

Related to vibration reduction analyzes, the next step is to evaluate damping recommendations through lab tests and prototyping. Furthermore, studying how to introduce damping in the intermediate shaft would be beneficial as it noticeably reduced vibration levels. A suggestion is the active magnetic bearing which potentially could influence angular displacements through its electromagnets and associated control system. The connection between reduced levels of torsional vibrations and fatigue damage is also interesting. An example of a case study could be; say that vibrations are reduced with a certain amount, what is then the corresponding decrease in fatigue?

The general focus of this research was mechanical vibrations. Further work could investigate propagation into the ship structure and other parts of the vessel such as the accommodation. If this is portrayed, the aspect of vibration isolation becomes relevant. Not only local vibration reduction is important, global consequences should also be addressed.

Bibliography

[1] JA. Aarvik. Software for shafting systems, 2005. DNV Software News, vol. 3, p. 11.

[2] SIMPACK AG. SIMPACK Reference Guide - Release 8.9, 2012. SIMDOC8905.

[3] J. Babicz. Encyclopedia of ship technology, September 2014. Wärtsilä.

[4] J.G. Balchen, T. Andersen, and B.A. Foss. *Reguleringsteknikk*. Institutt for teknisk kybernetikk, NTNU, 2003.

[5] Bicera. Handbook of torsional vibration, 1958. Cambridge Univeristy Press, London.

[6] S. Bilbao and J.O. Smith. Mus420/ee367a lecture 7d: Discrete-time lumped models, March 2014.

[7] E. Brodin. Engines with a barred speed range, 2016. DNV GL, Issuing unit: Machinery. Internal Technical Update No. 27.

[8] R.G. Budynas and J.N. Nisbett. *Shigley's Mechanical Engineering Design*. McGraw-Hill Education, 10th edition, 2015.

[9] The SHOPERA Consortium. Summary. `http://shopera.org/about/summary/`. Downloaded: 16/03/2018.

[10] Dassault Systems Simulia Corp. Simpack Documentation, 2016. Simpack Release 2017.

[11] G. Dahler. Technical course in vibrations in rotating machinery: Tvc - diesel engines, 2014. DNV GL, Maritime Advisory - Machinery & Systems.

[12] G. Dahler. Technical course in vibrations in rotating machinery: Tvc - engine vibration dampers, 2014. DNV GL, Maritime Advisory - Machinery & Systems.

[13] G. Dahler. Technical course in vibrations in rotating machinery: Tvc - mass-elastic system; inertias & shafts, 2014. DNV GL, Maritime Advisory - Machinery & Systems.

[14] G. Dahler, J.J. Iseskär, and J. Holm. Fuel efficient propeller design and torsional vibrations in propulsion machinery. *Torsional Vibration Symposium*, 2014.

[15] M.I. Friswell, J.E.T. Penny, S.D. Garvey, and A.W. Lees. *Dynamics of Rotating Machines*. Cambridge University Press, 2010.

[16] P. Girdhar and C. Scheffer. *Practical Machinery Vibration Analysis and Predictive Maintenance*. Newnes, 2004.

[17] DNV GL. Class guideline - calculation of shafts in marine applications. https://rules.dnvgl.com/docs/pdf/DNVGL/CG/2015-12/DNVGL-CG-0038.pdf. DNVGL-CG-0038, Edition December 2015. Downloaded: 14/12/2017.

[18] DNV GL. Nauticus machinery modules. https://www.dnvgl.com/services/nauticus-machinery-modules-2917, December 2014. Downloaded: 07/12/2017.

[19] DNV GL. Software nauticus machinery - torsional vibration. https://www.dnvgl.com/services/torsional-vibration-nauticus-machinery-2926, December 2014. Downloaded: 07/12/2017.

[20] DNV GL. Rules for classification: Part 4 systems and components, chapter 2 rotating machinery, general. https://rules.dnvgl.com/

docs/pdf/dnvgl/ru-ship/2017-01/DNVGL-RU-SHIP-Pt4Ch2.pdf, July 2016. Downloaded: 14/12/2017.

[21] DNV GL. Rules for classification: Part 4 systems and components chapter 3 rotating machinery - drivers. http://rules.dnvgl.com/docs/pdf/DNVGL/RU-SHIP/2017-07/DNVGL-RU-SHIP-Pt4Ch3.pdf, July 2017. Downloaded: 14/12/2017.

[22] Geislinger GmbH. *Geislinger Damper*, August 2016. Damper Catalogue Version 15.7.

[23] WAFO group. *WAFO - A Matlab Toolbox for Analysis of Random Waves and Loads - Tutorial for WAFO version 2017*. Math. Stat., Center for Math. Sci., Lund Univ., Lund, Sweden, 2017.

[24] E. Hau. *Wind Turbines - Fundamentals, Technologies, Application, Economics*. Springer, 2nd edition, 2006.

[25] IACS. Unified requirements. http://www.iacs.org.uk/publications/unified-requirements/. Downloaded: 14/12/2017.

[26] IACS. M68: Dimensions of propulsion shafts and their permissible torsional vibration stresses. Req.2005/Rev.1, 2014.

[27] IACS. M51: Factory acceptance test and shipboard trials of i.c. engines. Req. 1987/Rev.4, 2015.

[28] Y.G. Kim, S.J. Hwang, K.H. Cho, and U.K. Kim. Characteristics of propulsion shafting system in ships with engine acceleration problems in the barred speed range. *Ocean Engineering*, 145:479–491, 2017.

[29] Y.G. Kim, S.J. Hwang, K.H. Cho, and U.K. Kim. Characteristics of propulsion shafting system in ships with engine acceleration problems in the barred speed range. *Ocean Engineering*, 145(Supplement C):479 – 491, 2017.

[30] Y.G. Kim, S.J. Hwang, Y.H. Kim, S.W. Kim, K.H. Cho, and U.K. Kim. Control of torsional vibration for propulsion shafting with delayed

engine acceleration by optimum design of a viscous-spring damper. *J. Korean Soc. Mar. Eng., 40 (7)*, pages 580 – 586, 2016.

[31] S. Krüger and W. Abels. Hydrodynamic damping and added mass of modern screw propellers. June 2017.

[32] H. J. Landau. Sampling, data transmission, and the nyquist rate. *Proceedings of the IEEE*, 55(10):1701–1706, Oct 1967.

[33] Eric H. Maslen and G. Schweitzer. *Magnetic Bearings - Theory, Design, and Application to Rotating Machinery*. Springer-Verlag Berlin Heidelberg, 2009. Chapter 1 - Introduction and Survey.

[34] L. Murawski and A. Charchalis. Simplified method of torsional vibration calculation of marine power transmission system. *Marine Structures*, 39:335 – 349, 2014.

[35] A. Naess and T. Moan. *Stochastic Dynamics of Marine Structures*. Cambridge University Press, 2013.

[36] A.R. Nejad, Z. Gao, and T. Moan. On long-term fatigue damage and reliability analysis of gears under wind loads in offshore wind turbine drivetrains. *International Journal of Fatigue*, 61:116 – 128, 2014.

[37] The Association of German Engineers. Vdi 2039, torsional vibration of drivelines - calculation, measurement, reduction. http://www.vdi.eu/uploads/tx_vdirili/pdf/2360651.pdf. Downloaded: 15/12/2017.

[38] International Organization of Standardization. Iso 3046-5:2001, reciprocating internal combustion engines — performance — part 5: Torsional vibrations. https://www.iso.org/obp/ui/#iso:std:iso:3046:-5:ed-2:v1:en. Downloaded: 15/12/2017.

[39] International Maritime Organization. Eedi - rational, safe and effective. http://www.imo.org/en/MediaCentre/HotTopics/GHG/Pages/EEDI.aspx, August 2012. Downloaded: 17/10/2017.

[40] International Maritime Organization. Imo train the trainer (ttt) course on energy efficient ship operation. http://www.imo.org/en/OurWork/

Environment/PollutionPrevention/AirPollution/Documents/Air%20pollution/M2%20EE%20regulations%20and%20guidelines%20final.pdf, London, January 2016. Downloaded: 05/12/2017.

[41] E. Pedersen and H. Valland. Lecture notes in mechanical vibrations, course tmr4222, February 2014. Department of Marine Technology, NTNU.

[42] S. Ran, Y. Hu, and H. Wu. Design, modeling, and robust control of the flexible rotor to pass the first bending critical speed with active magnetic bearing. *Advances in Mechanical Engineering*, 10(2):1687814018757536, 2018.

[43] S.S. Rao. *Mechanical Vibrations*. Pearson Education, Inc., 4th edition, 2004.

[44] H. Rimstad. Dynamic analysis and modelling of slow rotating propulsion system. *NTNU, Marine Technology*, December 2017. TMR4530 - Marine Engineering Spezialization Project.

[45] M.K. Sethi, P. Kumar, and A. Kumar. Transient vibration reduction of a powertrain using mre based adaptive tuned vibration absorber. *Procedia Engineering*, 144(Supplement C):689 – 696, 2016. International Conference on Vibration Problems 2015.

[46] A.A. Shabana. *Dynamics of Multibody Systems*. Cambridge University Press, 4th edition, 2013.

[47] DNV GL Software. User manual - Nauticus Torsional Vibration, Version 12.3, November 2016.

[48] P. Stocia and R. Moses. *Spectral Analysis of Signals*. Prentice Hall, 2005.

[49] W.T. Thomson and M.D. Dahleh. *Theory of Vibration with Applications*. Prentice-Hall, Inc., 5th edition, 1998.

[50] MAN Diesel & Turbo. Basic Principles of Ship Propulsion, December 2011.

[51] MAN Diesel & Turbo. Derating - change of engine smcr. http://primeserv.man.eu/docs/librariesprovider5/primeserv-documents/de-rating.pdf?sfvrsn=2, January 2013. Downloaded: 13/12/2017.

[52] MAN Diesel & Turbo. Man b&w g60me-c9.2-tii, project guide. https://marine.man.eu/applications/projectguides/2stroke/content/printed/G60ME-C9_2-TII.pdf, July 2013. Downloaded: 08/12/2017.

[53] MAN Diesel & Turbo. Market update note: Light running margin (lrm). http://marine.man.eu/docs/librariesprovider6/Newsletter/Updates/MUN_2015-3.pdf, April 2015. Downloaded: 13/12/2017.

[54] MAN Diesel & Turbo. The dynamic limiter function. http://www.marine.man.eu/docs/librariesprovider6/test/5510-0188-00_the-dynamic-limiter-function_low.pdf?sfvrsn=6, July 2016. Downloaded: 13/12/2017.

[55] W. Ker Wilson. Practical solution of torsional vibration problems, 1942. Chapman & Hall Ltd, London.

[56] W. Ker Wilson. *Practical solution of torsional vibration problems*, volume one - Frequency calculations. Aberdeen University Press Limited, 1956.

[57] H.K. Woud and D. Stapersma. *Design of Propulsion and Electric Power Generation Systems*. IMarEST, 2002.

[58] Z. Zhang, B. Chen, and S.R.K. Nielsen. Coupled-mode flutter of wind turbines and its suppression using torsional viscous damper. *Procedia Engineering*, 199(Supplement C):3254 – 3259, 2017. X International Conference on Structural Dynamics, EURODYN 2017.

[59] Y. Zhao. Torsional vibration control in oilwell drilling. *IFAC-PapersOnLine*, 50(1):6035 – 6042, 2017. 20th IFAC World Congress.

Appendix A

Miscellaneous

A.1 Deriving rotational natural frequency

(Reference to 'Mechanical Vibrations' - Chapter 2.2 by Rao,S.S. [43])

Starting with the equation of motion under free vibrations:

$$J\ddot{\theta} + K\theta = 0$$

Assuming a solution on the form:

$$\theta(t) = A \cdot e^{st}$$

With its second derivative equal to:

$$\ddot{\theta}(t) = As^2 \cdot e^{st}$$

Leads to $\Rightarrow (JAs^2 + KA)e^{st} = 0$

This formula can be simplified to the characteristic equation:

$$\Rightarrow s^2 = -\frac{K}{J} \quad , \quad s = \pm\sqrt{-\frac{K}{J}}$$

Knowing that: $i = \sqrt{-1}$

Gives a solution of s as:

$$\Rightarrow s = \pm i\sqrt{\frac{K}{J}} = \pm i\omega_n$$

The natural frequency can then be written as:

$$\Rightarrow \omega_n = \sqrt{\frac{K}{J}} \quad \text{Q.E.D.}$$

The expression (formula 3.3) is derived.

A.2 Calculating propeller damping factor C - Ex. 77 rpm

The drive train model in Nauticus Machinery has a propeller damping at 77 revolutions per minute equal to 5.225E+04 Nms/rad. The extract from defined load case settings (Appendix C.2.1) underneath, shows how this is defined:

Propeller 13

Case	Engine speed [rpm]	Blade freq. [min-1]	Power [kW]	Damping [Nms/rad]	Propeller excitation 1st order [Nm]	2nd order [Nm]
77	77.0	385.0	8500.0	5.225E+04	7.379E+04	7.379E+04

Obtaining this value follows in the next paragraphs.

According to the variable propeller damping curve in figure 4.2, the percent of critical damping is equal to 5.5% at 77 rpm (100% of MCR).

In terms of the dynamic magnifier number $\tilde{M}$, this equals to:

$$\tilde{M} = \frac{100}{2 \cdot \zeta} = \frac{100}{2 \cdot 5.5} = 9.0909$$

By sticking to the dynamic magnifier approach, factor C at the relevant speed can be calculated in the unit of Nms/rad:

$$C = \frac{J \cdot \omega}{\tilde{M}} = \frac{58905 kgm^2 \cdot 77 \frac{2\pi}{60}}{9.0909} = 52.247 \ \frac{kNms}{rad}$$

The calculated propeller damping factor at MCR-condition coincides with the equivalent load case setting.

Appendix B

TVC Data for the Eco-Ship - Provided by DNV GL

B.1 Drive train specifications and TVC results

1. Specification

1.1. Main engine

Engine type	:	HYUNDAI-MAN B&W 5G60ME-C9.2
Max. continuous output	:	8,500 kW
Max. continuous speed	:	77.0 rpm
Cylinder bore	:	600 mm
Stroke	:	2,790 mm
No. of cylinder	:	5
Mean indicated pressure	:	17.9 bar
Ratio of connecting rod	:	0.500
Reciprocating mass	:	6,278 kg/cyl.
Gas harmonic	:	T248078
Firing order	:	1 4 3 2 5
Crank throw	:	FSB245000

1.2. Turning wheel

Moment of inertia	:	9,140 kgm^2
Weight	:	4,306 kg

1.3. Torsional vibration damper (spring type)

Type	:	**Geislinger, D280/FL**
Outer inertia	:	20,400 kgm^2
Inner inertia	:	869 kgm^2
Torsional stiffness	:	17 MNm/rad
Relative damping	:	295,000 Nms/rad
Perm. elastic torque cont.	:	489 kNm
Perm. elastic torque trans	:	733 kNm
Perm. thermal load	:	180 kW
Oil flow	:	160 l/min
Weight	:	18,500 kg

1.4. Propulsion shafting

Intermediate shaft

Diameter x length	:	Φ410 mm * 7,210 mm
Material	:	TS ≥ 800 N/mm^2

Propeller shaft

Diameter x length	:	Φ540 mm * 6,960 mm
Material	:	TS ≥ 600 N/mm^2

1.5. Propeller

Moment of Inertia in water	:	58,690 kgm^2
No. of blade	:	5
Weight	:	19,930 kg
Diameter	:	7.15 M

2. Conclusion

Torsional vibration is calculated with a view of confirming dynamic characteristic of whole propulsion shafting system, whose results are compared to relevant limit.

With normal firing condition, alternating torsional stresses satisfy the guidance limit with barred speed range due to 1node 5th order resonance.

In case of one cylinder misfiring condition, additional barred speed range is necessary for safe running.

Barred Speed Range	40 ~ 51 rpm
Additional Barred Speed Range	Above 57 rpm (Worst Case - No.4 Cyl. Misfire)

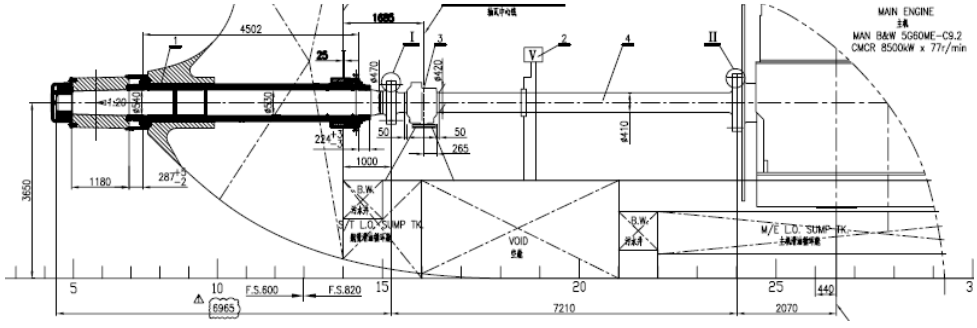

3. Mass elastic model for TVC

Mass ID/Description	Tang. harmon ID	Firing angle (deg)	Geo. mass (kg)	Mom. of inertia (kgm^2)	Rot. speed (r/min)	Mass damping (Nms or %)	Tors. flex. (mrad/Nm)	Diameters outer/inner (mm)	Relative damping (Nms or %)
MAIN SHAFT									
61 GEAR/FL OUT				20400	77.0	0.00%	58.824	9999.0/ 0.0	295000
88 G.IN+FLG+MC				1460	77.0	0.00%	0.000	820.0/150.0	1.00%
22 Moment Compnstr				4140	77.0	0.85%	0.423	820.0/150.0	1.00%
1 Cylinder	248078	0.0	6278	20080	77.0	0.85%	0.490	820.0/150.0	1.00%
2 Cylinder	248078	216.0	6278	20080	77.0	0.85%	0.496	820.0/150.0	1.00%
3 Cylinder	248078	144.0	6278	20080	77.0	0.85%	0.499	820.0/150.0	1.00%
4 Cylinder	248078	72.0	6278	20080	77.0	0.85%	0.474	820.0/150.0	1.00%
5 Cylinder	248078	288.0	6278	20080	77.0	0.85%	0.858	820.0/150.0	1.00%
27 Gendrive+Thrust				5590	77.0	0.85%	0.000	820.0/150.0	1.00%
28 Moment Compnstr				1630	77.0	0.85%	0.258	820.0/150.0	0
82 Turning Wheel				9877	77.0	0.50%	80.788	410.0/ 0.0	0
48 Flange				854.70	77.0	0.00%	9.881	580.0/ 0.0	0
78 Main Propeller				58905	77.0	See table	STANDARD		

4. Natural frequency and holzer tabulation

Model form no. 1, Cyclic frequency = 28.244 rad/s , = 8.699 Hz , = 221.96 CPM

Model form no. 2, Cyclic frequency = 82.071 rad/s , = 5.104 Hz , = 306.28 CPM

Model form no. 8, Cyclic frequency = 164.786 rad/s , = 26.219 Hz , = 1573.11 CPM

5. Normal firing

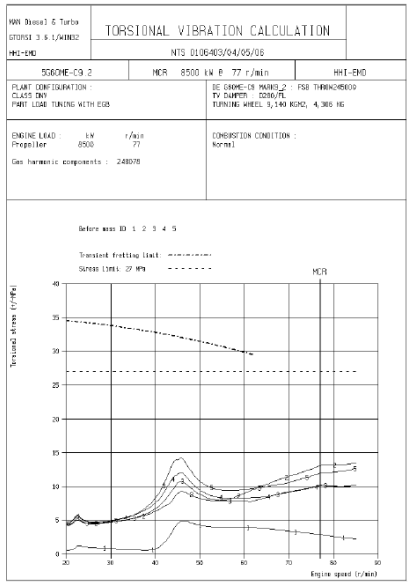

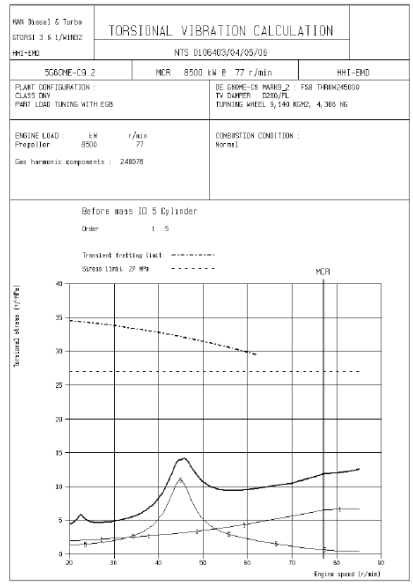

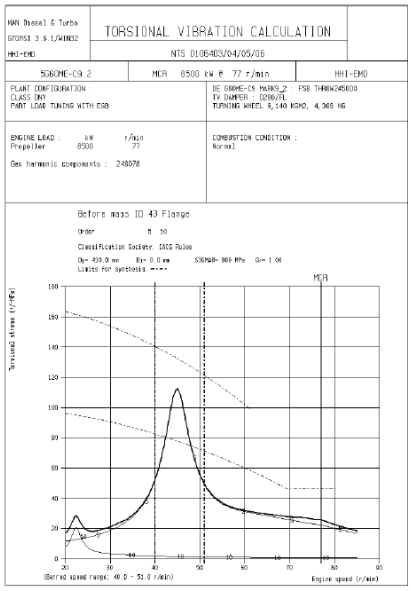

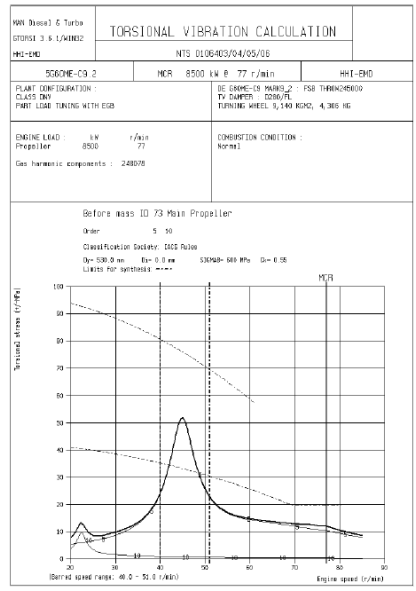

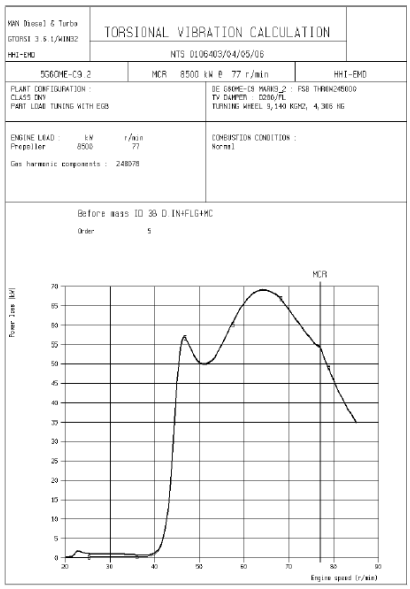
MAN Diesel & Turbo
GTORSI 3 6 1/WIN32
HHI-EMD
TORSIONAL VIBRATION CALCULATION
NTS D106403/04/05/06
5S60ME-C9.2
MCR 8500 kW @ 77 r/min
HHI-EMD
PLANT CONFIGURATION :
CLASS DNV
PART LOAD TUNING WITH EGB
DE ENGINE-CR MAIN3_2 : FSB THRRK24B009
TV DAMPER : D286/FL
TURNING WHEEL 9,140 KGM2, 4,386 MS
ENGINE LOAD : kW r/min
Propeller 8500 77
Gas harmonic components : 248078
COMBUSTION CONDITION :
Normal
Before mass ID 38 D IN+FLG+MC
Order 5
MCR
Power Loss (kW)
Engine speed (r/min)

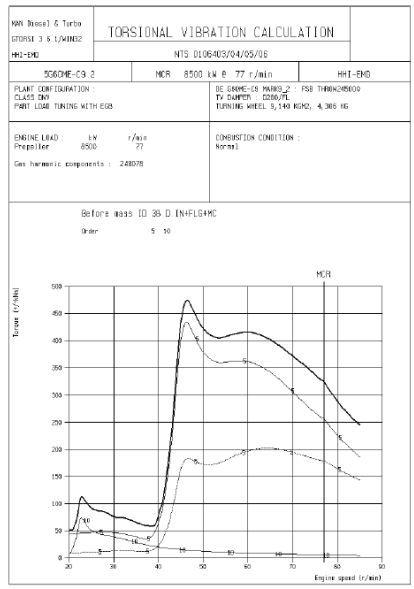
MAN Diesel & Turbo
GTORSI 3 6 1/WIN32
HHI-EMD
TORSIONAL VIBRATION CALCULATION
NTS D106403/04/05/06
5S60ME-C9.2
MCR 8500 kW @ 77 r/min
HHI-EMD
PLANT CONFIGURATION :
CLASS DNV
PART LOAD TUNING WITH EGB
DE ENGINE-CR MAIN3_2 : FSB THRRK24B009
TV DAMPER : D286/FL
TURNING WHEEL 9,140 KGM2, 4,386 MS
ENGINE LOAD : kW r/min
Propeller 8500 77
Gas harmonic components : 248078
COMBUSTION CONDITION :
Normal
Before mass ID 38 D IN+FLG+MC
Order 5 10
MCR
Torque (r/min)
Engine speed (r/min)

B.2 Propeller damping table

PROPELLER DAMPING <-> RPM DEPENDENCY

ID 73 STANDARD
F1 = 221.86 cpm
rpm1,rho1 0.0 0.0
rpm2,rho2 38.5 5.5
rpm3,rho3 77.0 5.5

Speed (r/min)	Physical damping (kNms , %critical)	
5	20	0.7
10	39	1.4
15	59	2.1
20	78	2.9
25	98	3.6
30	117	4.3
35	137	5.0
40	151	5.5
45	151	5.5
50	151	5.5
55	151	5.5
60	151	5.5
65	151	5.5
70	151	5.5
75	151	5.5
80	151	5.5

B.3 Engine excitation data

```
MAN Diesel              Harmonic analysis of            Bore:     0.600 m     Stroke: 2.790 m
Copenhagen              T A N G E N T I A L             Dpistrod: 0.233 m     Excen:  0.000 m
24 Aug 2012 11:04       PRESSURE  NO. 248078            Lconrod:  2.790 m     Sign:   FRK
                                                        Diagrams: 248078.f30
        ********************                            Tang. press.  G60ME-C Mk9.2 Tier2 EGB-PL pi=22 pmax=185
    No. * 2  4  8  0  7  8 *
        ********************                            FAMILY NO.  248078
Cosine components                       in MPa
                          Mean indicated pressure in bar
     0.0000  1.5714  3.1429  4.7143  6.2857  7.8571  9.4286 11.0000 12.5714 14.1429 15.7143 17.2857 18.8571 20.4286 22.0000 23.5714
Order

   1  0.0029  0.0705  0.1380  0.2056  0.2731  0.3407  0.4070  0.4704  0.5339  0.5974  0.6618  0.7262  0.7874  0.8423  0.8942  0.9357
   2  0.0013  0.0195  0.0376  0.0557  0.0738  0.0920  0.1065  0.1132  0.1198  0.1264  0.1321  0.1378  0.1403  0.1307  0.1098  0.0659
   3 -0.0026 -0.0051 -0.0076 -0.0100 -0.0125 -0.0150 -0.0220 -0.0390 -0.0561 -0.0736 -0.0955 -0.1175 -0.1364 -0.1627 -0.2067 -0.2698
   4  0.0005 -0.0112 -0.0228 -0.0345 -0.0461 -0.0578 -0.0735 -0.0980 -0.1226 -0.1474 -0.1745 -0.2017 -0.2244 -0.2502 -0.2902 -0.3408
   5  0.0008 -0.0167 -0.0341 -0.0515 -0.0690 -0.0864 -0.1071 -0.1351 -0.1630 -0.1907 -0.2156 -0.2405 -0.2637 -0.2884 -0.3187 -0.3545
   6 -0.0013 -0.0185 -0.0356 -0.0528 -0.0700 -0.0872 -0.1070 -0.1324 -0.1579 -0.1829 -0.2030 -0.2231 -0.2414 -0.2576 -0.2746 -0.2908
   7 -0.0003 -0.0175 -0.0347 -0.0519 -0.0691 -0.0863 -0.1052 -0.1277 -0.1502 -0.1721 -0.1880 -0.2039 -0.2176 -0.2270 -0.2349 -0.2370
   8  0.0000 -0.0160 -0.0320 -0.0480 -0.0641 -0.0801 -0.0967 -0.1149 -0.1330 -0.1504 -0.1607 -0.1709 -0.1799 -0.1844 -0.1851 -0.1780
   9 -0.0006 -0.0140 -0.0275 -0.0409 -0.0544 -0.0678 -0.0811 -0.0941 -0.1071 -0.1193 -0.1244 -0.1296 -0.1340 -0.1339 -0.1284 -0.1133
  10 -0.0003 -0.0123 -0.0244 -0.0365 -0.0485 -0.0606 -0.0717 -0.0809 -0.0901 -0.0987 -0.1009 -0.1031 -0.1054 -0.1036 -0.0957 -0.0779
  11 -0.0002 -0.0102 -0.0202 -0.0302 -0.0402 -0.0502 -0.0587 -0.0640 -0.0693 -0.0741 -0.0741 -0.0741 -0.0745 -0.0714 -0.0624 -0.0439
  12 -0.0003 -0.0083 -0.0164 -0.0244 -0.0324 -0.0404 -0.0466 -0.0486 -0.0506 -0.0523 -0.0511 -0.0499 -0.0490 -0.0448 -0.0351 -0.0165
  13 -0.0002 -0.0069 -0.0136 -0.0204 -0.0271 -0.0338 -0.0384 -0.0381 -0.0378 -0.0373 -0.0354 -0.0336 -0.0324 -0.0286 -0.0193 -0.0030
  14 -0.0002 -0.0053 -0.0104 -0.0156 -0.0207 -0.0259 -0.0287 -0.0265 -0.0243 -0.0221 -0.0200 -0.0179 -0.0166 -0.0131 -0.0046  0.0090
  15 -0.0001 -0.0041 -0.0081 -0.0121 -0.0160 -0.0200 -0.0217 -0.0182 -0.0147 -0.0114 -0.0096 -0.0079 -0.0066 -0.0034  0.0038  0.0147
  16  0.0000 -0.0031 -0.0062 -0.0092 -0.0123 -0.0153 -0.0161 -0.0117 -0.0074 -0.0033 -0.0016  0.0000  0.0011  0.0037  0.0094  0.0172
  17 -0.0001 -0.0023 -0.0044 -0.0065 -0.0086 -0.0108 -0.0107 -0.0060 -0.0012  0.0033  0.0049  0.0064  0.0073  0.0090  0.0134  0.0186
  18  0.0000 -0.0015 -0.0031 -0.0046 -0.0061 -0.0076 -0.0071 -0.0022  0.0027  0.0073  0.0085  0.0097  0.0103  0.0112  0.0142  0.0173
  19  0.0000 -0.0009 -0.0019 -0.0028 -0.0038 -0.0047 -0.0039  0.0011  0.0060  0.0106  0.0115  0.0123  0.0126  0.0128  0.0144  0.0156
  20 -0.0001 -0.0006 -0.0011 -0.0016 -0.0021 -0.0026 -0.0014  0.0033  0.0081  0.0125  0.0130  0.0135  0.0135  0.0132  0.0136  0.0135

Sine components                         in MPa
                          Mean indicated pressure in bar
     0.0000  1.5714  3.1429  4.7143  6.2857  7.8571  9.4286 11.0000 12.5714 14.1429 15.7143 17.2857 18.8571 20.4286 22.0000 23.5714
Order

   1  0.1606  0.2319  0.3033  0.3746  0.4459  0.5173  0.5992  0.7047  0.8101  0.9144  1.0071  1.0998  1.2238  1.3613  1.4538  1.6025
   2  0.2575  0.3379  0.4183  0.4987  0.5791  0.6595  0.7545  0.8818  1.0091  1.1349  1.2464  1.3579  1.5061  1.6635  1.7578  1.9165
   3  0.2530  0.3157  0.3785  0.4412  0.5039  0.5666  0.6424  0.7471  0.8518  0.9554  1.0481  1.1407  1.2608  1.3793  1.4381  1.5422
   4  0.2001  0.2492  0.2983  0.3475  0.3966  0.4458  0.5041  0.5828  0.6614  0.7391  0.8069  0.8747  0.9633  1.0466  1.0784  1.1380
   5  0.1549  0.1896  0.2243  0.2591  0.2938  0.3285  0.3689  0.4220  0.4750  0.5271  0.5700  0.6129  0.6723  0.7254  0.7342  0.7591
   6  0.1176  0.1413  0.1651  0.1888  0.2125  0.2363  0.2630  0.2963  0.3295  0.3620  0.3867  0.4114  0.4499  0.4826  0.4775  0.4812
   7  0.0882  0.1047  0.1212  0.1377  0.1543  0.1708  0.1883  0.2081  0.2280  0.2472  0.2608  0.2744  0.2999  0.3217  0.3130  0.3103
   8  0.0659  0.0755  0.0850  0.0945  0.1041  0.1136  0.1229  0.1316  0.1404  0.1490  0.1555  0.1620  0.1775  0.1902  0.1803  0.1741
   9  0.0479  0.0532  0.0585  0.0639  0.0692  0.0745  0.0787  0.0804  0.0821  0.0840  0.0869  0.0898  0.0994  0.1073  0.0989  0.0929
  10  0.0354  0.0377  0.0399  0.0421  0.0443  0.0466  0.0473  0.0446  0.0419  0.0395  0.0401  0.0406  0.0469  0.0531  0.0468  0.0440
  11  0.0259  0.0254  0.0250  0.0245  0.0240  0.0236  0.0215  0.0160  0.0105  0.0055  0.0053  0.0051  0.0092  0.0135  0.0091  0.0087
  12  0.0185  0.0169  0.0152  0.0136  0.0120  0.0103  0.0072  0.0007 -0.0058 -0.0116 -0.0114 -0.0111 -0.0080 -0.0043 -0.0061 -0.0033
  13  0.0135  0.0108  0.0081  0.0054  0.0026 -0.0001 -0.0041 -0.0108 -0.0176 -0.0238 -0.0236 -0.0235 -0.0211 -0.0176 -0.0173 -0.0116
  14  0.0097  0.0063  0.0029 -0.0005 -0.0039 -0.0073 -0.0116 -0.0180 -0.0244 -0.0301 -0.0298 -0.0295 -0.0275 -0.0241 -0.0224 -0.0152
  15  0.0069  0.0034  0.0000 -0.0035 -0.0070 -0.0104 -0.0145 -0.0200 -0.0255 -0.0304 -0.0298 -0.0291 -0.0271 -0.0235 -0.0203 -0.0117
  16  0.0049  0.0013 -0.0024 -0.0060 -0.0097 -0.0134 -0.0173 -0.0219 -0.0265 -0.0306 -0.0297 -0.0289 -0.0270 -0.0234 -0.0192 -0.0101
  17  0.0035  0.0000 -0.0036 -0.0071 -0.0107 -0.0142 -0.0178 -0.0214 -0.0250 -0.0282 -0.0271 -0.0260 -0.0244 -0.0210 -0.0162 -0.0074
  18  0.0025 -0.0008 -0.0041 -0.0074 -0.0107 -0.0140 -0.0171 -0.0198 -0.0224 -0.0247 -0.0237 -0.0226 -0.0210 -0.0177 -0.0129 -0.0048
  19  0.0017 -0.0014 -0.0046 -0.0077 -0.0108 -0.0140 -0.0167 -0.0184 -0.0201 -0.0215 -0.0204 -0.0194 -0.0177 -0.0145 -0.0099 -0.0027
  20  0.0012 -0.0016 -0.0045 -0.0073 -0.0102 -0.0130 -0.0153 -0.0162 -0.0171 -0.0179 -0.0167 -0.0154 -0.0139 -0.0110 -0.0067 -0.0008

MAN Diesel              Harmonic analysis of            Bore:     0.600 m     Stroke: 2.790 m
Copenhagen              T A N G E N T I A L             Dpistrod: 0.233 m     Excen:  0.000 m
24 Aug 2012 11:04       PRESSURE  NO. 248078            Lconrod:  2.790 m     Sign:   FRK
                                                        Diagrams: 248078.f30
        ********************                            Tang. press.  G60ME-C Mk9.2 Tier2 EGB-PL pi=22 pmax=185
    No. * 2  4  8  0  7  8 *
        ********************                            FAMILY NO.  248078
Resultants                              in MPa
                          Mean indicated pressure in bar
     0.0000  1.5714  3.1429  4.7143  6.2857  7.8571  9.4286 11.0000 12.5714 14.1429 15.7143 17.2857 18.8571 20.4286 22.0000 23.5714
Order
```

1	0.1606	0.2424	0.3332	0.4273	0.5229	0.6194	0.7243	0.8473	0.9702	1.0923	1.2051	1.3179	1.4552	1.6008	1.7067	1.8556
2	0.2576	0.3385	0.4200	0.5018	0.5838	0.6659	0.7620	0.8890	1.0161	1.1419	1.2534	1.3648	1.5127	1.6687	1.7612	1.9177
3	0.2530	0.3158	0.3785	0.4413	0.5041	0.5668	0.6428	0.7481	0.8536	0.9582	1.0524	1.1468	1.2682	1.3888	1.4529	1.5656
4	0.2001	0.2494	0.2992	0.3492	0.3993	0.4495	0.5094	0.5909	0.6727	0.7536	0.8255	0.8976	0.9891	1.0761	1.1167	1.1879
5	0.1549	0.1903	0.2269	0.2641	0.3018	0.3397	0.3842	0.4431	0.5022	0.5606	0.6094	0.6584	0.7222	0.7806	0.8004	0.8378
6	0.1176	0.1425	0.1689	0.1960	0.2238	0.2518	0.2839	0.3245	0.3654	0.4056	0.4368	0.4680	0.5106	0.5470	0.5508	0.5622
7	0.0882	0.1062	0.1261	0.1472	0.1690	0.1913	0.2157	0.2442	0.2730	0.3012	0.3215	0.3418	0.3705	0.3937	0.3913	0.3904
8	0.0659	0.0772	0.0908	0.1060	0.1222	0.1390	0.1564	0.1747	0.1934	0.2117	0.2236	0.2355	0.2527	0.2649	0.2584	0.2490
9	0.0479	0.0551	0.0647	0.0758	0.0880	0.1007	0.1130	0.1238	0.1349	0.1459	0.1518	0.1577	0.1669	0.1716	0.1620	0.1465
10	0.0354	0.0396	0.0468	0.0557	0.0657	0.0764	0.0859	0.0924	0.0994	0.1063	0.1085	0.1108	0.1153	0.1164	0.1065	0.0895
11	0.0259	0.0274	0.0321	0.0389	0.0468	0.0555	0.0626	0.0660	0.0701	0.0743	0.0743	0.0742	0.0750	0.0727	0.0631	0.0448
12	0.0185	0.0188	0.0224	0.0279	0.0346	0.0417	0.0471	0.0486	0.0509	0.0536	0.0523	0.0511	0.0496	0.0450	0.0356	0.0169
13	0.0135	0.0128	0.0158	0.0211	0.0272	0.0338	0.0386	0.0396	0.0417	0.0443	0.0426	0.0410	0.0387	0.0336	0.0259	0.0120
14	0.0097	0.0083	0.0109	0.0156	0.0211	0.0269	0.0310	0.0321	0.0344	0.0374	0.0359	0.0345	0.0321	0.0275	0.0229	0.0177
15	0.0069	0.0054	0.0081	0.0126	0.0175	0.0226	0.0261	0.0270	0.0294	0.0325	0.0313	0.0302	0.0279	0.0237	0.0207	0.0188
16	0.0049	0.0033	0.0066	0.0110	0.0156	0.0203	0.0236	0.0248	0.0275	0.0308	0.0298	0.0289	0.0271	0.0237	0.0213	0.0199
17	0.0035	0.0023	0.0057	0.0096	0.0137	0.0178	0.0208	0.0222	0.0250	0.0284	0.0275	0.0268	0.0254	0.0229	0.0210	0.0201
18	0.0025	0.0017	0.0051	0.0087	0.0123	0.0160	0.0186	0.0199	0.0226	0.0258	0.0252	0.0247	0.0234	0.0209	0.0192	0.0179
19	0.0017	0.0017	0.0049	0.0082	0.0115	0.0148	0.0171	0.0184	0.0209	0.0240	0.0234	0.0230	0.0217	0.0193	0.0175	0.0158
20	0.0012	0.0017	0.0046	0.0075	0.0104	0.0133	0.0153	0.0165	0.0190	0.0218	0.0211	0.0205	0.0194	0.0172	0.0152	0.0135

Phase angles in degrees

Mean indicated pressure in bar

Order	0.0000	1.5714	3.1429	4.7143	6.2857	7.8571	9.4286	11.0000	12.5714	14.1429	15.7143	17.2857	18.8571	20.4286	22.0000	23.5714
1	1.04	16.90	24.47	28.76	31.49	33.37	34.18	33.73	33.38	33.16	33.31	33.44	32.76	31.75	31.60	30.28
2	0.30	3.30	5.13	6.37	7.27	7.94	8.04	7.31	6.77	6.36	6.05	5.79	5.32	4.49	3.58	1.97
3	−0.59	−0.92	−1.14	−1.30	−1.42	−1.52	−1.96	−2.99	−3.77	−4.40	−5.21	−5.88	−6.17	−6.73	−8.18	−9.92
4	0.13	−2.57	−4.38	−5.67	−6.63	−7.39	−8.29	−9.55	−10.50	−11.28	−12.21	−12.98	−13.11	−13.45	−15.06	−16.67
5	0.28	−5.03	−8.65	−11.25	−13.21	−14.74	−16.19	−17.75	−18.94	−19.89	−20.72	−21.43	−21.42	−21.68	−23.46	−25.03
6	−0.62	−7.44	−12.18	−15.63	−18.23	−20.26	−22.13	−24.09	−25.61	−26.81	−27.70	−28.47	−28.21	−28.09	−29.90	−31.14
7	−0.16	−9.47	−15.96	−20.64	−24.13	−26.82	−29.19	−31.53	−33.38	−34.84	−35.79	−36.62	−35.96	−35.20	−36.89	−37.38
8	−0.03	−12.00	−20.66	−26.95	−31.62	−35.18	−38.21	−41.11	−43.45	−45.28	−45.94	−46.53	−45.38	−44.11	−45.75	−45.63
9	−0.68	−14.75	−25.14	−32.66	−38.18	−42.33	−45.89	−49.49	−52.51	−54.87	−55.07	−55.26	−53.43	−51.29	−52.40	−50.65
10	−0.46	−18.15	−31.46	−40.89	−47.58	−52.45	−56.62	−61.15	−65.06	−68.17	−68.34	−68.50	−65.98	−62.88	−63.94	−60.55
11	−0.44	−21.87	−39.00	−50.96	−59.13	−64.85	−69.86	−75.95	−81.38	−85.77	−85.92	−86.07	−82.96	−79.30	−81.68	−78.85
12	−1.01	−26.31	−47.04	−60.85	−69.74	−75.68	−81.24	−89.17	−96.52	−102.55	−102.58	−102.60	−99.24	−95.49	−99.78	−101.15
13	−0.76	−32.58	−59.32	−75.23	−84.41	−90.12	−96.03	−105.90	−115.03	−122.51	−123.71	−124.99	−122.98	−121.52	−131.92	−165.69
14	−0.92	−39.96	−74.32	−91.71	−100.55	−105.66	−111.95	−124.10	−135.02	−143.68	−146.11	−148.74	−148.81	−151.43	−168.41	149.23
15	−1.24	−50.09	−90.17	−106.16	−113.48	−117.55	−123.86	−137.76	−150.07	−159.54	−162.05	−164.77	−166.23	−171.86	169.36	128.50
16	−0.43	−67.89	−111.27	−123.29	−128.33	−131.06	−137.09	−151.83	−164.45	−173.91	−176.83	−179.95	177.62	171.04	153.91	120.34
17	−2.31	−90.42	−129.06	−137.50	−140.97	−142.85	−148.86	−164.44	−177.32	173.28	169.83	166.18	163.32	156.70	140.43	111.78
18	−0.87	−117.41	−143.34	−148.36	−150.45	−151.58	−157.47	−173.69	173.04	163.49	160.18	156.71	153.96	147.57	132.16	105.39
19	1.19	−147.09	−157.69	−159.86	−160.79	−161.30	−166.98	176.63	163.31	153.80	150.72	147.51	144.72	138.55	124.50	99.99
20	−3.07	−161.03	−166.66	−167.96	−168.54	−168.87	−174.67	168.36	154.68	145.06	142.03	138.81	135.86	129.83	116.31	93.22

Appendix C

Attachments to Analyzes in Nauticus Machinery

C.1 Free analysis

C.1.1 Input data

DNV GL
Test2 MASTER Propulsion System
REV7_NEWEng_NewIDs_M_TVD

Nauticus Torsional Vibrations
Version 12.3.89
By DNV GL - Software

Operating mode 1 - New operating mode
Load case 1 - New load case, 1-77 rpm,Propeller law - full pitch

DATA FOR MASSES AND DAMPERS

Mass No	DESCRIPTION	RPM RATIO [-]	MASS MOMENT OF INERTIA [kg*m^2]	DAMPING see note [N*s*m/rad]	FIRING ANGLE [deg]	TYPE
1	OuterTVD	1,000	2,0400E+004	0,000E+000		Lump mass
2	InnerTVD	1,000	1,4800E+003	0,000E+000		Lump mass
3	MomentComponstr1	1,000	4,1400E+003	-58,8		Lump mass
4	Cylinder1	1,000	2,0030E+004	-58,8	0	Cylinder
5	Cylinder2	1,000	2,0030E+004	-58,8	216	Cylinder
6	Cylinder3	1,000	2,0030E+004	-58,8	144	Cylinder
7	Cylinder4	1,000	2,0030E+004	-58,8	72	Cylinder
8	Cylinder5	1,000	2,0030E+004	-58,8	288	Cylinder
9	CamdriveThrust	1,000	5,5900E+003	-58,8		Lump mass
10	MomentComponstr2	1,000	1,8300E+003	-58,8		Lump mass
11	TurningWheel	1,000	9,3770E+003	-100,0		Lump mass
12	Flange	1,000	3,5470E+002	0,000E+000		Lump mass
13	Propeller	1,000	5,8905E+004	-9,1		Propeller

Note: Negative sign on mass damping means dynamic magnifier

DATA FOR SHAFT ELEMENTS

SHAFT No	NODES		RPM RATIO [-]	TORSIONAL STIFFNESS [N*m/rad]	DAMPING see note [N*s*m/rad]	DIAMETER OUTER [mm]	DIAMETER INNER [mm]	TYPE
1	1	2	1,000	1,700E+007	2,950E+005	0,0	0,0	DamperStiffness
2	2	3	1,000	1,000E+012	-50,0	820,0	150,0	Shaft
3	3	4	1,000	2,364E+009	-50,0	820,0	150,0	Shaft
4	4	5	1,000	2,041E+009	-50,0	820,0	150,0	Crankthrow
5	5	6	1,000	2,008E+009	-50,0	820,0	150,0	Crankthrow
6	6	7	1,000	2,004E+009	-50,0	820,0	150,0	Crankthrow
7	7	8	1,000	2,110E+009	-50,0	820,0	150,0	Crankthrow
8	8	9	1,000	2,793E+009	-50,0	820,0	150,0	Shaft
9	9	10	1,000	1,000E+012	-50,0	820,0	150,0	Shaft
10	10	11	1,000	3,876E+009	0,000E+000	820,0	150,0	Shaft
11	11	12	1,000	3,248E+007	0,000E+000	410,0	0,0	Shaft
12	12	13	1,000	1,066E+008	0,000E+000	530,0	0,0	Shaft

Note: Negative sign on shaft damping means dynamic magnifier

Operating mode 1 - New operating mode
Load case 1 - New load case, 1-77 rpm,Propeller law - full pitch

ENGINE DATA

Index:	#1
Manufacturer:	MAN
Type:	B&W 5G60ME-C9.2
Crank throw:	
Mass numbers:	3,4,5,6,7,8,9,10
RPM (@MCR):	77,0 rpm
Total power (@MCR):	8500,0 kW
Firing order:	1-4-3-2-5
Firing interval:	Even
Firing type:	Consecutive
Number of strokes:	2
Firing angle between banks:	0,00 deg
Cylinder diameter:	600,0 mm
Length of stroke:	2790,0 mm
Connecting rod ratio:	0,5
Compression ratio:	0
Reciprocating mass (per cylinder):	6278 kg
Number of cylinders:	5

DAMPER DATA

Damper type:	Steel
Node numbers:	1-2
Inertia outer member:	20400,00000 kg*m^2
Inertia inner member:	1480,00000 kg*m^2
Dynamic magnifier:	0,000
Damping coefficient:	295000,000 N*s*m/rad
Torsional stiffness:	1,700E+007 N*m/rad

PROPELLER DATA

Index:	#13
Manufacturer:	
Type:	
Ice class notation:	No ice class
MCR Power:	8500,0 kW
MCR Speed:	77,0 rpm
Bollard Speed:	65,5 rpm
Ducted propeller:	No
Pitch type:	Fixed pitch
Number of propeller blades:	5
Damping method:	Variable (Knuckle point 0,52)
Boss diameter:	0,0 mm
Blade diameter:	7150,0 mm
Pitch ratio:	1,000
Expanded area ratio (Ae/Ao):	0,000
Inertia, in air (@MCR):	0,000E+000 kg*m^2
Inertia, entrained water (@MCR):	5,891E+004 kg*m^2
Propeller excitation in % of shaft torque (Nm):	7,0%
Propeller excitation (*2) in % of shaft torque (Nm):	7,0%

C.1.2 Natural frequencies and mode shapes

DNV GL
Test2 MASTER Propulsion System
REV7_NEWEng_NewIDs_M_TVD

Nauticus Torsional Vibrations
Version 12.3.89
By DNV GL - Software

NATURAL FREQUENCIES AND MODE SHAPES
Operating mode 1 - New operating mode
Load case 1 - New load case, 1-77 rpm,Propeller law - full pitch

Mode number		**1**	**2**	**3**
Natural frequency (rad/s)		23,24	32,06	164,38
Natural frequency (vibs/min)		221,93	306,18	1569,74
Natural frequency (Hz)		3,70	5,10	26,16
Node no.	**Description**			
1	OuterTVD	2,8842E+000	-3,9054E+000	-3,3738E-002
2	InnerTVD	1,0148E+000	9,1266E-001	1,0603E+000
3	MomentComponst	1,0147E+000	9,1274E-001	1,0602E+000
4	Cylinder1	1,0000E+000	9,4516E-001	1,0000E+000
5	Cylinder2	9,7762E-001	9,7317E-001	6,6501E-001
6	Cylinder3	9,4960E-001	9,9166E-001	1,4529E-001
7	Cylinder4	9,1640E-001	1,0000E+000	-4,1470E-001
8	Cylinder5	8,8017E-001	9,9816E-001	-8,4025E-001
9	CamdriveThrust	8,4939E-001	9,8941E-001	-9,9884E-001
10	MomentComponst	8,4930E-001	9,8938E-001	-9,9913E-001
11	TurningWheel	8,2625E-001	9,8113E-001	-1,0618E+000
12	Flange	-2,0542E+000	-2,9480E-001	-2,5146E-001
13	Propeller	-2,9281E+000	-6,8256E-001	1,8049E-002

Mode number		**4**	**5**	**6**
Natural frequency (rad/s)		318,64	449,40	550,65
Natural frequency (vibs/min)		3042,83	4291,49	5258,29
Natural frequency (Hz)		50,71	71,52	87,64
Node no.	**Description**			
1	OuterTVD	7,8982E-003	-3,8495E-003	1,9800E-003
2	InnerTVD	-9,5444E-001	9,2910E-001	-7,1846E-001
3	MomentComponst	-9,5431E-001	9,2884E-001	-7,1815E-001
4	Cylinder1	-7,3088E-001	4,8956E-001	-2,0562E-001
5	Cylinder2	2,5628E-001	-9,8972E-001	1,0000E+000
6	Cylinder3	1,0000E+000	-4,9928E-001	-7,9922E-001
7	Cylinder4	7,3038E-001	1,0000E+000	-1,7994E-001
8	Cylinder5	-2,2981E-001	5,0667E-001	9,2632E-001
9	CamdriveThrust	-7,8770E-001	-5,9970E-001	-2,5221E-001
10	MomentComponst	-7,8881E-001	-6,0212E-001	-2,5507E-001
11	TurningWheel	-1,0377E+000	-1,1674E+000	-9,5760E-001
12	Flange	-3,2100E-001	-5,5428E-001	-9,6685E-001
13	Propeller	5,8251E-003	5,0114E-003	5,8051E-003

Mode number		**7**	**8**	**9**
Natural frequency (rad/s)		614,42	629,16	758,89
Natural frequency (vibs/min)		5867,24	6008,05	7246,83
Natural frequency (Hz)		97,79	100,13	120,78
Node no.	**Description**			
1	OuterTVD	8,5582E-004	-5,4475E-004	4,0044E-003
2	InnerTVD	-3,8684E-001	2,5822E-001	-2,7634E+000
3	MomentComponst	-3,8663E-001	2,5807E-001	-2,7611E+000
4	Cylinder1	-4,2395E-002	1,7044E-002	1,0000E+000
5	Cylinder2	5,1345E-001	-3,2838E-001	-2,9555E-001
6	Cylinder3	-8,5507E-001	6,1717E-001	8,5596E-002

7	Cylinder4	1,0000E+000	-8,7719E-001	-2,5193E-002
8	Cylinder5	-8,2200E-001	1,0000E+000	7,3198E-003
9	CamdriveThrust	2,7046E-002	-4,2071E-001	1,6475E-003
10	MomentComponst	2,9361E-002	-4,2374E-001	1,6264E-003
11	TurningWheel	6,2128E-001	-1,1282E+000	-4,2721E-003
12	Flange	3,5462E+000	4,3737E+001	2,1394E-003
13	Propeller	-1,7082E-002	-2,0087E-001	-6,7437E-006

Mode number		**10**	**11**	**12**
Natural frequency (rad/s)		1104,68	26964,04	30288,29
Natural frequency (vibs/min)		10548,95	257487,62	289231,86
Natural frequency (Hz)		175,82	4291,46	4820,53
Node no.	**Description**			
1	OuterTVD	4,0538E-008	0,0000E+000	-1,9734E-002
2	InnerTVD	-5,9324E-005	0,0000E+000	2,1724E+004
3	MomentComponst	-5,9218E-005	-3,0174E-019	-7,7708E+003
4	Cylinder1	1,1223E-004	3,8564E-016	1,0000E+000
5	Cylinder2	-1,0333E-003	-2,7511E-012	-1,1109E-004
6	Cylinder3	1,0381E-002	1,9946E-008	1,2142E-008
7	Cylinder4	-1,0480E-001	-1,4491E-004	-1,3404E-012
8	Cylinder5	1,0000E+000	1,0000E+000	2,8973E-014
9	CamdriveThrust	-6,9162E+000	-5,2118E+003	-8,7630E-013
10	MomentComponst	-6,8911E+000	1,5956E+004	-5,9268E-013
11	TurningWheel	3,5467E+000	-9,0764E+000	2,3521E-014
12	Flange	-3,9234E-001	1,1438E-003	-7,4088E-013
13	Propeller	5,8268E-004	-2,8467E-009	-1,7422E-014

C.2 Forced analysis

C.2.1 Load case settings

DNV GL
Test2 MASTER Propulsion System
REV7_NEWEng_NewIDs_M_TVD

Nauticus Torsional Vibrations
Version 12.3.89
By DNV GL - Software

LOAD CASE SETTINGS
Operating mode 1 - New operating mode
Load case 1 - New load case, 1-77 rpm,Propeller law - full pitch

Diesel Case	1 Speed [rpm]	Power [kW/cyl]	P.Max [bar]	P.Inlet [bar]	P.Comp [bar]	MIP [bar]	MEP [bar]
1	1.0	0.0	0.0	0.0	0.0	1.7	0.0
2	2.0	0.0	0.0	0.0	0.0	1.7	0.0
3	3.0	0.1	0.0	0.0	0.0	1.7	0.0
4	4.0	0.2	0.0	0.0	0.0	1.7	0.0
5	5.0	0.5	0.0	0.0	0.0	1.8	0.1
6	6.0	0.8	0.0	0.0	0.0	1.8	0.1
7	7.0	1.3	0.0	0.0	0.0	1.8	0.1
8	8.0	1.9	0.0	0.0	0.0	1.9	0.2
9	9.0	2.7	0.0	0.0	0.0	1.9	0.2
10	10.0	3.7	0.0	0.0	0.0	2.0	0.3
11	11.0	5.0	0.0	0.0	0.0	2.0	0.3
12	12.0	6.4	0.0	0.0	0.0	2.1	0.4
13	13.0	8.2	0.0	0.0	0.0	2.2	0.5
14	14.0	10.2	0.0	0.0	0.0	2.2	0.6
15	15.0	12.6	0.0	0.0	0.0	2.3	0.6
16	16.0	15.3	0.0	0.0	0.0	2.4	0.7
17	17.0	18.3	0.0	0.0	0.0	2.5	0.8
18	18.0	21.7	0.0	0.0	0.0	2.6	0.9
19	19.0	25.5	0.0	0.0	0.0	2.7	1.0
20	20.0	29.8	0.0	0.0	0.0	2.8	1.1
21	21.0	34.5	0.0	0.0	0.0	2.9	1.2
22	22.0	39.6	0.0	0.0	0.0	3.1	1.4
23	23.0	45.3	0.0	0.0	0.0	3.2	1.5
24	24.0	51.5	0.0	0.0	0.0	3.3	1.6
25	25.0	58.2	0.0	0.0	0.0	3.5	1.8
26	26.0	65.4	0.0	0.0	0.0	3.6	1.9
27	27.0	73.3	0.0	0.0	0.0	3.8	2.1
28	28.0	81.7	0.0	0.0	0.0	3.9	2.2
29	29.0	90.8	0.0	0.0	0.0	4.1	2.4
30	30.0	100.5	0.0	0.0	0.0	4.3	2.5
31	31.0	110.9	0.0	0.0	0.0	4.4	2.7
32	32.0	122.0	0.0	0.0	0.0	4.6	2.9
33	33.0	133.8	0.0	0.0	0.0	4.8	3.1
34	34.0	146.4	0.0	0.0	0.0	5.0	3.3
35	35.0	159.7	0.0	0.0	0.0	5.2	3.5
36	36.0	173.7	0.0	0.0	0.0	5.4	3.7
37	37.0	188.6	0.0	0.0	0.0	5.6	3.9
38	38.0	204.3	0.0	0.0	0.0	5.8	4.1
39	39.0	220.9	0.0	0.0	0.0	6.0	4.3
40	40.0	238.3	0.0	0.0	0.0	6.3	4.5
41	41.0	256.6	0.0	0.0	0.0	6.5	4.8
42	42.0	275.9	0.0	0.0	0.0	6.7	5.0
43	43.0	296.1	0.0	0.0	0.0	7.0	5.2
44	44.0	317.2	0.0	0.0	0.0	7.2	5.5
45	45.0	339.3	0.0	0.0	0.0	7.5	5.7
46	46.0	362.5	0.0	0.0	0.0	7.7	6.0
47	47.0	386.6	0.0	0.0	0.0	8.0	6.3
48	48.0	411.8	0.0	0.0	0.0	8.3	6.5
49	49.0	438.1	0.0	0.0	0.0	8.6	6.8
50	50.0	465.5	0.0	0.0	0.0	8.8	7.1
51	51.0	494.0	0.0	0.0	0.0	9.1	7.4
52	52.0	523.6	0.0	0.0	0.0	9.4	7.7
53	53.0	554.4	0.0	0.0	0.0	9.7	8.0
54	54.0	586.4	0.0	0.0	0.0	10.0	8.3
55	55.0	619.5	0.0	0.0	0.0	10.3	8.6
56	56.0	653.9	0.0	0.0	0.0	10.7	8.9
57	57.0	689.6	0.0	0.0	0.0	11.0	9.2
58	58.0	726.5	0.0	0.0	0.0	11.3	9.5

59	59.0	764.8	0.0	0.0	0.0	11.6	9.9
60	60.0	804.3	0.0	0.0	0.0	12.0	10.2
61	61.0	845.2	0.0	0.0	0.0	12.3	10.5
62	62.0	887.5	0.0	0.0	0.0	12.7	10.9
63	63.0	931.1	0.0	0.0	0.0	13.0	11.2
64	64.0	976.2	0.0	0.0	0.0	13.4	11.6
65	65.0	1022.6	0.0	0.0	0.0	13.8	12.0
66	66.0	1070.6	0.0	0.0	0.0	14.2	12.3
67	67.0	1120.0	0.0	0.0	0.0	14.5	12.7
68	68.0	1170.9	0.0	0.0	0.0	14.9	13.1
69	69.0	1223.3	0.0	0.0	0.0	15.3	13.5
70	70.0	1277.2	0.0	0.0	0.0	15.7	13.9
71	71.0	1332.8	0.0	0.0	0.0	16.1	14.3
72	72.0	1389.9	0.0	0.0	0.0	16.5	14.7
73	73.0	1448.6	0.0	0.0	0.0	16.9	15.1
74	74.0	1508.9	0.0	0.0	0.0	17.4	15.5
75	75.0	1570.9	0.0	0.0	0.0	17.8	15.9
76	76.0	1634.6	0.0	0.0	0.0	18.2	16.4
77	77.0	1700.0	0.0	0.0	0.0	18.7	16.8

Propeller 13

Case	Engine speed [rpm]	Blade freq. [min-1]	Power [kW]	Damping [Nms/rad]	Propeller excitation 1st order [Nm]	2nd order [Nm]
1	1.0	5.0	0.0	1.695E+01	1.245E+01	1.245E+01
2	2.0	10.0	0.1	6.779E+01	4.978E+01	4.978E+01
3	3.0	15.0	0.5	1.525E+02	1.120E+02	1.120E+02
4	4.0	20.0	1.2	2.711E+02	1.991E+02	1.991E+02
5	5.0	25.0	2.3	4.237E+02	3.111E+02	3.111E+02
6	6.0	30.0	4.0	6.101E+02	4.480E+02	4.480E+02
7	7.0	35.0	6.4	8.304E+02	6.098E+02	6.098E+02
8	8.0	40.0	9.5	1.085E+03	7.965E+02	7.965E+02
9	9.0	45.0	13.6	1.373E+03	1.008E+03	1.008E+03
10	10.0	50.0	18.6	1.695E+03	1.245E+03	1.245E+03
11	11.0	55.0	24.8	2.051E+03	1.506E+03	1.506E+03
12	12.0	60.0	32.2	2.440E+03	1.792E+03	1.792E+03
13	13.0	65.0	40.9	2.864E+03	2.103E+03	2.103E+03
14	14.0	70.0	51.1	3.321E+03	2.439E+03	2.439E+03
15	15.0	75.0	62.8	3.813E+03	2.800E+03	2.800E+03
16	16.0	80.0	76.3	4.338E+03	3.186E+03	3.186E+03
17	17.0	85.0	91.5	4.897E+03	3.597E+03	3.597E+03
18	18.0	90.0	108.6	5.491E+03	4.032E+03	4.032E+03
19	19.0	95.0	127.7	6.118E+03	4.493E+03	4.493E+03
20	20.0	100.0	148.9	6.779E+03	4.978E+03	4.978E+03
21	21.0	105.0	172.4	7.473E+03	5.489E+03	5.489E+03
22	22.0	110.0	198.2	8.202E+03	6.024E+03	6.024E+03
23	23.0	115.0	226.5	8.965E+03	6.584E+03	6.584E+03
24	24.0	120.0	257.4	9.761E+03	7.169E+03	7.169E+03
25	25.0	125.0	290.9	1.059E+04	7.779E+03	7.779E+03
26	26.0	130.0	327.2	1.146E+04	8.413E+03	8.413E+03
27	27.0	135.0	366.5	1.235E+04	9.073E+03	9.073E+03
28	28.0	140.0	408.7	1.329E+04	9.757E+03	9.757E+03
29	29.0	145.0	454.1	1.425E+04	1.047E+04	1.047E+04
30	30.0	150.0	502.7	1.525E+04	1.120E+04	1.120E+04
31	31.0	155.0	554.7	1.629E+04	1.196E+04	1.196E+04
32	32.0	160.0	610.1	1.735E+04	1.274E+04	1.274E+04
33	33.0	165.0	669.1	1.845E+04	1.355E+04	1.355E+04
34	34.0	170.0	731.8	1.959E+04	1.439E+04	1.439E+04
35	35.0	175.0	798.3	2.076E+04	1.525E+04	1.525E+04
36	36.0	180.0	868.7	2.196E+04	1.613E+04	1.613E+04
37	37.0	185.0	943.1	2.320E+04	1.704E+04	1.704E+04
38	38.0	190.0	1021.6	2.447E+04	1.797E+04	1.797E+04
39	39.0	195.0	1104.4	2.578E+04	1.893E+04	1.893E+04
40	40.0	200.0	1191.6	2.711E+04	1.991E+04	1.991E+04
41	41.0	205.0	1283.2	2.782E+04	2.092E+04	2.092E+04
42	42.0	210.0	1379.4	2.850E+04	2.195E+04	2.195E+04
43	43.0	215.0	1480.3	2.918E+04	2.301E+04	2.301E+04
44	44.0	220.0	1586.0	2.986E+04	2.409E+04	2.409E+04
45	45.0	225.0	1696.6	3.053E+04	2.520E+04	2.520E+04

46	46.0	230.0	1812.3	3.121E+04	2.634E+04	2.634E+04
47	47.0	235.0	1933.0	3.189E+04	2.749E+04	2.749E+04
48	48.0	240.0	2059.1	3.257E+04	2.868E+04	2.868E+04
49	49.0	245.0	2190.5	3.325E+04	2.988E+04	2.988E+04
50	50.0	250.0	2327.3	3.393E+04	3.111E+04	3.111E+04
51	51.0	255.0	2469.8	3.461E+04	3.237E+04	3.237E+04
52	52.0	260.0	2617.9	3.528E+04	3.365E+04	3.365E+04
53	53.0	265.0	2771.9	3.596E+04	3.496E+04	3.496E+04
54	54.0	270.0	2931.8	3.664E+04	3.629E+04	3.629E+04
55	55.0	275.0	3097.7	3.732E+04	3.765E+04	3.765E+04
56	56.0	280.0	3269.7	3.800E+04	3.903E+04	3.903E+04
57	57.0	285.0	3448.0	3.868E+04	4.044E+04	4.044E+04
58	58.0	290.0	3632.7	3.935E+04	4.187E+04	4.187E+04
59	59.0	295.0	3823.9	4.003E+04	4.332E+04	4.332E+04
60	60.0	300.0	4021.6	4.071E+04	4.480E+04	4.480E+04
61	61.0	305.0	4226.1	4.139E+04	4.631E+04	4.631E+04
62	62.0	310.0	4437.3	4.207E+04	4.784E+04	4.784E+04
63	63.0	315.0	4655.5	4.275E+04	4.940E+04	4.940E+04
64	64.0	320.0	4880.8	4.343E+04	5.098E+04	5.098E+04
65	65.0	325.0	5113.1	4.410E+04	5.258E+04	5.258E+04
66	66.0	330.0	5352.8	4.478E+04	5.421E+04	5.421E+04
67	67.0	335.0	5599.8	4.546E+04	5.587E+04	5.587E+04
68	68.0	340.0	5854.3	4.614E+04	5.755E+04	5.755E+04
69	69.0	345.0	6116.4	4.682E+04	5.925E+04	5.925E+04
70	70.0	350.0	6386.2	4.750E+04	6.098E+04	6.098E+04
71	71.0	355.0	6663.8	4.818E+04	6.274E+04	6.274E+04
72	72.0	360.0	6949.4	4.885E+04	6.452E+04	6.452E+04
73	73.0	365.0	7242.9	4.953E+04	6.632E+04	6.632E+04
74	74.0	370.0	7544.7	5.021E+04	6.815E+04	6.815E+04
75	75.0	375.0	7854.7	5.089E+04	7.001E+04	7.001E+04
76	76.0	380.0	8173.1	5.157E+04	7.189E+04	7.189E+04
77	77.0	385.0	8500.0	5.225E+04	7.379E+04	7.379E+04

C.2.2 Explanation of 'synthesis'

Harmonic components vs. Synthesis

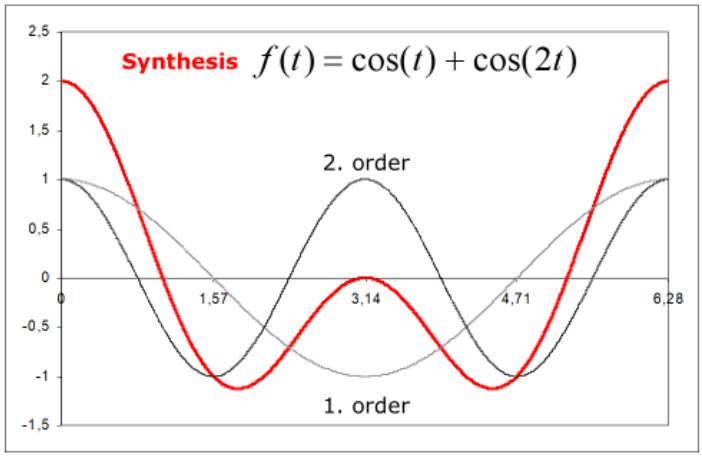

Ungraded

Harmonic components vs. Synthesis

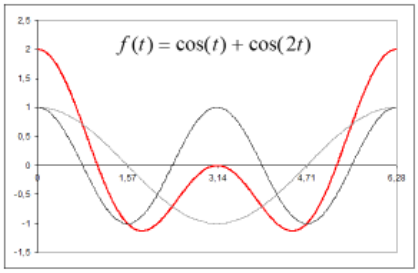

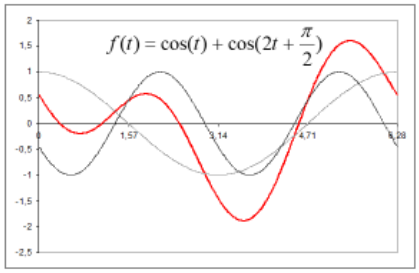

Synthesis : Sum of harmonic functions with phase angles (vector sum)

Algebraic sum *: Sum of amplitudes of all components*

Ungraded

C.2.3 Maximum torque and stress amplitudes

DNV GL
Test2 MASTER Propulsion System
REV7_NEWEng_NewIDs_M_TVD

Nauticus Torsional Vibrations
Version 12.3.89
By DNV GL - Software

Operating mode 1 - New operating mode
Load case 1 - New load case, 1-77 rpm,Propeller law - full pitch

MAXIMUM VIBRATORY TORQUE AMPLITUDES | TOP 5

Shaft ID	Description	RPM [rpm]	Torque [kN*m]
11	Stiffness1112	45	1,687E+003
12	Stiffness1213	45	1,680E+003
10	Stiffness1011	45	1,602E+003
7	Crankthrow78	45	1,599E+003
9	Stiffness910	45	1,585E+003

MAXIMUM VIBRATORY STRESS AMPLITUDES | TOP 5

Shaft ID	Description	RPM [rpm]	Stress [N/mm^2]
11	Stiffness1112	45	1,247E+002
12	Stiffness1213	45	5,747E+001
10	Stiffness1011	45	1,489E+001
7	Crankthrow78	45	1,486E+001
9	Stiffness910	45	1,473E+001

C.3 Excel sheet for sensitivity analysis

The Excel sheet where results from the sensitivity analysis are evaluated is attached in the delivered zip-file in DAIM. Its file name is 'Sensitivity_Analysis_NM.xlsx'.

Appendix D

Attachments to Simpack Simulation

D.1 Values of absolute and relative damping in Simpack

All damping factors are calculated by use of Equation 3.22, according to the constant magnifier model.

Table D.1: Relative shaft damping

Shaft	**Damping factor** C_{rel} [Nms/rad]
Damp. stiff.	295000
Shaft 2-3	1925
Shaft 3-4	9313
CT1	9313
CT2	9313
CT3	9313
CT4	9313
Shaft 8-9	2599
Shaft 9-10	851
Shaft 10-11	0
Interm. shaft	0
Prop. shaft	0

Table D.2: Absolute mass damping

ID	**Inertia**	**Damping factor** C_{abs} [Nms/rad]
1	TVD outer	0
2	TVD inner	0
3	MomentCompnstr1	1636
4	1st cylinder	7916
5	2nd cylinder	7916
6	3rd cylinder	7916
7	4th cylinder	7916
8	5th cylinder	7916
9	Camdrive+Thrust	2209
10	MomentCompnstr2	723
11	Turning wheel	2180
12	Flange	0
13	Propeller	Not approached

D.2 Example of a Simpack model

An example of a Simpack model, with document format '.spck', is attached in the zip-file delivered together with this report in DAIM. The selected example is simulation at resonance speed, namely 45 rpm.

The file name of the actual model is 'SimpackModel_45rpmOperation.spck'. The associated text-file of harmonic input torque is also attached in the same folder, named 'EngineTorque_45rpm.if2'.

D.3 MATLAB files for variable reference speed

D.3.1 Simulink setup

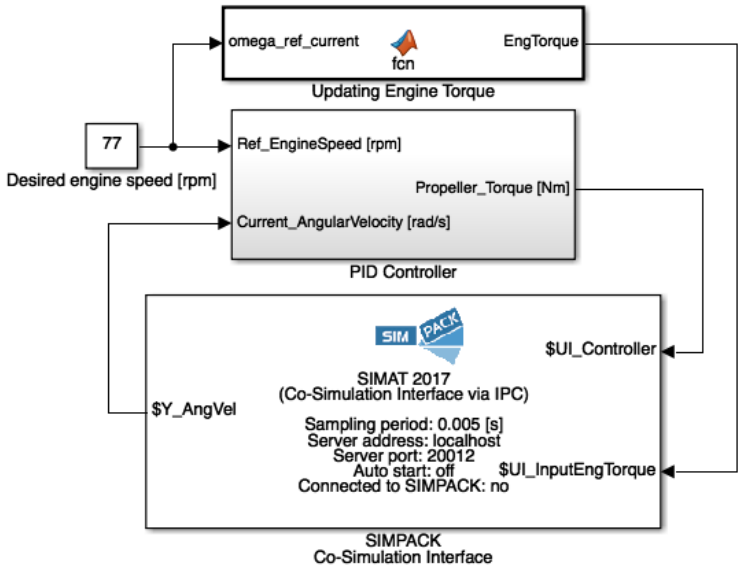

D.3.2 MATLAB function for updating engine torque

```
%Updating engine torque in Simulink

%Calculates engine torque for all cylinders at a given rpm, applies this
%torque in Simpack at the joint of cylinder 1 (through a force element)

function EngTorque = fcn(omega_ref_current)
EngTorque = 177.79*omega_ref_current^2; %Engine/Propeller curve [Nm]
end
```

D.3.3 MATLAB script for updating reference speed

```
%Run this script to start co-simulation with variable omega_ref

%Simulation is finished after about 300s (reached 77 rpm then)
%Step wise change: 11-77 rpm

%Set initial omega_ref
init = '11';%Initially omega_ref = 11 rpm
set_param('Controller_Rev12_PID_EngineTorque/Desired engine speed [rpm]','
    Value', init)
%Start simulation
set_param('Controller_Rev12_PID_EngineTorque','SimulationCommand','start');

%Update omega_ref
X = zeros(1,6);%Vector with simulation time events [sec] where omega_ref is
    changed
for i = 11:11:66 %6 different i
    omega_ref = i+11;%22,33,44,...,77 rpm
    omega_ref_char = num2str(omega_ref);% Value of constant block is a string
    pause(7000) %Pause real seconds, not sim time seconds
    X(i/11) = get_param('Controller_Rev12_PID_EngineTorque','SimulationTime')
        ;
    set_param('Controller_Rev12_PID_EngineTorque/Desired engine speed [rpm]',
        'Value', omega_ref_char);
end

%Make a vector with the simulation time difference between initialization of
    two omega_ref
Time_Diff = zeros(1,5);
for i = 1:1:5
 Time_Diff(i) = X(i+1)-X(i);
end
```

D.4 Result file - eigenvalues, eigenvectors and energies

```
# Simpack Modal Result File - Eigenvalues, Eigenvectors and Energies
# Version          :  2.0
# Creation Date    : 18-06-23
# Simpack Version  : 20170
# File Type        : modal damped
# Model Input File : DriveTrain_Rev19_Teng_45rpm_20012
# Damping of Force Elements and Flexible Bodies enabled
# Units            :    1.000 kg,    1.000 m,    1.000 s,    1.000 N,    1.000 rad
# Amplifications   : CG-xyz= 1.0E+00, CG-phi= 1.0E+00, body.el= 1.0E+00, force.st= 1.0E+00
# Amplification of Eigenvalue Components does not influence Energies
# ------------------------------------------------------------------------
   26      # number of stored eigenvalues
   13      # number of bodies
    0      # number of modal coordinates
    0      # number of force element states
# ------------------------------------------------------------------------
#                  E I G E N V A L U E S
   26      # number of Eigenvalues (total)
    2      # number of Eigenvalues with positive Real Parts
    1      # number of Zero Eigenvalues
#
#   No.     |  Real-Part      Imag.-Part | Nat.Damping  Frequency | Undamped Frequency |
#           |    [1/s]         [rad/s]   |     [-]         [Hz]   |      f0  [Hz]      |
# ----------+----------------------------+------------------------+--------------------+
#    1      | -7.6271E-08  +  0.0000E+00 |    0.0000       0.0000 |                    |
#    2      |  2.2910E-01  +  0.0000E+00 |    1.0000       0.0000 |                    |
#    3/   4 | -3.9609E-01 +/- 2.3586E+01 |    0.0168       3.7538 |        3.7543      |
#    5/   6 | -7.7369E+00 +/- 3.0712E+01 |    0.2443       4.8879 |        5.0406      |
#    7/   8 | -2.3421E+00 +/- 1.6417E+02 |    0.0143      26.1289 |       26.1315      |
#    9/  10 | -2.1595E+00 +/- 3.1857E+02 |    0.0068      50.7015 |       50.7027      |
#   11/  12 | -1.8717E+00 +/- 4.4937E+02 |    0.0042      71.5195 |       71.5202      |
#   13/  14 | -1.5252E+00 +/- 5.5064E+02 |    0.0028      87.6376 |       87.6379      |
#   15/  16 | -8.6726E-01 +/- 6.1442E+02 |    0.0014      97.7888 |       97.7888      |
#   17/  18 | -4.5428E-02 +/- 6.2915E+02 |    0.0001     100.1326 |      100.1326      |
```

```
#   19/  20 | -1.8385E+01 +/- 7.5774E+02 |    0.0243     120.5986 |      120.6341      |
#   21/  22 |  1.0841E-03 +/- 1.1046E+03 |   -0.0000     175.8105 |      175.8105      |
#   23/  24 | -1.6824E-01 +/- 2.6964E+04 |    0.0000    4291.3840 |     4291.3840      |
#   25/  26 | -7.4520E+01 +/- 3.0287E+04 |    0.0025    4820.4053 |     4820.4199      |
# ------------------------------------------------------------------------------------
EV.No:              3 /   4             |                  5 /   6             |
#      Re          Im          f0 [Hz]  |      Re          Im          f0 [Hz]  |
   -3.9609E-01   2.3586E+01   3.754E+00 -7.7369E+00   3.0712E+01   5.041E+00  |
# --------------------------------------|--------------------------------------|
#       Amplitude  Phase    Energy      |       Amplitude  Phase    Energy      |
#                  [deg]    kin. /      |                  [deg]    kin. /      |
#                           modal       |                           modal       |
# --------------------------------------|--------------------------------------|
body.cm: $B_TVD_outer
          0.8174   158.63   0.2314        1.0000     0.00   1.0000
body.cm: $B_TVD_inner
          0.3849  -173.87   0.0037        0.1946   159.26   0.0027
body.cm: $B_Flange
          0.6928    -0.85   0.0029        0.0754   -86.17   0.0001
body.cm: $B_Propeller
          1.0000     0.00   1.0000        0.1311   -59.01   0.0496
body.cm: $G_Engine.$B_MomentComponstr1
          0.3849  -173.87   0.0104        0.1947   159.26   0.0077
body.cm: $G_Engine.$B_Cylinder1
          0.3808  -173.61   0.0493        0.2000   161.07   0.0393
body.cm: $G_Engine.$B_Cylinder2
          0.3741  -173.33   0.0476        0.2047   162.79   0.0411
body.cm: $G_Engine.$B_Cylinder3
          0.3651  -173.05   0.0453        0.2078   164.21   0.0424
body.cm: $G_Engine.$B_Cylinder4
          0.3542  -172.76   0.0427        0.2093   165.31   0.0430
body.cm: $G_Engine.$B_Cylinder5
          0.3419  -172.49   0.0397        0.2089   166.09   0.0428
body.cm: $G_Engine.$B_CamdriveThrust
          0.3312  -172.28   0.0104        0.2073   166.48   0.0118
body.cm: $G_Engine.$B_MomentComponstr2
          0.3312  -172.28   0.0034        0.2073   166.48   0.0039
body.cm: $B_TurningWheel
```

```
          0.3232  -172.12   0.0166        0.2059   166.72   0.0195

# ----------------------------------------------------------------------

EV.No:              7 /   8             |

#      Re           Im          f0 [Hz]  |

   -2.3421E+00   1.6417E+02   2.613E+01 |

# --------------------------------------|

#       Amplitude  Phase    Energy      |

#                  [deg]    kin. /      |

#                           modal       |

# --------------------------------------|

body.cm: $B_TVD_outer

          0.0956  -105.10   0.0105

body.cm: $B_TVD_inner

          1.0000     0.00   0.0834

body.cm: $B_Flange

          0.2367  -179.61   0.0011

body.cm: $B_Propeller

          0.0170    -1.36   0.0010

body.cm: $G_Engine.$B_MomentComponstr1

          1.0000     0.00   0.2333

body.cm: $G_Engine.$B_Cylinder1

          0.9413     1.20   1.0000

body.cm: $G_Engine.$B_Cylinder2

          0.6249     2.74   0.4407

body.cm: $G_Engine.$B_Cylinder3

          0.1372    11.38   0.0213

body.cm: $G_Engine.$B_Cylinder4

          0.3925   177.68   0.1738

body.cm: $G_Engine.$B_Cylinder5

          0.7919   179.70   0.7078

body.cm: $G_Engine.$B_CamdriveThrust

          0.9408  -179.94   0.2788

body.cm: $G_Engine.$B_MomentComponstr2

          0.9411  -179.94   0.0913

body.cm: $B_TurningWheel

          0.9999  -179.82   0.5282

# ----------------------------------------------------------------------
```

Appendix E

Attachments to Time Domain Post-Processing

E.1 The WAFO codes

All WAFO scripts and functions are attached in the zip-file delivered in DAIM together with this report. The name of its folder is 'WAFO_Version2017'.

E.2 Investigation of power spectra

E.2.1 MATLAB script for construction of PSD plots

Comment: Required WAFO functions, such as 'dat2spec', are attached in the zip-file together with this report (reference to Appendix E.1)

```
%Time series of shaft torque
fileID = fopen('ForceTorque_Stiff1213_30rpm.txt','r'); %Open txt-file
formatSpec = '%f %f'; %Read floats
sizeA = [2 6001]; %Dimensions
A = fscanf(fileID,formatSpec,sizeA); %Read data
fclose(fileID);
x = A';%Transpose, 2 columns

%Plotting power spectrum
sampling_fre = 200 ; %Sampling frequency [Hz]
```

```
dt = 1/sampling_fre; %Time step
tmax = length(x)/sampling_fre; %Max sim time (30 s)

L = 2000; %L=5000, how corse the plot becomes
plotflag = 3; %Plots the density, S, and 10log10(S) together
S1 = dat2spec([x(:,1) x(:,2)],L); %Calculate PSD by use of WAFO

figure(1); %S against Hz
omeg1 = S1.w / (2*pi); %Hz
spect1 = S1.S;
semilogy(omeg1,spect1); %y-axis log
xlim([0 80]) %80 Hz max on x-axis
xlabel('Frequency [Hz]');
ylabel('S(w) [(Nm)^2/(rad/s)]'); %S normalized at rad/s
```

E.2.2 Plots of power spectral density

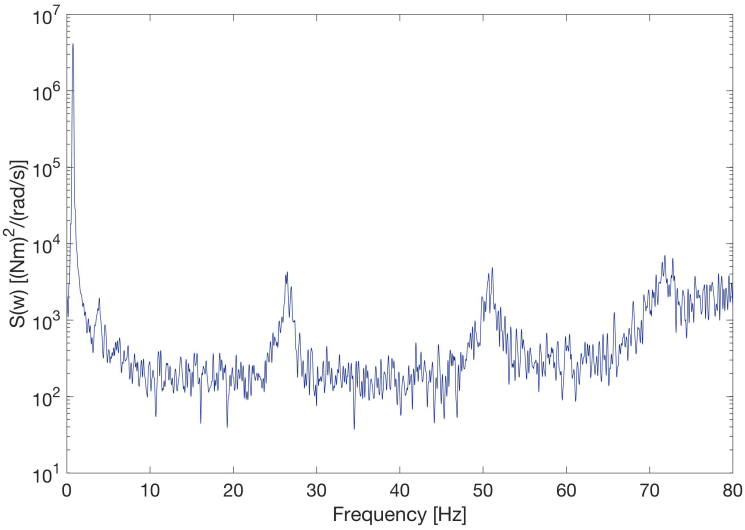

Figure E.1: Power spectrum of damper stiffness (from torque at 45 rpm)

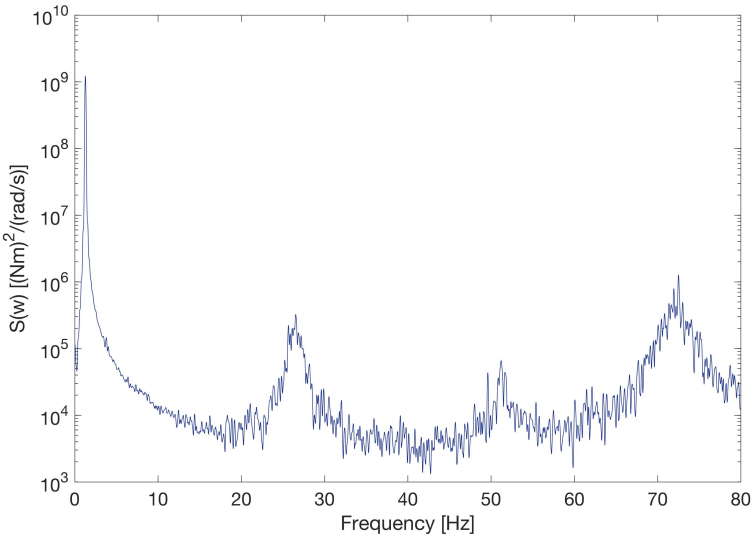

Figure E.2: Power spectrum of third crank throw (from torque at 77 rpm)

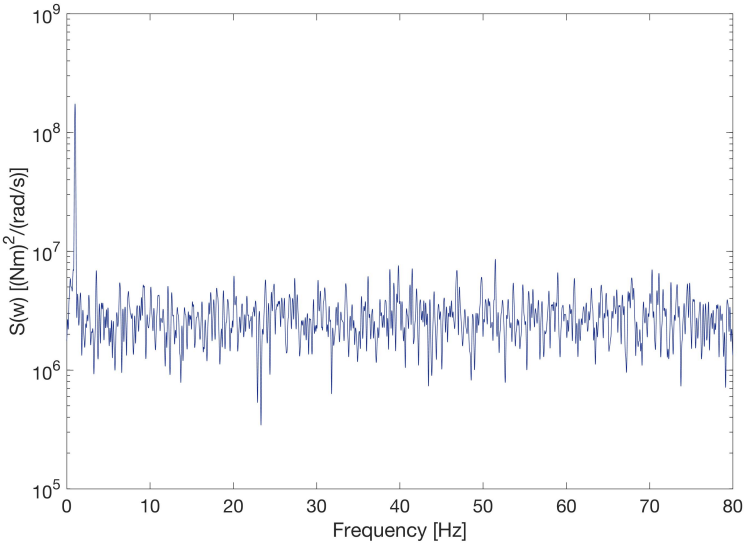

Figure E.3: Power spectrum of Shaft 10-11 (from torque at 60 rpm)

E.3 MATLAB script for calculations of fatigue damage

Comment: Utilized WAFO functions such as 'dat2rfm' and 'tp2rfc' are attached in the zip-file together with this report (reference to Appendix E.1)

```
%FATIGUE DAMAGE ANALYSIS
%This example is for 45 rpm operation at the intermediate shaft

%READ FROM TXT-FILE OF TORQUE SERIES AND CREATE MATRIX x
fileID = fopen('ForceTorque_45rpm_Stiff1112.txt','r'); %Open txt-file
formatSpec = '%f %f'; %Read floats
sizeA = [2 6001]; %Dimensions
A = fscanf(fileID,formatSpec,sizeA); %Read data
fclose(fileID);
x = A';%Transpose, 2 columns

%CALCULATE TIME SERIES OF TORSIONAL STRESS
%tau = T*r/I    %I varies with shaft
%DampStiff - Must remove 2nd [RFM,u]
r_damp = 4999.5/1000;%m
d_out_damp = 2*r_damp;%m
I_DampStiff = pi/32*(d_out_damp^4);%m^4
%All other shafts (hollow)
r_hollow = 410/1000;%m
d_out_hollow = 2*r_hollow;%m
d_in_hollow = 150/1000;%m
I_Hollow = pi/32*(d_out_hollow^4 - d_in_hollow^4);%m^4
%Intermediate shaft
r_interm = 205/1000;%m
d_out_interm = 2*r_interm;%m
I_Interm = pi/32*(d_out_interm^4);%m^4
%Propeller shaft
r_prop = 265/1000;%m
d_out_prop = 2*r_prop;%m
I_Prop = pi/32*(d_out_prop^4);%m^4
%Torque i Nm --> Stress in N/m^2 --> Stress*10^-6 N/mm^2 = MPa
%x(:,2) = (x(:,2)*r_damp/I_DampStiff)*10^-6;
%x(:,2) = (x(:,2)*r_hollow/I_Hollow)*10^-6;
x(:,2) = (x(:,2)*r_interm/I_Interm)*10^-6;
%x(:,2) = (x(:,2)*r_prop/I_Prop)*10^-6;

%PLOT TORSIONAL STRESS AGAINST TIME
time = x(:,1); %45, 45.005, ...
stress = x(:,2); %Torsional stress in MPa
figure
plot(time,stress) %Plot torsional stress in MPa against time
title('Intermediate Shaft - Torsional stress at 45 rpm operation')
xlabel('Simulation time [s]')
ylabel('Torsional stress [MPa]')
set(gca,'fontsize', 12);
%CREATE ZOOM IN
axes('Position',[.63 .15 .25 .25]); %Position of new box in current figure
box on %Put box around new pair of axes
indexOfInterest = (time > 49.4) & (time < 50.02); %Desired area time axis
plot(time(indexOfInterest),stress(indexOfInterest));
set(gca,'XAxisLocation','top','fontsize',12);%X-axis above box,new fontsize
axis tight;

%PLOT RAIN FLOW MATRIX
```

```
55 [RFM,u] = dat2rfm(x,0,64); %Default parameters (h=0, n=64)
56 figure
57 cmatplot(u,u,RFM,3);
58 title('Rain flow matrix')
59 xlabel('Min stress [MPa]')
60 ylabel('Max stress [MPa]')
61 set(gca,'fontsize', 12);
62
63 %PLOT RFC HISTOGRAM
64 tp = dat2tp(x) ; %Calculate turning point
65 rfc = tp2rfc(tp) ; %Calculate the rfc by use of 4-point algorithm
66 for i=1:length(rfc)
67     range(i)=rfc(i,2)-rfc(i,1);
68 end
69 figure
70 histogram(range);
71 title('Histogram from rain flow cycle counting')
72 xlabel('Stress range, S [MPa]')
73 ylabel('Number of cycles, n')
74 set(gca,'fontsize', 12);
75
76 %CALCULATE ACCUMULATED FATIGUE DAMAGE
77 beta = 6.225; %=m, slope parameter
78 log_Kc = 23.613;
79 Kc = 10^log_Kc;
80 epcilon = 1/Kc; %1/K_c;
81 RFC = tp2rfc(tp);
82 dam45rpm=cc2dam(RFC,beta,epcilon)*2;
83 %Times 2 since RFC calc. half amplitudes
```